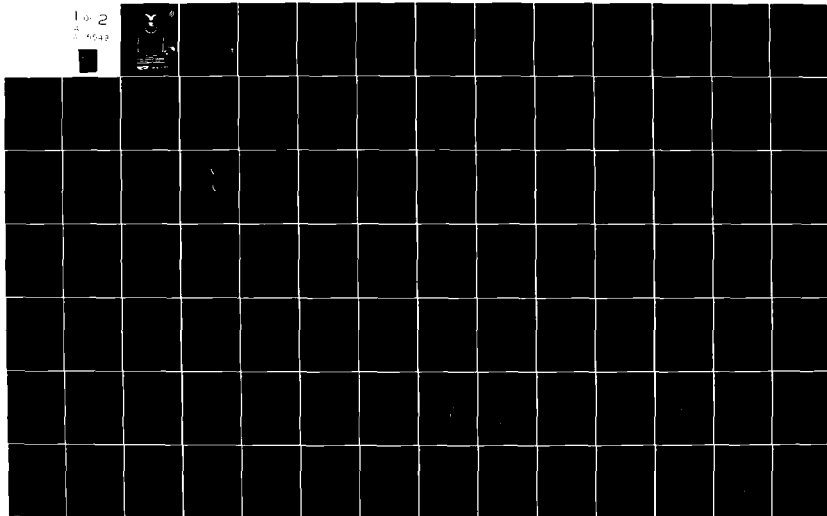


AD-A115 549 AIR FORCE INST OF TECH WRIGHT-PATTERSON AFB OH SCHOO--ETC F/G 20/4.
CALCULATING AIRCRAFT CONTROLLABILITY QUALITY.(U)
DEC 79 J M YARGER
UNCLASSIFIED AFIT/8AE/AA/79D-19

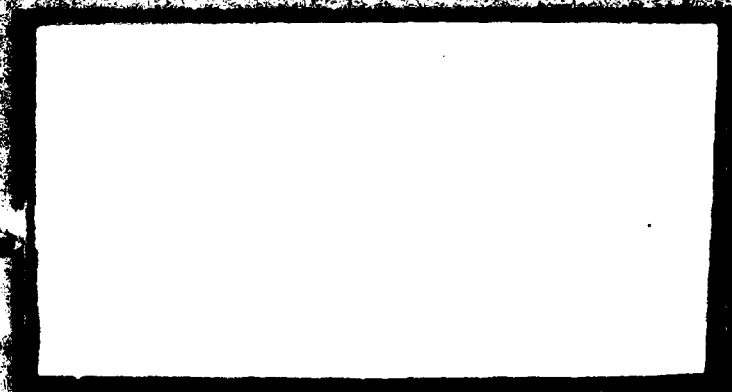
NL

10-2

5643



- AD A115549 -



AFIT/GAE/AA/79D-19

C

CALCULATING AIRCRAFT
CONTROLLABILITY QUALITY

THESIS

AFIT/GAE/AA/79D-19

John M. Yarger
Capt USAF

DTIC
ELECTE
JUN 15 1982
H

DISTRIBUTION STATEMENT A

Approved for public release;
Distribution Unlimited

AFIT/CAE/AA/79D-19

CALCULATING AIRCRAFT
CONTROLLABILITY QUALITY

THESIS

Presented to the Faculty of the School of Engineering
of the Air Force Institute of Technology
Air University
in Partial Fulfillment of the
Requirements for the Degree of
Master of Science

by

John M. Yarger, B.S.

Capt USAF

Graduate Aeronautical Engineering

December 1979

Approval for public release; distribution unlimited

Preface

This thesis project could never have been completed without the invaluable help of several individuals. My thesis advisor, Capt James Silverthorn, provided the initial insights into the theoretical material of this project, and his interim evaluations were crucial in identifying and correcting several obscure software problems. Dr. Robert Schwantz and Capt Jerrel Southern of the AFFDL catalyzed the entire project by their assistance with the finer points of the FLEXSTAB computer program. Capt Jerry Stinson of the AFIT Computer Center lent his superior support and experience to make the final software system a reality. My wife, Sibbi, deserves even more credit. She remained confident, supportive, and positive through even the worst of the problems and delays. Most of all, I thank and praise the Lord Jesus Christ for this opportunity to learn to trust and obey Him more fully.

John M. Yarger



Accession For	
NTIS GRA&I	<input checked="checked" type="checkbox"/>
DTIC TAB	<input type="checkbox"/>
Unannounced	<input type="checkbox"/>
Justification	
By	
Distribution/	
Availability Codes	
Dist	Avail and/or Special
A	

Contents

	<u>Page</u>
Preface	11
List of Figures	v
List of Tables	1x
List of Symbols	x
Abstract	xv
I. Introduction	1
Background	1
Application of the Concept	5
Control System Concept and Aircraft Selection	5
Purpose	7
Goals	7
Assumptions	10
Approach and Overview	10
II. Aerodynamic Data Generation	11
Basic Theory and Outputs	11
Control Surface Definition	11
Discussion of Data	14
III. Data Conversion to State Space Representation	17
IV. Control System Analysis	24
Basic Theory	24
Software Implementation	30
V. Results	31
Aircraft Traits	31
1) LES 230-Y Longitudinal Case	31
2) LES 230-Y Lateral/Directional Case	33
3) Modified LES 230-Y Longitudinal Case	34
4) Modified LES 230-Y Lateral/Direction Case	35
Traits Discussion	37
Direct Aircraft Comparison	38
1) Longitudinal Vector 1	39
2) Longitudinal Vector 2	39
3) Lateral/Directional Vector 1	39
4) Lateral/Directional Vector 2	39
Experimental Control System Evaluation	39
Method Evaluation	40

Contents (Cont'd)

	<u>Page</u>
VI. Conclusions and Recommendations	46
Conclusions	46
Recommendations	48
Bibliography	50
Appendix A: Aircraft Specifications and FLEXSTAB Results	52
Appendix B: Sample Output Data for LES 230-Y	57
Appendix C: Sample Output Data for Modified LES 230-Y	81
Appendix D: Sample Data for Direct Aircraft Comparison	111
Appendix E: GRAMOP Program User's Guide	128
Vita	134

List of Figures

<u>Figure</u>		<u>Page</u>
1	Yawing Moment Due to Individual Tip Deflection	6
2	Baseline Boeing LES 230-Y	8
3	Boeing LES 230-Y With Experimental Control Surfaces	9
4	Aerodynamic Paneling Approximation	13
5	Linearity Restrictions	42
B1	Baseline LES Longitudinal $\bar{V}_1(t_f)$	58
B2	Baseline LES Longitudinal Response to Reach $\bar{V}_1(t_f = 1.5$ Seconds)	59
B3	Baseline LES Longitudinal Controls to Reach $\bar{V}_1(t_f = 1.5$ Seconds)	60
B4	Baseline LES Longitudinal $\bar{V}_2(t_f)$	61
B5	Baseline LES Longitudinal $\bar{V}_3(t_f)$	62
B6	Baseline LES Longitudinal $\bar{V}_4(t_f)$	63
B7	Baseline LES Longitudinal $\bar{V}_5(t_f)$	64
B8	Baseline LES Longitudinal Response to Reach $\bar{V}_5(t_f = 1.5$ Seconds)	65
B9	Baseline LES Longitudinal Controls to Reach $\bar{V}_5(t_f = 1.5$ Seconds)	66
B10	Baseline LES Longitudinal Response to Reach $\bar{V}_5(t_f = 4.0$ Seconds)	67
B11	Baseline LES Longitudinal Controls to Reach $\bar{V}_5(t_f = 4.0$ Seconds)	68
B12	\log_{10} of Baseline LES Weighted Control Costs for All Longitudinal Basis Vectors	69
B13	Baseline LES Lateral/Directional $\bar{U}_1(t_f)$	70
B14	Baseline LES Lateral/Directional Response to Reach $\bar{U}_1(t_f = 2.25$ Seconds)	71
B15	Baseline LES Lateral/Directional Controls to Reach $\bar{U}_1(t_f = 2.25$ Seconds)	72

List of Figures (Contd)

<u>Figure</u>		<u>Page</u>
B16	Baseline LES Lateral/Directional $\bar{V}_2(t_f)$	73
B17	Baseline LES Lateral/Directional $\bar{V}_3(t_f)$	74
B18	Baseline LES Lateral/Directional $\bar{V}_4(t_f)$	75
B19	Baseline LES Lateral/Directional Response to Reach $\bar{V}_4(t_f = 2.0 \text{ Seconds})$	76
B20	Baseline LES Lateral/Directional Controls to Reach $\bar{V}_4(t_f = 2.0 \text{ Seconds})$	77
B21	Baseline LES Lateral/Directional Response to Reach $\bar{V}_4(t_f = 8.0 \text{ Seconds})$	78
B22	Baseline LES Lateral/Directional Controls to Reach $\bar{V}_4(t_f = 8.0 \text{ Seconds})$	79
B23	\log_{10} of Baseline LES Weighted Control Costs for All Lateral/Directional Basis Vectors	80
C1	Experimental LES Longitudinal $\bar{V}_1(t_f)$	82
C2	Experimental LES Longitudinal Response to Reach $\bar{V}_1(t_f = 1.5 \text{ Seconds})$	83
C3	Experimental LES Longitudinal Controls to Reach $\bar{V}_1(t_f = 1.5 \text{ Seconds})$	84
C4	Experimental LES Longitudinal Response to Reach $\bar{V}_1(t_f = 4.0 \text{ Seconds})$	85
C5	Experimental LES Longitudinal Controls to Reach $\bar{V}_1(t_f = 4.0 \text{ Seconds})$	86
C6	Experimental LES Longitudinal $\bar{V}_2(t_f)$	87
C7	Experimental LES Longitudinal $\bar{V}_3(t_f)$	88
C8	Experimental LES Longitudinal $\bar{V}_4(t_f)$	89
C9	Experimental LES Longitudinal $\bar{V}_5(t_f)$	90
C10	Experimental LES Longitudinal Response to Reach $\bar{V}_5(t_f = 3.0 \text{ Seconds})$	91
C11	Experimental LES Longitudinal Controls to Reach $\bar{V}_5(t_f = 3.0 \text{ Seconds})$	92

List of Figures (Cont'd)

Figure		Page
C12	Experimental LES Longitudinal Response to Reach $\bar{U}_5(t_f = 8.0 \text{ Seconds})$	93
C13	Experimental LES Longitudinal Controls to Reach $\bar{U}_5(t_f = 8.0 \text{ Seconds})$	94
C14	\log_{10} of Experimental LES Weighted Control Costs for All Longitudinal Basis Vectors	95
C15	Experimental LES Lateral/Directional $\bar{U}_1(t_f)$	96
C16	Experimental LES Lateral/Directional Response to Reach $\bar{U}_1(t_f = 2.0 \text{ Seconds})$	97
C17	Experimental LES Lateral/Directional Controls to Reach $\bar{U}_1(t_f = 2.0 \text{ Seconds})$	98
C18	Experimental LES Lateral/Directional Response to Reach $\bar{U}_1(t_f = 4.0 \text{ Seconds})$	99
C19	Experimental LES Lateral/Directional Controls to Reach $\bar{U}_1(t_f = 4.0 \text{ Seconds})$	100
C20	Experimental LES Lateral/Directional $\bar{U}_2(t_f)$	101
C21	Experimental LES Lateral/Directional $\bar{U}_3(t_f)$	102
C22	Experimental LES Lateral/Directional $\bar{U}_4(t_f)$	103
C23	Experimental LES Lateral/Directional Response to Reach $\bar{U}_4(t_f = 2.0 \text{ Seconds})$	104
C24	Experimental LES Lateral/Directional Controls to Reach $\bar{U}_4(t_f = 2.0 \text{ Seconds})$	105
C25	Experimental LES Lateral/Directional Response to Reach $\bar{U}_4(t_f = 8.0 \text{ Seconds})$	106
C26	Experimental LES Lateral/Directional Controls to Reach $\bar{U}_4(t_f = 8.0 \text{ Seconds})$	107
C27	Experimental LES Lateral/Directional Response to Reach $\bar{U}_4(t_f = 9.5 \text{ Seconds})$	108
C28	Experimental LES Lateral/Directional Controls to Reach $\bar{U}_4(t_f = 9.5 \text{ Seconds})$	109
C29	\log_{10} of Experimental LES Weighted Control Costs for All Lateral/Directional Basis Vectors	110

List of Figures (Cont'd)

<u>Figure</u>		<u>Page</u>
D1	Baseline LES Longitudinal Response to Reach Longitudinal Vector 1	112
D2	Baseline LES Longitudinal Controls to Reach Longitudinal Vector 1	113
D3	Experimental LES Longitudinal Response to Reach Longitudinal Vector 1	114
D4	Experimental LES Longitudinal Controls to Reach Longitudinal Vector 1	115
D5	Baseline LES Longitudinal Response to Reach Longitudinal Vector 2	116
D6	Baseline LES Longitudinal Controls to Reach Longitudinal Vector 2	117
D7	Experimental LES Longitudinal Response to Reach Longitudinal Vector 2	118
D8	Experimental LES Longitudinal Controls to Reach Longitudinal Vector 2	119
D9	Baseline LES Lateral/Directional Response to Reach Lateral Vector 1	120
D10	Baseline LES Lateral/Directional Controls to Reach Lateral Vector 1	121
D11	Experimental LES Lateral/Directional Response to Reach Lateral Vector 1	122
D12	Experimental LES Lateral/Directional Controls to Reach Lateral Vector 1	123
D13	Baseline LES Lateral/Directional Response to Reach Lateral Vector 2	124
D14	Baseline LES Lateral/Directional Controls to Reach Lateral Vector 2	125
D15	Experimental LES Lateral/Directional Response to Reach Lateral Vector 2	126
D16	Experimental LES Lateral/Directional Controls to Reach Lateral Vector 2	127

List of Tables

<u>Table</u>		<u>Page</u>
I	Perturbation Substitutions	18
II	Baseline Boeing LES 230-Y State Space Matrices	21
III	Experimental LES 230-Y State Space Matrices	22
IV	Eigenvalues of Aircraft A Matrices	23
V	Direct Comparison Final State Vectors	38
A.I	Aircraft Data Specifications	53
A.II	Trim Parameters	54
A.III	FLEXSTAB Stability and Control Derivatives	55

List of Symbols

<u>Symbol</u>	<u>Definition</u>	<u>Usual Dimension</u>
a	Speed of sound	ft/sec
a.c.	Aerodynamic center	
A_{ij}, a_{ij}	Aerodynamic influence coefficients	ft ² /rad
b	(Wing) span	ft
c	Chord	ft
\bar{c}	Mean aerodynamic (geometric) chord	ft
D	Drag	lbs
g	Acceleration of gravity	ft/sec ²
I_{xx}, I_{yy}, I_{zz}	Moments of inertia about X, Y, Z axes respectively	slug ft ²
$I_{xy}, I_{yx}, I_{yz}, I_{zy}, I_{xz}, I_{zx}$	Products of inertia in XYZ system	slug ft ²
L	Rolling moment (about X)	ft lbs
ℓ	Perturbed rolling moment	ft lbs
L	Lift	lbs
m	Mass (airplane)	slugs
\bar{M}	Applied moment	ft lbs
M	Pitching moment	ft lbs
M	Mach number	
m	Perturbed pitching moment	ft lbs
N	Yawing moment	ft lbs
n	Perturbed yawing moment	ft lbs
P	Roll rate (About X)	rad/sec
p	Perturbed roll rate (about x)	rad/sec

List of Symbols (Cont'd)

<u>Symbol</u>	<u>Definition</u>	<u>Usual Dimension</u>
Q	Pitch rate	rad/sec
q	Perturbed pitch rate	rad/sec
\bar{q}	Dynamic pressure	lbs/ft ²
R	Yaw rate (About Z)	rad/sec
r	Perturbed yaw rate	rad/sec
S	Surface area, Reference (wing) area	ft ²
t	Time	sec
T	Thrust	lbs
U	Forward velocity (along X)	ft/sec
u	Perturbed forward velocity (along X)	ft/sec
V	Side velocity (along Y)	ft/sec
v	Perturbed side velocity	ft/sec
W	Downward velocity (along Z)	ft/sec
w	Perturbed downward velocity	ft/sec
α	Angle of attack	rad
δ_E	Elevator angle	deg, rad
δ_A	Aileron angle	deg, rad
δ_R	Rudder angle	deg, rad
ρ	Air density	slug/ft ³
γ	Flight path angle	rad
Θ, θ	Pitch attitude angle (total, perturbed)	rad
Φ, ϕ	Bank (roll) angle (total, perturbed)	rad
C_L	Lift coefficient (airplane)	

<u>Symbol</u>	<u>Definition</u>	<u>Usual Dimension</u>
C_D	Drag coefficient (airplane)	
C_m	Pitching moment coefficient (airplane)	
C_l	Rolling moment coefficient	
C_n	Yawing moment coefficient	
C_y	Side force coefficient	
C_{L_α}	Airplane lift curve slope	rad^{-1}
C_{L_δ}	Control surface lift effectiveness (planform)	rad^{-1}
C	Control surface lift effectiveness (section)	rad^{-1}
C_{D_0}	Drag coefficient for zero angle of attack, zero elevator and zero stabilizer angle	
C_{D_α}	Variation of drag coefficient with angle of attack	rad^{-1}
$C_{D_{\delta_E}}$	Variation of drag coefficient with elevator angle	$\text{deg}^{-1}, \text{rad}^{-1}$
\bar{C}_{D_0}	Drag coefficient at zero lift coefficient, zero elevator angle and zero stabilizer angle	
C_{L_0}	Lift coefficient for zero angle of attack, zero elevator angle and zero stabilizer angle	
$C_{L_{\delta_E}}$	Variation of lift coefficient with elevator angle	$\text{deg}^{-1}, \text{rad}^{-1}$
C_{m_0}	Pitching moment coefficient for zero angle of attack, zero elevator angle and zero stabilizer angle	
C_{m_α}	Variation of pitching moment coefficient with angle of attack (i.e., static longitudinal stability)	rad^{-1}
$C_{m_{\delta_E}}$	Variation of pitching moment coefficient with elevator angle (i.e., longitudinal control power)	$\text{deg}^{-1}, \text{rad}^{-1}$

<u>Symbol</u>	<u>Definition</u>	<u>Usual Dimension</u>
$C_{l\beta}$	Variation of rolling moment coefficient with sideslip angle (i.e., dihedral angle)	rad^{-1}
$C_{l\delta_A}$	Variation of rolling moment coefficient with aileron angle (i.e., lateral control power)	$\frac{\text{deg}^{-1}}{\text{rad}}$
$C_{l\delta_R}$	Variation of rolling moment coefficient with rudder angle	$\frac{\text{deg}^{-1}}{\text{rad}}$
$C_{n\beta}$	Variation of yawing moment coefficient with sideslip angle	rad^{-1}
$C_{n\delta_R}$	Variation of yawing moment coefficient with rudder angle	$\frac{\text{deg}^{-1}}{\text{rad}}$
$C_{n\delta_A}$	Variation of yawing moment coefficient with aileron angle	$\frac{\text{deg}^{-1}}{\text{rad}}$
$C_{y\beta}$	Variation of side force coefficient with sideslip angle	rad^{-1}
$C_{y\delta_R}$	Variation of side force coefficient with rudder angle	$\frac{\text{deg}^{-1}}{\text{rad}}$
$C_{y\delta_A}$	Variation of side force coefficient with aileron angle	$\frac{\text{deg}^{-1}}{\text{rad}}$
C_{D_u}	Variation of drag coefficient with speed (i.e., speed damping)	
C_{L_u}	Variation of lift coefficient with speed	
C_{m_u}	Variation of pitching moment coefficient with speed	
$C_{D\dot{\alpha}}$	Variation of drag coefficient with rate of change of angle of attack	
$C_{L\dot{\alpha}}$	Variation of lift coefficient with rate of change of angle of attack	
$C_{m\dot{\alpha}}$	Variation of pitching moment coefficient with rate of change of angle of attack	

<u>Symbol</u>	<u>Definition</u>	<u>Usual Dimension</u>
C_{D_q}	Variation of drag coefficient with pitch rate	
C_{L_q}	Variation of lift coefficient with pitch rate	
C_{m_q}	Variation of pitching moment coefficient with pitch rate	
$C_{y_{\dot{\beta}}}$	Variation of side-force coefficient with rate of change of sideslip angle	
$C_{l_{\dot{\beta}}}$	Variation of rolling moment coefficient with rate of change of sideslip angle	
$C_{n_{\dot{\beta}}}$	Variation of yawing moment coefficient with rate of change of sideslip angle	
C_{y_p}	Variation of side-force coefficient with roll rate	
C_{l_p}	Variation of rolling moment coefficient with roll rate	
C_{n_p}	Variation of yawing moment coefficient with roll rate	
C_{y_r}	Variation of side-force coefficient with yaw rate	
C_{l_r}	Variation of rolling moment coefficient with yaw rate	
C_{n_r}	Variation of yawing moment coefficient with yaw rate	

Abstract

A quantitative measure of linear system controllability quality was developed, implemented in a software program, and demonstrated through a preliminary evaluation of an experimental aircraft flight control system. Aerodynamic data (stability and control derivatives) were first calculated with linear aerodynamics software, then used in the linearized perturbation motion equations to generate a linear state space representation of aircraft motion. This representation was then used as the differential constraint equation for a quadratic cost functional which minimizes the control energy required to reach a specified final state.

The singular value decomposition of the controllability Grammian, which appears in the solution to this optimal control problem, yields a unique, time-varying, orthogonal set of basis vectors (\bar{V}_i , $i=1,2,\dots,n$) which are ranked by the control energy required to move the linear system along each vector. Each \bar{V}_i is the least costly (in control energy) direction to control in the orthogonal complement to that subspace of (R^n) containing \bar{V}_j , $j=1,2,\dots,(i-1)$.

The experimental flight control system consists of variable incidence wingtips acting as elevons and rudders, used on a supersonic-cruise lightweight fighter. The evaluation included both comparison of basis vector sets between baseline and modified aircraft and direct comparison of the control magnitudes required to reach sample final states. Results show the experimental controls are unsuitable due to

- 1) poor longitudinal and lateral control power
- 2) no yaw/rudder control available due to symmetry restrictions

in the linear aerodynamics software.

CALCULATING AIRCRAFT
CONTROLLABILITY QUALITY

1. Introduction

Background

In the field of linear system analysis, the concept of controllability is well known; i.e., it is determined by the rank of the controllability matrix

$$[B \mid AB \mid A^2B \mid \cdots \mid A^{n-1}B] \quad (1)$$

of the linear system described by the state space matrix equation

$$\dot{\bar{x}} = A\bar{x} + B\bar{u} \quad (2)$$

However, this measure of linear system behavior is largely qualitative. Either the controllability matrix is of full rank or it is not; therefore, the linear system is either completely controllable or it is not. Although there is a transformation matrix which separates the state space into completely controllable and completely uncontrollable modes, this is still only a qualitative result. The only information gained about the system's controllability characteristics is a "yes-or-no" answer as to whether a given mode is controllable or not. In terms of "ease" or "difficulty" of controlling the controllable modes, this method gives no quantitative measure of system controllability. Neither is there any quantitative indication of "how close to uncontrollable" are the controllable modes.

Compare this situation with that of stability analysis. The

techniques used in stability analysis not only determine the qualitative "yes-or-no" answer concerning stability of each mode, but also quantitatively describe the characteristic modes of system motion (e.g., exponential growth, exponential decay, damped sinusoid, etc.). In addition, there are quantitative methods to measure the stability characteristics of the system, such as time constants, damping ratio, etc. We now explore a similar quantitative measure of system controllability characteristics which would be useful as a control system analysis tool.

This study developed a method to identify that unique, time-varying set of characteristic directions in state space (R^n) which describes the system controllability quality. In this set, the n directions are mutually orthogonal and therefore the set spans (R^n). Also, these directions can be ranked according to the relative amount of control energy required to reach a fixed-magnitude final state located along each respective direction. Not only can these directions be ranked with respect to each other, but they also indicate the easiest and hardest to attain directions in the entire system state space (R^n). The definitions of these special directions are:

Direction 1) the easiest direction of all to attain (i.e., least control energy to reach) in the entire system state space (R^n);

Direction 2) the easiest direction of all to control (least control energy to reach) in (R^{n-1}), that particular subspace of (R^n) which is the orthogonal complement to the one-dimensional subspace spanned by direction 1.

...

...

Direction i) the easiest direction of all to control in (R^{n-i+1}) , that particular subspace of (R^n) which is the orthogonal complement to the $(i-1)$ -dimensional subspace spanned by directions 1 through $(i-1)$.

...

...

Direction n) the most difficult direction of all to control (most control energy to reach) in the entire state space system (R^n) . This new quantitative measure of controllability quality, then, consists of the relative amounts of control energy required to move the linear system along each orthogonal direction in this unique, time-varying set.

The development of this quantitative measure of linear system controllability appears in detail in Chapter IV and employs the following rationale. First, consider the functional

$$J(\bar{u}(t)) = \frac{1}{2} \int_0^{t_f} \bar{u}^T(\tau) R \bar{u}(\tau) d\tau \quad (3)$$

When the matrix R is limited to diagonal form, with only non-negative diagonal elements, the integrand $(\bar{u}^T R \bar{u})$ becomes $\frac{1}{2} \sum_{i=1}^n u_i^2 R_{ii}$, which may be interpreted physically as "control energy", analogous to the expression for kinetic energy, $\frac{1}{2} mV^2$. Restricting R to non-negative diagonal form, then, the entire functional expression $J(\bar{u}(t))$ is the net control energy used during the time interval $[0, t_f]$. Now let the linear system begin at zero initial state and alternately drive it to the same final state, \bar{x}_f , at the same final time, t_f , by using two different control input histories, $\bar{u}^1(t)$ and $\bar{u}^2(t)$, which result in

two different respective state space trajectories, $\bar{x}^1(t)$ and $\bar{x}^2(t)$. In general, one of these control histories will require less control energy than the other, as measured by the relative magnitudes of their respective functionals, $J_1 = J(\bar{u}^1(t))$ and $J_2 = J(\bar{u}^2(t))$; i.e., for a fixed final time and final state, the control history-response trajectory combination with the smaller $J(\bar{u}(t))$ is "easier" to attain since it requires less control energy.

Second, we use this control energy functional to make the quantitative evaluations of the controllability characteristics of the linear system. Rather than comparing arbitrary control histories which drive the system to an arbitrary final state, we wish to select those specific final states which can be used to identify absolute limits of control system capabilities. The minimum control energy is found by solving the following constrained optimization problem:

Find the $u(t)$ that minimizes the quadratic functional

$$J(\bar{u}(t_f)) = \frac{1}{2} \int_0^{t_f} \bar{u}^T(\tau) R \bar{u}(\tau) d\tau \quad (4)$$

where R is positive definite, subject to the linear differential constraint

$$\dot{\bar{x}} = A \bar{x} + B \bar{u}$$

where $\bar{x}(0) = \bar{0}$ and $\bar{x}_f = \bar{x}(t_f)$ are specified. Using the singular value decomposition of the controllability Gramian,

$$W_c(t) = \int_0^t \Phi(\tau) B B^T \Phi^T(\tau) d\tau \quad (5)$$

where $\Phi(t)$ is the state transition matrix, e^{At} , we calculate the unique set of n characteristic directions, defined above, in (R^n)

which describe system controllability quality.

Application of the Concept

To demonstrate one possible application of this quantitative controllability measure, consider a "controllability comparison" between two different aircraft. Presently, the qualitative determination that one aircraft is controllable while the other is not is the only relative measure of controllability performance. If the two aircraft are either both controllable or both uncontrollable, no information has been gained from which to decide any relative merit of either aircraft system. In such cases, we have no quantitative information as to which aircraft is "more controllable". A typical application of this new quantitative controllability measure, then, is to generate these quantitative results for different aircraft and compare them in order to deduce some general conclusions about relative controllability performance between the two aircraft-control system combinations. Rather than compare two totally different aircraft, this study considered the comparison of two different control systems installed on the same basic aircraft. Specifically, this was a preliminary evaluation of a new flight control system concept compared to a more conventional flight control system.

Control System Concept and Aircraft Selection

Most current aircraft flight control systems involve three separate sets of control surfaces, each set primarily producing moments about only a single axis of rotation of the aircraft. An alternative to this one-axis moment control surface is the all-flying horizontal tail which generates both rolling and pitching moments by using asymmetric and symmetric stabilizer deflections, respectively.

Logically, the simplest moment control system using such a multi-axis concept would be a single surface, or set of surfaces, which would provide moments about all three axes of rotation. The experimental control system tested in this study is an attempt to use such a system, and is configured as follows.

The new flight control surfaces are the wingtips (Figure 1), which act as conventional elevons to generate pitch and roll control, and are deflected individually to produce yawing moment. Two different forces produce yawing moments in this case: first, asymmetric drag of the single deflected tip; and second, side force of the deflected tip.

Using the moment equation

$$\bar{M}_z = \bar{R}_y \times \bar{F}_x + \bar{R}_x \times \bar{F}_y \quad (6)$$

Figure 1 shows the wingtip drag force, F_{D_x} , acting through a y-axis

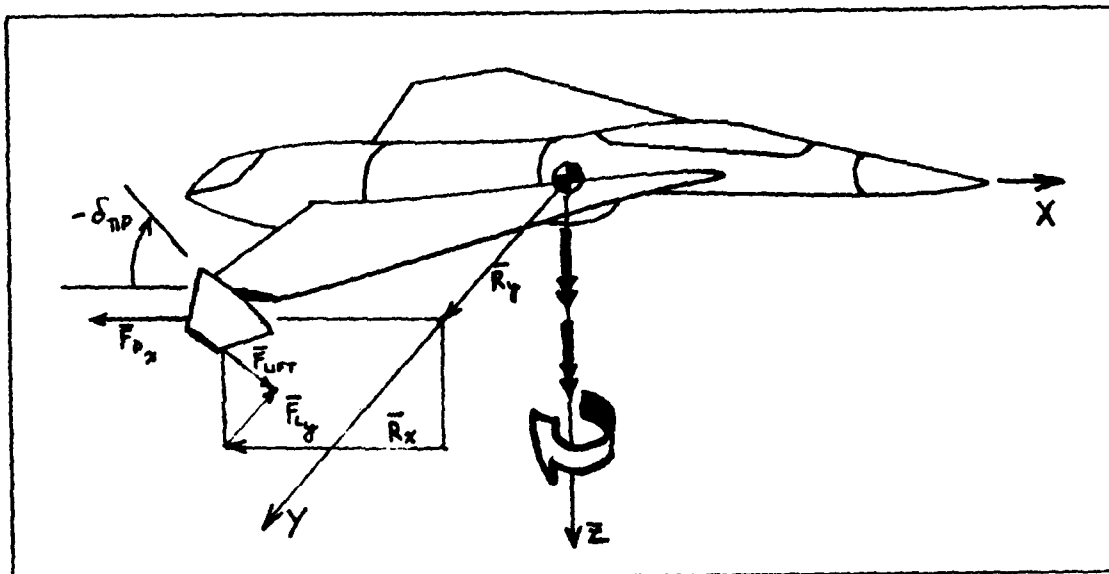


Figure 1. Yawing Moment Due to Individual Tip Deflection

moment arm, together with F_{Ly} , the side force component of the net wingtip lift force F_L , acting through an x-axis moment arm, combining to produce the resultant M_z yawing moment.

The aircraft chosen for this new control system is the Boeing Lightweight Experimental Supercruiser (LES) model 230-Y (Figures 2 and 3). There are two reasons for this choice. First, geometry data was available from Boeing for modeling the 230-Y with FLEXSTAB to calculate the necessary aerodynamic data. Second, as a contractor-funded design, the 230-Y represents a practical, physically realistic baseline control system against which to compare the new system.

Purpose

The purpose of this study was to both develop a quantitative measure of linear system controllability characteristics and to demonstrate this measure as the main tool in a preliminary evaluation of an unorthodox aircraft flight control system.

Goals

There are three separate goals of this study. The first goal is the theoretical development of this quantitative measure of linear system controllability. The second goal is the implementation of the software to calculate this quantitative measure. The third goal is the practical demonstration of this software by both using it to calculate the degree of controllability of three different aircraft/flight condition combinations, then using these results to make a preliminary evaluation of the particular flight control systems used on the experimental aircraft.

Assumptions

First, this study assumed a rigid aircraft ignoring the effect of

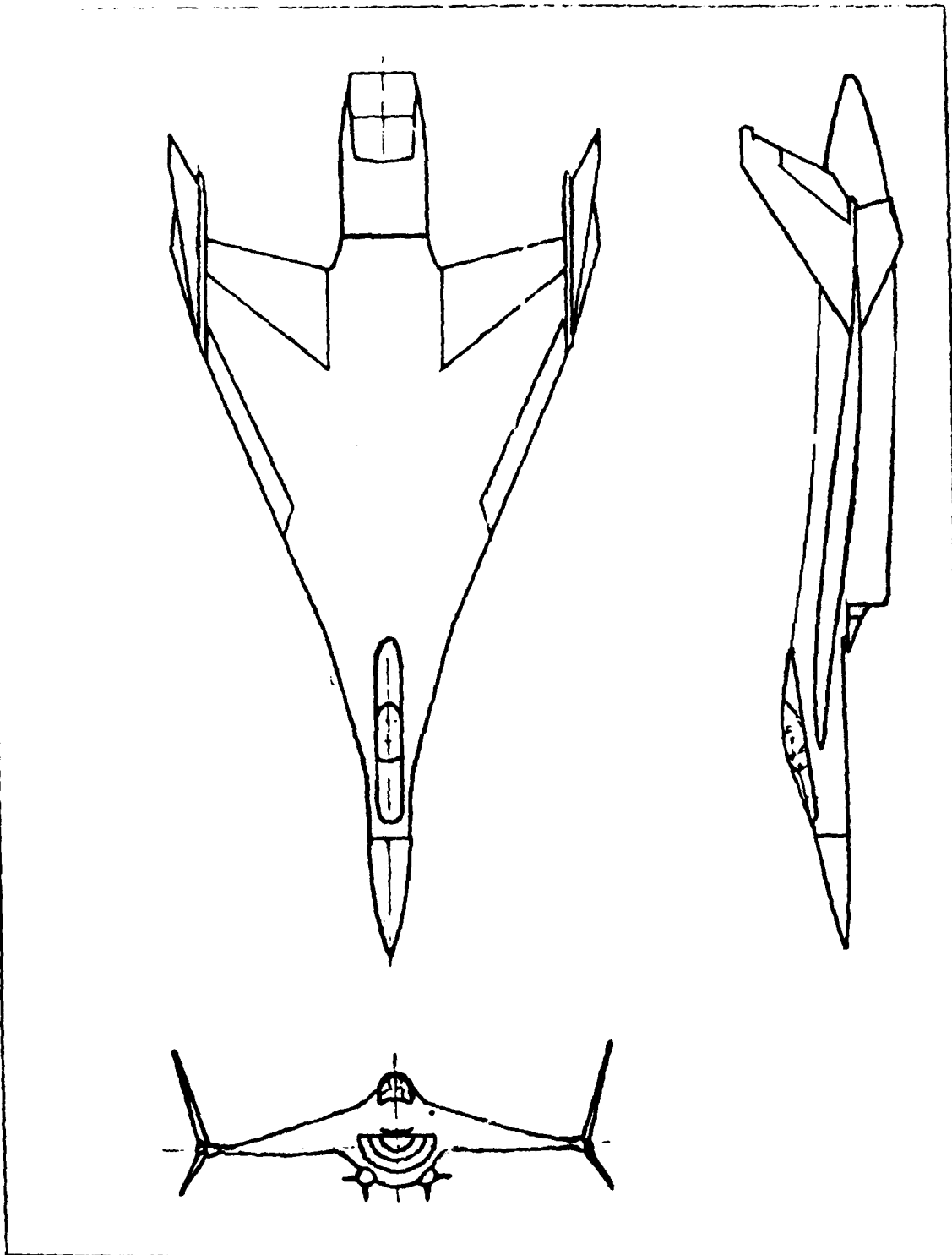


Figure 2. Baseline Boeing LES 230-Y

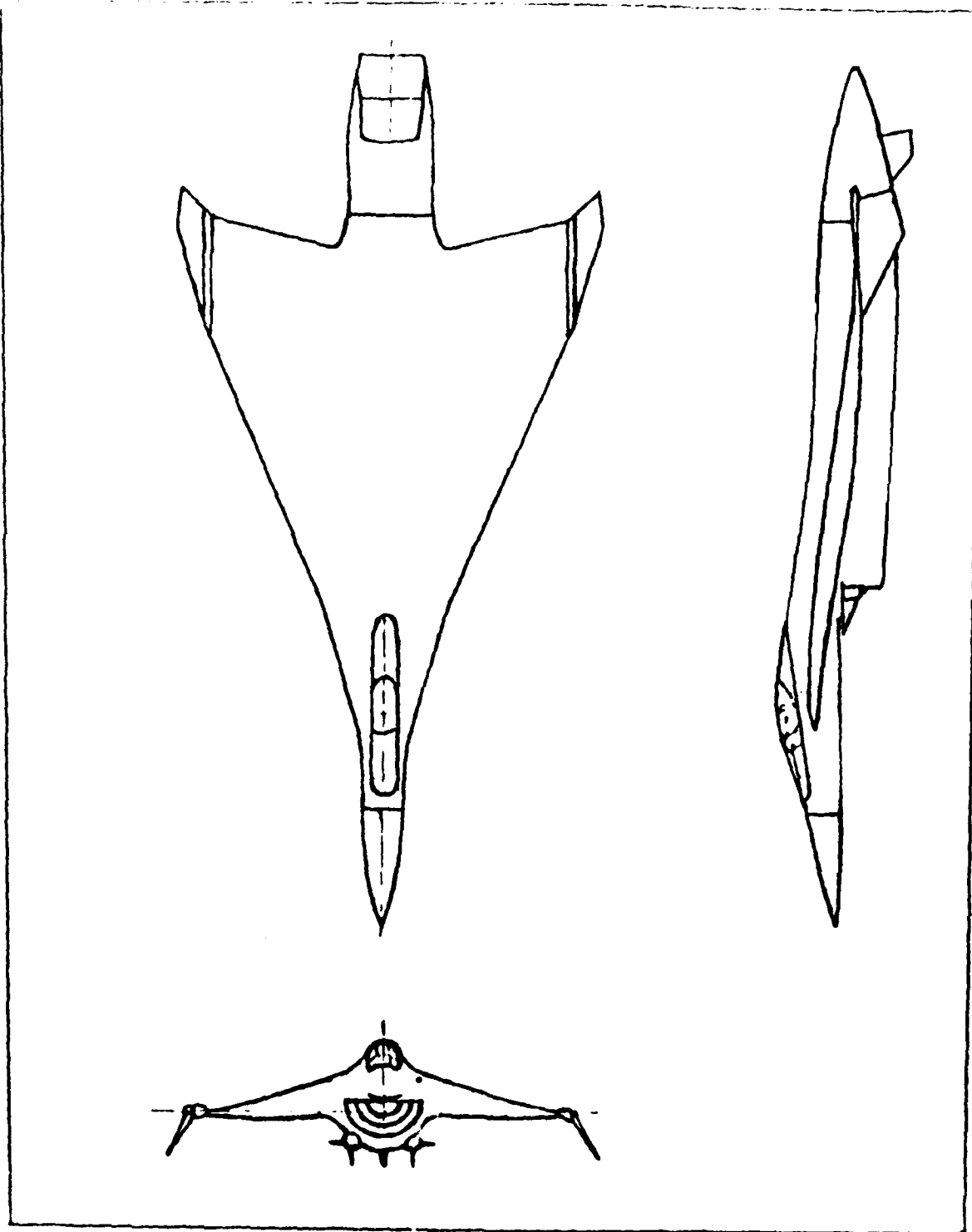


Figure 3. Boeing LES 230-Y With Experimental Control Surfaces

structural dynamics on the design of the control systems. The second restriction was to address only linear systems, which permits linearization of both dynamics and aerodynamics. The fairly unconventional aircraft configuration chosen for analysis reasonably precluded the use of the theoretical/empirical DATCOM methods developed from more orthodox configurations. Instead, the FLEXSTAB (References 1 and 2) digital computer program, based on linear aerodynamic theory, was used in this study. Although wind tunnel testing would provide the most accurate aerodynamic data, the linear modeling of aerodynamics should not significantly impair the accuracy of the results, since the study is limited to the same small perturbation region about some equilibrium.

Approach and Overview

The first step in the study was to use the FLEXSTAB program to estimate the aircraft stability and control characteristics. This data is presented and discussed in Chapter II.

The second step was to convert the stability and control derivatives from FLEXSTAB, using the linearized equations of motion, into the constant-coefficient matrices of the linear system state space representation. The results, along with a derivation of the linearized aircraft equations of motion, are given in Chapter III.

The third step was to quantitatively measure the degree of control capability of each linear system at the defined flight condition. Theoretical development of this quantitative measure is presented in Chapter IV. The results of the control system evaluation, in terms of this measure of controllability, are given in Chapter V. Chapter VI lists the conclusions and recommendations of this study.

11. Aerodynamic Data Generation

Basic Theory and Outputs

Aircraft flight characteristics were calculated using the FLEXSTAB computer program (References 1 and 2). FLEXSTAB uses an aerodynamic theory based on a first-order, linear, small-perturbation approximation to the unsteady, inviscid, irrotational, velocity potential equation:

$$\begin{aligned} a^2 \nabla^2 \Phi = & \frac{\partial^2}{\partial t^2} (\Phi - \Phi_\infty) + \frac{\partial}{\partial t} [(\nabla \Phi)^2 - (\nabla \Phi_\infty)^2] + \\ & + \frac{1}{2} \nabla \Phi \cdot \nabla (\nabla \Phi)^2 - \nabla (\Phi - \Phi_\infty) \cdot \frac{\partial}{\partial t} (\nabla \Phi_\infty), \end{aligned} \quad (7)$$

where a is the local speed of sound for both subsonic and supersonic flow. This partial differential equation has the physical boundary condition of zero normal velocity

$$\nabla \cdot \nabla \Phi = 0 \quad (8)$$

at $F(x,y,z,t) = 0$, the aircraft surface.

Details of this method are presented in Reference 1.

The net FLEXSTAB outputs are: (1) for a straight and level flight condition at the trim airspeed U_1 , with all other trim parameters and control surface deflections set to zero, the aerodynamic force derivatives are calculated; (2) these derivatives are used in linearized equilibrium equations to calculate the actual trim values for all the aircraft state and control variables; and (3) these trim values are finally used to calculate the stability and control derivatives for the trimmed reference flight condition.

Control Surface Definitions

FLEXSTAB assumes the aircraft to be symmetrical with respect to

the XZ plane, as in Figure 4, and only accepts control surfaces located either on the XZ plane or else located symmetrically with respect to the XZ plane. Also, control surface pairs not on the XZ plane must be deflected symmetrically, like elevators, or asymmetrically, like ailerons. The effect of a single surface deflection on either side of the XZ plane cannot be modeled. This FLEXSTAB restriction, then, reduces the experimental flight control system to a pair of wingtips acting as elevons, with no provision for rudder effects except for the coincidental lateral/directional effects of ordinary aileron deflections. For conventional control systems, the following sign convention for control deflections is adopted: down elevator, right aileron up, and left rudder deflections are taken as positive. For the experimental control system, wingtip deflections δ_{tipR} and δ_{tipL} are defined as positive for wingtip trailing edge down. Applying this convention to all three moment axes, wingtip deflections generate the same moments as the following conventional controls:

positive δ_{tipR} equivalent to positive δ_E , negative δ_A

positive δ_{tipL} equivalent to positive δ_E , positive δ_A

Using the following definitions for control surface deflections for the unconventional aircraft,

$$+\delta_E = \frac{1}{2}(\delta_{tipR} + \delta_{tipL}) \quad (9)$$

$$+\delta_A = \frac{1}{2}(-\delta_{tipR} + \delta_{tipL}) \quad (10)$$

$$+\delta_R = \frac{1}{2}(\delta_{tipR} - \delta_{tipL}) = -\delta_A \quad (11)$$

it is apparent that there is no "pure" rudder deflections possible. Any roll or yaw effects due to rudder are already contained in the

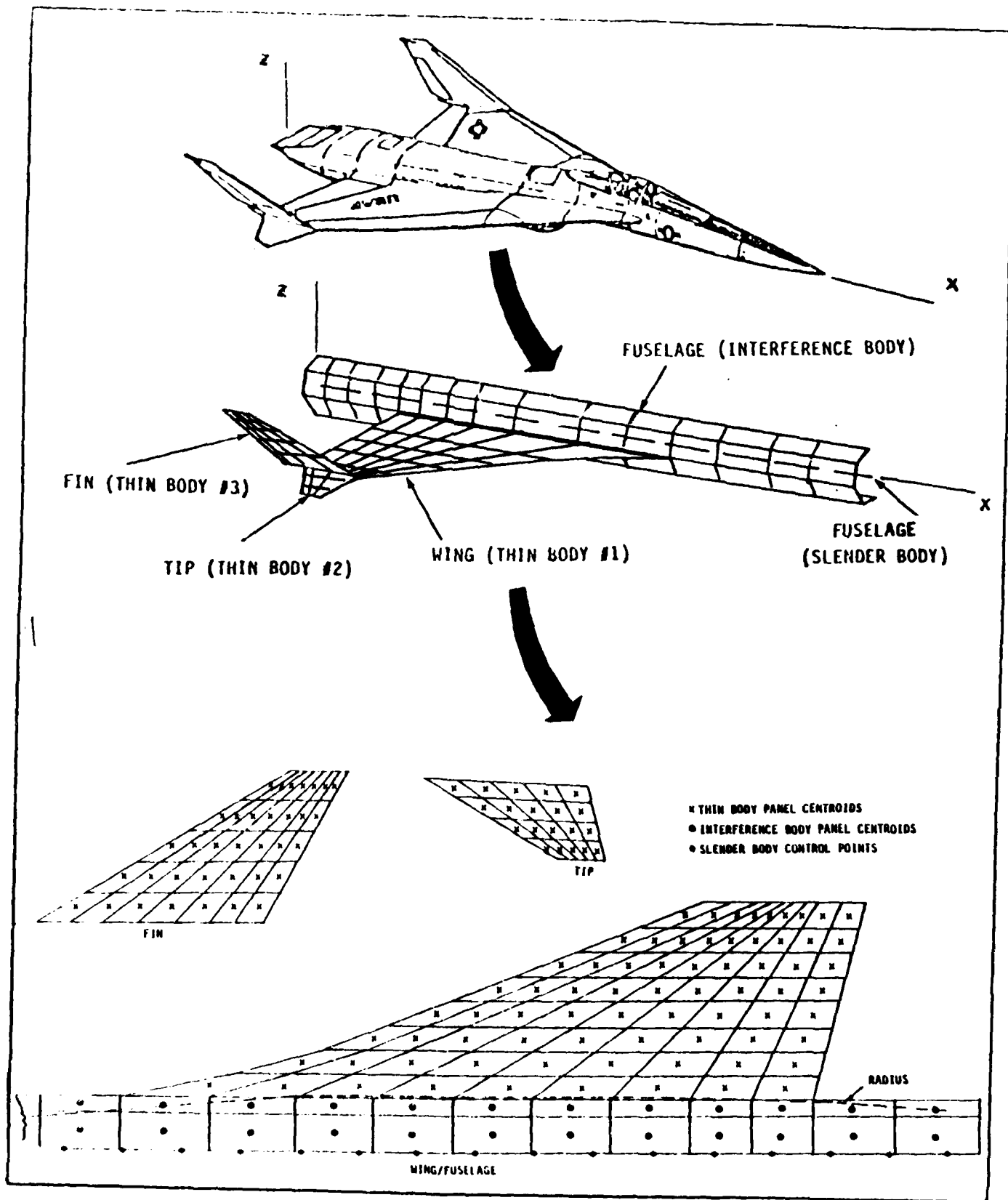


Figure 4. Aerodynamic Paneling Approximation

aileron derivatives, and any pitch effects due to rudder are already contained in the elevator derivatives.

Since some rudder surface must be defined in FLEXSTAB, a strake was included as an artificial rudder to allow FLEXSTAB to always successfully trim the experimentally-controlled aircraft, but all strake-related rudder control derivatives were discarded.

Discussion of Data

Tables A.I, A.II, and A.III show the respective FLEXSTAB-computed results for both the baseline and experimental LES 230-Y aircraft at the indicated flight condition. Comparing the two LES 230-Y models, the differences in several trim and stability parameters warrant explanation: (1) trim values for angle of attack, thrust, and elevator; and (2) static longitudinal stability, $C_{m_{\alpha}}$. The trim angle of attack difference is probably due to the baseline aircraft's wingtip-mounted vertical fins. They provide an endplate effect which generates a stronger lift distribution than for the fin-less experimental aircraft. The baseline aircraft can thus produce the same amount of lift at a smaller angle of attack. The baseline aircraft's larger trim thrust is also due to its vertical fins, which produce more drag (thereby requiring more thrust) than the fin-less experimental aircraft. This erroneously large disparity in trim thrusts is due to the inherent inability of FLEXSTAB linear theory to accurately predict drag data. Experimental wingtip trim deflection of 35° would certainly produce even more drag and require more trim thrust than would the baseline fins plus elevators trimmed at only 4° deflection.

The difference in trim elevator settings is due to the differences between the two types of elevator control surfaces. Table A.III shows

that the experimental elevons are far less effective, as measured by $C_{m\delta_E}$ and $C_{L\delta_E}$. The reasons for this include: (a) the experimental wingtip elevons are physically much smaller in surface area than the baseline trailing edge elevons, so can generate less change in net lift per degree of deflection; (b) the control surface center of pressure for the baseline elevons has a longer moment arm, with respect to the aircraft center of gravity, than for the experimental wingtip elevons, so the experimental surfaces produce less change in pitching moment for the same amount of change in net lift; (c) the extreme wingtip anhedral (60°) reduces by half the vertical component of the change in net lift used to generate changes in pitching moment. These three effects combine to severely limit the experimental wingtip elevons' pitch effectiveness. Since an aircraft would never be designed to fly with such large trim settings, a better preliminary design approach would be to modify the trailing edge camber of the wing (i.e., to "design in" more up-elevator) to allow a more reasonable trim elevator setting for the experimental aircraft. Also, more control power could be gained by increasing the physical size of the wingtip elevons.

The experimental aircraft is also statically unstable in pitch, as seen by a positive $C_{m\alpha}$ in Table A.III. Both LES models were balanced at the same percent mean aerodynamic chord, and in fact have the same identical wing geometry, M.A.C., and longitudinal location of M.A.C. FLEXSTAB output data shows that the trim neutral point was slightly behind the CG for the baseline aircraft (stable), and was slightly ahead of the CG (unstable) for the experimental aircraft. This

neutral point shift between identically-winged aircraft is also due to the presence of vertical fins. Since this study was not directed toward aircraft design, these results were left as is, and the analysis continued after noting the problems discussed above.

The stability and control derivative data of Table A.III is now converted to the linear state space representation of aircraft perturbation motion by the conversion process described in the next chapter.

III. Data Conversion to State Space Representation

Converting FLEXSTAB-generated stability and control derivatives into the linear state space representation for the various aircraft-flight condition combinations begins with the six nonlinear differential equations of motion and the two kinematic relationships:

$$m(\dot{U} - VR + WQ) = -mg_0 \sin \Theta + F_{Ax} + F_{Tx} \quad (12)$$

$$m(\dot{V} + UR - WP) = mg_0 \sin \Phi \cos \Theta + F_{Ay} + F_{Ty} \quad (13)$$

$$m(\dot{W} - UQ + VP) = mg_0 \cos \Phi \cos \Theta + F_{Az} + F_{Tz} \quad (14)$$

$$I_{xx} \dot{P} - I_{xz}(\dot{R} + PQ) + (I_{zz} - I_{yy})RQ = L_A + L_T \quad (15)$$

$$I_{yy} \dot{Q} + (I_{xx} - I_{zz})PR + I_{xz}(P^2 - R^2) = M_A + M_T \quad (16)$$

$$I_{zz} \dot{R} - I_{xz} \dot{P} + (I_{yy} - I_{xx})PQ + I_{xz}QR = N_A + N_T \quad (17)$$

$$\dot{\Phi} = P + Q \sin \Phi \tan \Theta + R \cos \Phi \tan \Theta \quad (18)$$

$$\dot{\Theta} = Q \cos \Phi - R \sin \Phi \quad (19)$$

The first step is to form the perturbed state equations of motion with respect to steady state flight. Steady state flight implies (14:2.25) that all motion variables remain constant. The perturbation substitution (for each force and moment component and for all the motion variables) expresses the instantaneous value of each variable as the sum of the equilibrium value (i.e., trim value) denoted by the subscript ()₁, plus the perturbation away from the equilibrium value (denoted by the small case symbol). Table I shows the complete list of perturbation substitutions for all parameters involved.

The second step is to apply the two fundamental linearity restrictions on the magnitude of all perturbations: (1) the small angle

Table I
Perturbation Substitutions

$$X = X_1 + x$$

$$\left(\begin{array}{l} \text{total} \\ \text{value} \end{array} \right) = \left(\begin{array}{l} \text{steady} \\ \text{state} \\ \text{value} \end{array} \right) + \left(\begin{array}{l} \text{perturbation} \\ \text{value} \end{array} \right)$$

subscript ()_A - aerodynamic force or moment

subscript ()_T - thrust force or moment

$$U = U_1 + u$$

$$V = V_1 + v$$

$$W = W_1 + w$$

$$P = P_1 + p$$

$$Q = Q_1 + q$$

$$R = R_1 + r$$

$$\theta = \theta_1 + \phi$$

$$\dot{\theta} = \dot{\theta}_1 + \dot{\phi}$$

$$F_{A_x} = F_{A_{x1}} + f_{A_x}$$

$$F_{T_x} = F_{T_{x1}} + f_{T_x}$$

$$F_{A_y} = F_{A_{y1}} + f_{A_y}$$

$$F_{T_y} = F_{T_{y1}} + f_{T_y}$$

$$F_{A_z} = F_{A_{z1}} + f_{A_z}$$

$$F_{T_z} = F_{T_{z1}} + f_{T_z}$$

$$L = L_{A_1} + l_A$$

$$L_T = L_{T_1} + l_T$$

$$M = M_{A_1} + m_A$$

$$M_T = M_{T_1} + m_T$$

$$N = N_{A_1} + n_A$$

$$N_T = N_{T_1} + n_T$$

approximation

$$\cos \theta \approx 1.0, \quad \theta \approx \sin \theta \approx \tan \theta \quad (20)$$

(2) all perturbation magnitudes are small enough that any produce or cross-product of perturbations is negligible with respect to the perturbations themselves. Removing the equilibrium terms and neglecting all nonlinear perturbation terms produces the following linearized equations of perturbed motion in stability axes:

$$(\dot{u} - V_1 r - R_1 v + W_1 \delta + Q_1 w) = -g_0 \theta \cos \Phi_1 + \frac{\bar{g}_1 \bar{s}}{M} \left[\left\{ -(C_{D_u} + 2C_{D_z}) \right\} \frac{u}{U_1} + (C_{L_z} - C_{D_x}) \alpha - (C_{D_z} \frac{\bar{c}}{2U_1}) \dot{\alpha} - (C_{D_z} \frac{\bar{c}}{2U_1}) \delta - C_{D_{\delta}} \delta \right] \quad (21)$$

$$(\dot{v} + U_1 r + R_1 u - W_1 p - P_1 w) = -g_0 \theta \sin \Phi_1 \sin \Theta_1 + g_0 \phi \cos \Phi_1 \cos \Theta_1 + \frac{\bar{g}_1 \bar{s}}{M} \left[C_{Y_p} \beta + (C_{Y_p} \frac{b}{2U_1}) \dot{\beta} + (C_{Y_p} \frac{b}{2U_1}) p + (C_{Y_r} \frac{b}{2U_1}) r + C_{Y_{\delta_A}} \delta_A + C_{Y_{\delta_R}} \delta_R \right] \quad (22)$$

$$(\dot{w} - U_1 \delta - Q_1 u + V_1 p + P_1 v) = -g_0 \theta \cos \Phi_1 \sin \Theta_1 - g_0 \phi \sin \Phi_1 \cos \Theta_1 + \frac{\bar{g}_1 \bar{s}}{M} \left[\left\{ -(C_{L_u} + 2C_{L_z}) \right\} \frac{u}{U_1} - (C_{L_z} + C_{D_z}) \alpha - (C_{L_z} \frac{\bar{c}}{2U_1}) \dot{\alpha} - (C_{L_z} \frac{\bar{c}}{2U_1}) \delta - C_{L_{\delta}} \delta \right] \quad (23)$$

$$I_{xx} \dot{p} - I_{xz} \dot{r} - I_{xz} (P_1 \delta + Q_1 r) + (I_{zz} - I_{yy}) (R_1 \delta + Q_1 v) = \bar{g}_1 \bar{s} b \left[C_{L_p} \beta + (C_{L_p} \frac{b}{2U_1}) \dot{\beta} + (C_{L_p} \frac{b}{2U_1}) p + (C_{L_r} \frac{b}{2U_1}) r + C_{L_{\delta_A}} \delta_A + C_{L_{\delta_R}} \delta_R \right] \quad (24)$$

$$I_{yy} \dot{\delta} + (I_{xx} - I_{zz}) (P_1 r + R_1 p) + 2I_{xz} (P_1 p - R_1 v) = \bar{g}_1 \bar{s} \bar{c} \left[\left\{ (C_{m_u} + 2C_{m_z}) \right\} \frac{u}{U_1} + (C_{m_z} + C_{m_{r_z}}) \alpha + (C_{m_z} \frac{\bar{c}}{2U_1}) \dot{\alpha} + (C_{m_z} \frac{\bar{c}}{2U_1}) \delta + C_{m_{\delta}} \delta \right] \quad (25)$$

$$I_{zz} \dot{r} - I_{xz} \dot{p} + (I_{yy} - I_{xx}) (P_1 \delta + Q_1 r) + I_{xz} (Q_1 v + R_1 \delta) = \bar{g}_1 \bar{s} b \left[(C_{n_p} + C_{n_{r_p}}) \beta + (C_{n_p} \frac{b}{2U_1}) \dot{\beta} + (C_{n_p} \frac{b}{2U_1}) p + (C_{n_r} \frac{b}{2U_1}) r + C_{n_{\delta_A}} \delta_A + C_{n_{\delta_R}} \delta_R \right] \quad (26)$$

$$\dot{\theta} = g \cos \Phi_1 - r \sin \Phi_1 - (\omega_1 \sin \Phi_1 + R \cos \Phi_1) \phi \quad (27)$$

$$\begin{aligned} \dot{\phi} = & \varphi + \tan \Theta_1 (g \sin \Phi_1 + r \cos \Phi_1 + (Q_1 \cos \Phi_1 - R_1 \sin \Phi_1) \phi) + \\ & + (\omega_1 \sin \Phi_1 + R_1 \cos \Phi_1) \Theta \sec^2 \Theta_1 \end{aligned} \quad (28)$$

$$\dot{h} = (-U_1 \cos \alpha_1) \alpha + (U_1 \cos \alpha_2) \Theta \quad (29)$$

The third step is to substitute the FLEXSTAB-generated stability and control derivatives into these linearized equations of perturbed motion (21) - (29) as the constant coefficients of the motion and control variables

$$\bar{x}_{LONG} = (u, \alpha, \beta, \Theta, h)^T, \quad \bar{x}_{LAT} = (\beta, \phi, p, r)^T \quad (30)$$

$$\bar{u}_{LONG} = (\delta_E, \delta_T)^T, \quad \bar{u}_{LAT} = (\delta_A, \delta_R)^T \quad (31)$$

Solving this system for the time derivatives of the state variables \bar{x} yields the state space representation of the aircraft perturbation motion with respect to steady state conditions:

$$\dot{\bar{x}} = A\bar{x} + B\bar{u} \quad (32)$$

where the coefficient matrices A and B are made up of combinations of the constant coefficients from the original motion and kinematic equations.

Tables II and III show the resulting A and B matrices calculated for both LES 230-Y models tested, for both the longitudinal and lateral/directional modes. These A and B matrix pairs define the physical differential constraint equation of the optimal control problem discussed in the next chapter. All longitudinal and lateral/directional mode eigenvalues of both aircraft A matrices are included in Table IV.

Table II Baseline Boeing LES 230-Y State Space Matrices

$$\dot{\bar{x}} = A\bar{x} + B\bar{u}$$

A_{LONG}					B_{LONG}				
-0.020197	-0.34862	-0.44982	-0.56124	0.0	-0.1944	32.174			
-0.012762	-0.36777	0.99185	-0.0013325	0.0	-0.1877	0.0			
-0.054589	-1.4697	-0.46440	0.0001436	0.0	-11.232	0.0			
0.0	0.0	1.0	0.0	0.0	0.0	0.0			
0.0	-13.596	0.0	13.596	0.0	0.0	0.0			
A_{LAT}					B_{LAT}				
-0.099551	0.041246	0.031718	-0.99644		-0.0017	-0.0421			
0.0	0.0	1.0	0.032350		0.0	0.0			
-8.9937	0.0005783	-0.82049	0.50340		-40.578	-8.4278			
5.0474	-0.0000707	0.0029823	-0.23643		-2.8473	4.045			

$$x_{LONG} = [u \text{ (FT/SEC)}, \alpha \text{ (DEG)}, q \text{ (DEG/SEC)}, \dot{\alpha} \text{ (DEG)}, h \text{ (FT)}]^T$$

$$x_{LAT} = [\dot{\psi} \text{ (DEG)}, \phi \text{ (DEG)}, p \text{ (DEG/SEC)}, r \text{ (DEG/SEC)}]^T$$

$$u_{LONG} = [\dot{\xi}_e \text{ (DEG)}, \dot{\xi}_r \text{ (% aircraft weight)}]^T$$

$$u_{LAT} = [\dot{\xi}_A \text{ (DEG)}, \dot{\xi}_\lambda \text{ (DEG)}]^T$$

Table III Experimental LES 230-Y State Space Matrices

$$\dot{\bar{x}} = A\bar{x} + B\bar{u}$$

	A_{LONG}				B_{LONG}	
$x_{LONG} = [u \text{ (FT/SEC)}, \alpha \text{ (DEG)}, q \text{ (DEG/SEC)}, \theta \text{ (DEG)}, h \text{ (FT)}]^T$	-0.01212	-0.32661	-0.51092	-0.56116	0.0	0.0
$x_{LAT} = [\beta \text{ (DEG)}, \phi \text{ (DEG)}, p \text{ (DEG/SEC)}, r \text{ (DEG/SEC)}]^T$	-0.013089	-0.32100	0.99170	-0.0015140	0.0	0.0
$u_{LONG} = [\delta_{\eta_R} \text{ (DEG)}, \delta_{\eta_L} \text{ (DEG)}, \delta_r \text{ (% aircraft weight)}]^T$	-0.054978	1.8317	-0.44702	0.00022572	0.0	0.0
$u_{LAT} = [\delta_{\eta_R} \text{ (DEG)}, \delta_{\eta_L} \text{ (DEG)}]^T$	0.0	0.0	1.0	0.0	0.0	0.0
	0.0	-13.596	0.0	13.596	0.0	0.0
	A_{LAT}				B_{LAT}	
	-0.023925	0.041239	0.037091	-0.99910	-0.0075	0.0075
	0.0	0.0	1.0	0.036797	0.0	0.0
	7.8557	0.00019884	-0.60578	0.20727	5.4375	-5.4375
	-0.62152	-0.00030922	-0.66696	-0.011022	0.9353	-0.9353

Table IV
Eigenvalues of Aircraft A Matrices

AIRCRAFT	LONGITUDINAL EIGENVALUES	LATERAL-DIRECTIONAL EIGENVALUES
Baseline	0.0	
LES	-0.016	.005526
	0.0289	-0.1602 \pm j 2.307
	-0.4326 \pm j 1.2	-0.8415
Experimental	1.01	
LES	-.02829 \pm j .1118	1.119
	0.0	-.88 \pm j 0.5634
	-1.733	.0006578

IV. Control System Analysis

The flight control systems are now evaluated quantitatively by their ability to maneuver the aircraft from the reference flight condition to a specified final flight condition differing from the reference by small perturbations in the motion variables \bar{x} of equation (32). For a given reference flight condition, equation (32) models the physical changes in aircraft motion \bar{x} caused by control deflections \bar{u} , when the instantaneous flight condition is sufficiently close to the reference condition characterized by equation (32). The quantitative measure developed in this study is discussed in the optimal control technique described below

Basic Theory

The problem is to select the optimal control time history, $u(t)$, which minimizes the functional performance index

$$J(\bar{u}(t)) = \frac{1}{2} \int_0^{t_f} \bar{u}^T(t) R \bar{u}(t) dt \quad (33)$$

where R is a positive definite matrix, and where t_f is specified and both $\bar{x}(t)$ and $\bar{u}(t)$ are subject to the constraint equation,

$$\dot{\bar{x}} = A\bar{x} + B\bar{u}, \quad (34)$$

and $\bar{x}(t_0) = \bar{x}_0 = \bar{0}$ and $\bar{x}(t_f) = \bar{x}_f$ are specified. Since $\bar{x}(t)$ can be expressed as

$$\bar{x}(t) = \Phi(t)x_0 + \int_0^t \Phi(t-\tau)B\bar{u}(\tau)d\tau, \quad (35)$$

the state variables' time history, $\bar{x}(t)$, is dependent on the control variables' time history, $\bar{u}(t)$. We can treat them as independent, for

the purpose of generating the first necessary condition for optimality, by introducing n Lagrange multipliers $\bar{\lambda}$ to form the augmented performance index

$$J_A(\bar{u}(t)) = \frac{1}{2} \int_0^{t_f} \bar{u}^T(\tau) R \bar{u}(\tau) d\tau + \bar{\lambda}^T \left\{ \int_0^{t_f} \Phi(t_f - \tau) B \bar{u}(\tau) d\tau - \bar{x}_f \right\} \quad (36)$$

Since the constraint is introduced involving the constant vector \bar{x}_f , $\bar{\lambda}$ is also a constant vector. Combining the separate integrands of equation (76) yields

$$J_A(\bar{u}(t)) = \frac{1}{2} \int_0^{t_f} (\bar{u}^T(\tau) R \bar{u}(\tau) + \bar{\lambda}^T \Phi(t_f - \tau) B \bar{u}(\tau)) d\tau - \bar{\lambda}^T \bar{x}_f \quad (37)$$

Defining the Hamiltonian function as

$$\mathcal{H}(\bar{u}(\tau), \bar{\lambda}) = \frac{1}{2} \bar{u}^T(\tau) R \bar{u}(\tau) + \bar{\lambda}^T \Phi(t_f - \tau) B \bar{u}(\tau) \quad (38)$$

we now express the augmented performance index as

$$J_A(\bar{u}(t)) = \int_0^{t_f} \mathcal{H}(\bar{u}(\tau), \bar{\lambda}) d\tau - \bar{\lambda}^T \bar{x}_f \quad (39)$$

The superscript $(*)$ is hereafter used to denote quantities evaluated at the optimal condition, i.e., at the minimum value of $J_A(\bar{u}(t))$.

Examining a non-optimal, neighboring control $\bar{u}(t)$, lying close to the optimal $\bar{u}^*(t)$, but differing from the optimum by a variation $\delta \bar{u}(t)$,

$$\bar{u}(t) = \bar{u}^*(t) + \delta \bar{u}(t) = \bar{u}^*(t) + \epsilon \bar{\eta}(t) \quad (40)$$

where $|\epsilon|$ is a small number. Note that $\bar{\eta}(t)$ may be chosen arbitrarily.

Note also that both the initial and final conditions $\bar{x}_0 = \bar{0}$ and $\bar{x}(t_f) = \bar{x}_f$ are always optimal, since they are located on the optimum trajectory $\bar{x}^*(t)$ connecting \bar{x}_0 and \bar{x}_f . From the calculus of

variations, any value of $J_A(\bar{u})$, where $\bar{u} \neq \bar{u}^*$, must be greater than or equal to the optimum (minimum) $J_A(\bar{u}^*)$. The necessary conditions for optimality of $\bar{u}^*(t)$ are found by expanding $J_A(\bar{u})$ in a Taylor series expansion about the optimum $J_A(\bar{u}^*)$,

$$J_A(\bar{u}) = \int_0^{t_f} \mathcal{H}[(\bar{u}^* + \epsilon \bar{\eta}), \bar{\lambda}] d\tau - \bar{\lambda}^T \bar{x}_f \quad (41)$$

Expanding further, we have

$$J_A(\bar{u}) = \underbrace{\int_0^{t_f} (\mathcal{H}[\bar{u}^*, \bar{\lambda}] + \frac{\partial \mathcal{H}}{\partial \bar{u}} \bigg|_{*} \epsilon \bar{\eta}(\tau)) d\tau}_{- \bar{\lambda}^T \bar{x}_f} + \theta(\epsilon^2) \quad (42)$$

The underlined terms are just $J_A(\bar{u}^*)$, and the ϵ is factored out to give

$$J_A(\bar{u}) = J_A(\bar{u}^*) + \epsilon \left\{ \int_0^{t_f} \left[\frac{\partial \mathcal{H}}{\partial \bar{u}} \bigg|_{*} \bar{\eta}(\tau) \right] d\tau \right\} + \theta(\epsilon^2) \quad (43)$$

Since ϵ can be chosen arbitrarily small, all terms of order ϵ^2 and higher can be made negligibly small with respect to the ϵ -term. Also, since ϵ can be chosen to be either positive or negative, the only way $J_A(\bar{u})$ can always be greater than or equal to $J_A(\bar{u}^*)$, for all permissible ϵ and $\bar{\eta}(t)$, is to require that the coefficient of the ϵ -term in equation (43) always be zero. This necessary condition for $\bar{u}^*(t)$ to be the optimal control is then

$$\int_0^{t_f} \frac{\partial \mathcal{H}}{\partial \bar{u}} \bigg|_{*}^T \bar{\eta}(\tau) d\tau = 0 \quad (44)$$

Applying the fundamental Lemma of the calculus of variations, the necessary condition for optimality becomes

$$\frac{\partial \mathcal{H}}{\partial \bar{u}} \bigg|_{*} = (R\bar{u} + B^T \Phi^T(t_f - \tau) \bar{\lambda}) \bigg|_{*} = 0, \text{ or} \quad (45)$$

$$\bar{u}^*(\tau) = -R^{-1} B^T \Phi^T(t_f - \tau) \bar{\lambda} \quad (46)$$

Substituting equation (46) for $\bar{u}(t)$ into equation (35) gives

$$\bar{x}(t_f) = - \left[\int_0^{t_f} \Phi(t_f - \tau) B R^{-1} B^T \Phi^T(t_f - \tau) d\tau \right] \bar{\lambda} = \bar{x}_f \quad (47)$$

By changing the dummy variable of integration from τ to $(t_f - \tau)$, the integral in equation (47) becomes

$$\int_0^{t_f} \Phi(\tau) B R^{-1} B^T \Phi^T(\tau) d\tau$$

Expressing the combination $BR^{-1}B^T$ as $B_R B_R^T$, where

$$B_R = BR^{-\frac{1}{2}} \quad , \quad (48)$$

the integral becomes

$$\int_0^{t_f} \Phi(\tau) B_R B_R^T \Phi^T(\tau) d\tau$$

This integral-matrix expression is defined in the literature (8:402) as the symmetric $(n \times n)$ controllability Gramian, $W_c(t_f)$. For both $t_0 = 0$ and $t = t_f$ specified in this optimization problem, the bracketed integral in equation (47) becomes $W_c(t_f)$. Substituting this form for the integral, equation (47) becomes

$$\bar{x}(t_f) = -W_c(t_f) \bar{\lambda} \quad (49)$$

and equation (46) becomes

$$\bar{u}^*(\tau) = R^{-1} B^T \Phi^T(t_f - \tau) W_c^{-1}(t_f) \bar{x}(t_f) \quad (50)$$

Substituting this expression for $\bar{u}(t)$ into equation (33) gives

$$J(\bar{u}(t)) = \frac{1}{2} \int_0^{t_f} \bar{x}^T(t_f) W_c^{-1}(t_f) \Phi(t_f - \tau) B R^{-1} B^T \Phi^T(t_f - \tau) W_c^{-1}(t_f) \bar{x}(t_f) d\tau \quad (51)$$

All factors involving $\bar{x}(t_f)$ and $W_c(t_f)$, are invariant over the interval of integration, and may be factored out of the integrand to give

$$J(\bar{u}(t)) = \frac{1}{2} \bar{x}^T(t_f) W_c^{-1}(t_f) \left\{ \int_0^{t_f} \bar{\Phi}(t_f, \tau) B R^{-1} B^T \bar{\Phi}^T(t_f, \tau) d\tau \right\} W_c^{-1}(t_f) \bar{x}(t_f) \quad (52)$$

The integral in this equation is $W_c(t_f)$, so

$$J(\bar{u}(t)) = \frac{1}{2} \bar{x}_f^T W_c^{-1}(t_f) \bar{x}_f \quad (53)$$

Since W_c is a symmetric matrix, the optimal cost functional is

$$J(\bar{u}^*(t)) = \frac{1}{2} \bar{x}_f^T W_c^{-1}(t_f) \bar{x}_f \quad (54)$$

The controllability Gramian can be decomposed into

$$W_c(t_f) = P_W \Sigma_W P_W^T \quad (55)$$

where

$$\Sigma_W = \begin{bmatrix} \lambda_1 & & \phi \\ & \ddots & \\ \phi & & \lambda_n \end{bmatrix}$$

is a diagonal matrix of eigenvalues of $W_c(t_f)$, and $P_W = \begin{bmatrix} \bar{v}_1 & \vdots & \bar{v}_n \end{bmatrix}$

is an orthogonal matrix of column vectors which are the eigenvectors of $W_c(t_f)$. Because $W_c(t_f)$ is symmetric, the eigenvalues and eigenvectors are the same as the singular values and singular vectors, respectively. Substituting (55) into (54) gives

$$\begin{aligned} J(\bar{u}^*(t)) &= \frac{1}{2} \bar{x}_f^T P_W \Sigma_W^{-1} P_W^T \bar{x}_f = \\ &= \frac{1}{2} (\bar{x}_f^T P_W) \Sigma_W^{-1} (P_W^T \bar{x}_f)^T \end{aligned} \quad (56)$$

The quantity $(\bar{x}_f^T P_W)$ is expanded to give

$$\bar{x}_f^T W = x_f^T \begin{bmatrix} \bar{v}_1 & \dots & \bar{v}_n \end{bmatrix} = \begin{bmatrix} (\bar{x}_f^T, \bar{v}_1) & \dots & (\bar{x}_f^T, \bar{v}_n) \end{bmatrix} \quad (57)$$

which is a row vector of scalars, $[c_1, c_2, \dots, c_n]$, where c_i is the inner (scalar) product between \bar{x}_f and \bar{v}_i , i.e. c_i is the projection of \bar{x}_f along the eigenvector \bar{v}_i of $W_c(t_f)$.

$$c_i = (\bar{x}_f, \bar{v}_i) \quad (58)$$

Substituting this result into equation (56) gives

$$J(\bar{u}^*(t)) = \frac{1}{2} [c_1, \dots, c_n] \Sigma^{-1} \begin{bmatrix} c_1 \\ \vdots \\ c_n \end{bmatrix} = \frac{1}{2} \sum_{i=1}^n \frac{c_i^2}{\lambda_i} \quad (59)$$

This is a weighted sum of squares (c_i^2) of the components of \bar{x}_f along each of the eigenvectors \bar{v}_i . The individual weights ($1/\lambda_i$), as reciprocals of the eigenvalues λ_i of $W_c(t_f)$, are now ordered in ascending order; i.e., where λ_1 is the largest eigenvalue from the singular value decomposition of $W_c(t_f)$, so $(1/\lambda_1)$ is now the smallest weighting.

The final conclusion from this form of the cost functional is that an \bar{x}_f , of fixed magnitude, selected along each of the "ranked" eigenvector directions \bar{v}_i , will give (in ascending order) cost values $J_1(\bar{u}^*)$, the control energy required to reach \bar{x}_f . That is, if \bar{x}_f is a unit vector along \bar{v}_1 , then the control cost to reach \bar{x}_f will be just $1/\lambda_1$. If \bar{x}_f is a unit vector along \bar{v}_2 , then the control cost to reach \bar{x}_f will be just $1/\lambda_2 > 1/\lambda_1$. Also, if \bar{x}_f is along \bar{v}_n , the control cost to reach \bar{x}_f will be $1/\lambda_n > 1/\lambda_1, i = 1, 2, \dots, (n-1)$. This characteristic is the desired measure of relative controllability quality throughout the entire state space. That is, since all

$\bar{v}_1 \perp \bar{v}_j$, the eigenvector set will completely span the state space (R^n), and therefore forms a set of basis vectors for the state space. Also, since the controllability Gramian is time-varying, the ranked eigenvector-basis vector set is also time-varying. This implies the importance of obtaining time histories of the $\bar{v}_i(t)$ vectors over some finite time interval of interest.

Software Implementation

This controllability quality measure, derived from the controllability Gramian, has been successfully implemented in the computer program GRAMOP, whose output includes two sets of plots (and print):

- 1) a set of n "traits" plots, plus a cost history plot;
- 2) a set of state trajectory and optimal control history plots

for each user-defined final time t_f and final state $\bar{x}(t_f)$.

The i^{th} trait plot (e.g., figure B1) shows the history, versus final time, of the i^{th} -ranked (i^{th} -smallest amount of control energy required) response direction $\bar{v}_i(t_f)$ in state space. Recall from the above that $\bar{v}_i(t_f)$ is one of the n mutually orthogonal, time-varying eigenvector/basis vector directions spanning (R^n), and that $\bar{v}_i(t_f)$ is just the i^{th} eigenvector of the controllability Gramian $W_c(t_f)$. The cost history plot shows the relative control costs needed to reach each one of these n ranked directions in state space.

The control and state trajectory history plots show, respectively:

- (1) the optimal control history $\bar{u}^*(t)$ that drives the system from zero initial state to the user-defined final state, using minimum control energy and
- (2) the corresponding state trajectory history $\bar{x}(t)$ along which the system travels. Chapter V presents the GRAMOP results for the two aircraft studied.

V. Results

For this study, two separate aircraft/flight condition combinations were analyzed:

- 1) LES 230-Y - Mach 0.8, 35,000 ft, steady level cruise
- 2) Modified LES 230-Y - Mach 0.8, 35,000 ft, steady level cruise

The two LES aircraft were modeled using the FLEXSTAB aerodynamic paneling program to generate stability and control derivatives for the indicated flight conditions. These derivatives were used to produce a state space system of equations for each aircraft/flight condition combination. These systems of equations were used as the constraint equation (34) in the GRAMOP program in order to calculate and plot the basic longitudinal and lateral/directional controllability characteristics of each aircraft when flying at the indicated flight conditions. These state and control history plots are best interpreted by first noting the vertical axis scaling of each separate plot variable. This scaling clearly indicates which variables are dominant, in terms of relative magnitude, in each response vector time history. Each test case is discussed in detail.

Aircraft Traits

1) LES 230-Y Longitudinal Case

This Boeing-designed aircraft has wing trailing edge elevons and rudders on the wingtip-mounted vertical fins, as shown in Figure 2. This aircraft is used as the baseline for the modified LES, to explore changes within a single aircraft design.

a) Direction 1 (Figure B1)

For the baseline LES, this easiest-to-control response is a combination

of pitch rate, pitch angle, and angle of attack up until about 2 seconds, when it becomes almost entirely an altitude change, with some minor velocity change, for times beyond 2 seconds. Sample state and control trajectories at 1.5 seconds (Figures B2 and B3) show very small throttle and elevator requirements to drive the aircraft along this direction. This is consistent with a fighter aircraft designed for high maneuverability.

b) Direction 2 (Figure B4)

This response begins as mostly negative velocity, angle of attack, and pitch angle, but quickly (1.0 seconds) inverts to a combination of velocity change with opposite pitch angle and opposite angle of attack.

c) Direction 3 (Figure B5)

This response exhibits several changes in behavior, beginning as mostly pitch angle and angle of attack, then (around 1.3 seconds) changes to predominantly altitude until about 3 seconds, when it becomes mostly pitch rate.

d) Direction 4 (Figure B6)

This vector begins as mostly altitude, quickly (at 1 second) changes to mostly velocity, with a minor and fairly equal-magnitude combination of pitch angle, pitch rate, and angle of attack.

e) Direction 5 (Figure B7)

The most difficult response vector remains mostly a combination of angle of attack and opposite pitch angle through the final time interval tested. The altitude component dies out very rapidly (at about 0.5 sec.) while the opposite pitch angle component grows rapidly at the same time. The difficulty of this response is apparent in the

extremely large elevator control magnitudes required to achieve it over short t_f , as seen in Figure B9. The linearity assumptions of the constraint equation are grossly exceeded.

f) Cost Plot (Figure B12)

This figure shows the relative costs of response along each $\bar{v}_i(t_f)$. GRAMOP correctly shows that no two cost traces overlap, since $J(u_i)$ must always be less than $J(u_j)$ for $j > i$ at any final time, t_f . It is important to notice that all cost lines tend to decrease sharply as t_f increases out to about 2 seconds, then all lines remain somewhat constant over later final times. Also, the control histories generally show progressively smaller control deflections used as final time increases through the 2-second area, which accounts for the sharp drop in cost magnitude through that interval.

2) LES 230-Y - Lateral/Directional Case

a) Direction 1 (Figure B13)

This easiest response begins as almost entirely roll rate, which quickly diminishes and is replaced by roll angle. Control history Figure B15 shows minimal control requirements, again attributable to the aircraft's combat mission design.

b) Direction 2 (Figure B16)

This response direction history begins as mostly yaw rate, which dies out very rapidly (at about 0.3 sec.) and is replaced by roll angle, which is then (at 1.5 sec.) gradually replaced by roll rate as the dominant component.

c) Direction 3 (Figure B17)

This response begins as mostly roll angle, then very quickly (at about .5 sec.) becomes mostly yaw rate and remains that way throughout the

rest of the time interval tested.

d) Direction 4 (Figure B18)

This response is mostly sideslip throughout the entire time interval tested. Control magnitudes are small, but usually increasing steadily with increasing t_f (see Figures B20 and B22).

e) Cost Plot (Figure B23)

The cost plot characteristics are similar to the longitudinal case cost plot.

3) Modified LES 230-Y Longitudinal Case

The modifications to the Boeing design LES 230-Y include removal of the wingtip/vertical fins, elevons "locked" in the wing surface, and the anhedral wingtips used as the only set of control surfaces (Figure 3).

a) Direction 1 (Figure C1)

This response begins as almost entirely pitch rate, then, around 1 second, gradually becomes mostly a combination of both some lesser velocity and angle of attack changes along with a larger altitude change. Consistent with this change, the trend between the two sample trajectories, Figures C2 through C5, as final time is increased, is toward virtually no throttle changes and only elevator movement. Note also that all control input histories show both left and right wingtips' movements are identical, which is consistent with both tips acting together as elevators. Control magnitude drops with larger final times.

b) Direction 2 (Figure C6)

This response history begins as mostly velocity change, then changes to a fairly equal combination of pitch rate and opposite altitude

change between 1 and 2 seconds. It then gradually becomes a new combination of all variables - positive velocity and altitude changes along with negative angle of attack, pitch angle, and pitch rate.

c) Direction 3 (Figure C7)

This response begins as a combination of angle of attack and pitch angle, then changes at 1 second to a combination of altitude and opposite pitch rate. At 2 seconds it again changes to mostly velocity change with a minor pitch rate component.

d) Direction 4 (Figure C8)

This response begins as altitude change, then (around 1 second) changes to a fairly constant combination of pitch rate and opposite pitch angle, with minor opposite angle of attack.

e) Direction 5 (Figure C9)

This most difficult response history is always mostly angle of attack with opposite pitch angle. Figures C10 through C13 show that this response is unattainable within the linear region of either state or control motion until around 8 seconds final time.

f) Cost Plot (Figure C14)

Cost plot trends generally follow those of the other aircraft.

4) Modified LES 230-Y Lateral/Directional Case

a) Direction 1 (Figure C15)

This response is predominantly roll rate over all times. Beyond 4 seconds, roll rate and roll angle components are roughly equal, while there is slight opposite yaw rate beginning around 2 seconds. The sample trajectories (Figures C16 through C19) show that less and less control is required as t_f increases. Also, note that the only control command available is pure aileron, as the right and left tips'

trajectories are mirror images of each other. This is also consistent with FLESTAB symmetry restrictions as well as the stated definition of aileron deflection.

b) Direction 2 (Figure C20)

This response direction is mostly roll angle except at 1.5 seconds, when opposite roll rate briefly dominates, then quickly diminishes until 2 seconds. At that time, opposite roll rate again grows until it is the secondary component, with roll angle still dominating.

c) Direction 3 (Figure C21)

This direction is dominated at all times by negative yaw rate. At about 1 second, a minor positive sideslip angle component begins. At about 3 seconds, another minor negative roll rate component begins. This plot shows the first evidence of some numerical problems in the software at around 9 seconds, as all vector components abruptly shift values. This is due to numerical ill-conditioning of the A and B matrix combination for the aircraft, which results in the final time Grammian and its inverse being incorrectly computed by the existing library matrix subroutines. A specially-written Grammian inverse subroutine, which made use of the singular value decomposition of the matrix, eased the numerical problems to some extent but did not remove them completely.

d) Direction 4 (Figure C22)

This most difficult response is always dominated by sideslip, with a minor yaw rate component beginning around 2 seconds. Numerical problems again appear around 9 seconds, as discussed above. The very poor controllability of this direction is shown in Figures C23 and C24 (2.0 seconds) where extremely large state and control magnitudes

are required. Also, Figures C25 and C27 show numerical problems, since the state trajectories never reach \bar{x}_f exactly. This is also attributed to the particular routines used to compute the Gramian.

e) Cost Plot (Figure C29)

Cost trends still follow those of all other cases. However, the numerical problem affects the highest two cost lines, around 9 seconds. Clearly this aircraft/flight control system combination is very badly behaved in the lateral/directional mode.

Traits Discussion

The response characteristics of these two aircraft/control system combinations all exhibited certain trends:

1) Each ranked response direction appears to be divided into three distinct areas: a) the very short final time range (0 to 2 seconds) where the state directions remain somewhat constant; b) a "transition region", usually from final times of 2 to 5 seconds, where the state variable components are changing from their short-time to long-time constant values; and c) the long final time region, later than 5 seconds, where the directions are again fairly constant in the state space, but different from the previous directions. These three "bands" may be physically interpreted as the dominance of the short period/Dutch roll modes and phugoid/spiral modes in the first and third t_f bands, respectively, and the transition between the two modes during the second band.

2) It is very difficult for the flight control system to drive the aircraft along these "worst" directions, since they usually combine conflicting state variable motions, e.g., positive angle of attack along with negative pitch angle and rate, as shown in Figure C9.

From a pilot's viewpoint, these directions usually represent highly unorthodox aircraft motions that are neither required nor naturally occur during normal aircraft use. Figures C11 and C13 again show that larger final times require less control magnitude, probably due to the aircraft's dynamic response approaching \bar{x}_f with relatively little extra help from the control system.

Direct Aircraft Comparison

These aircraft/control system combinations were also studied using a direct, "head to head" comparison. Each aircraft is "flown" to the same arbitrary set of state vectors for both the longitudinal and lateral cases, and the state and control trajectories are compared to see which aircraft required the least control and state variable displacements. Four different final state vectors were used (see Table V), each at three different final times of 2.5, 5.0, and 7.5 seconds. Certain final time examples show results typical of results

Table V
Direct Comparison Final State Vectors

VECTOR	t_f	u (FT/SEC)	α (DEG)	q (DEG/SEC)	ϕ (DEG)	h (FT)
LONG. #1	7.5	-5.0	3.0	0.25	5.0	25.0
LONG. #2	5.0	-25.0	8.0	12.0	8.0	75.0
VECTOR	t_f	β (DEG)	ϕ (DEG)	$\dot{\phi}$ (DEG/SEC)	$\dot{\psi}$ (DEG/SEC)	
LAT. #1	7.5	0.0	60.0	25.0	0.0	
LAT. #2	2.5	10.0	5.0	2.0	5.0	

for all three times, within a given final state vector, and these samples are included for all four state vectors in Appendix D. These typical examples are now discussed in detail.

1) Longitudinal Vector 1 (Figures D1 through D4)

Overall, the LES baseline aircraft is by far the most controllable and hence requires the least control energy to maneuver. The experimental tip controls require much more deflection than the baseline LES controls.

2) Longitudinal Vector 2 (Figures D5 through D8)

Again, the LES baseline aircraft is by far the most controllable for the least control movement. Now the experimental LES aircraft shows control magnitudes just over linearity limits.

3) Lateral/Directional Vector 1 (Figures D9 through D13)

The LES baseline aircraft is still the best, with the experimental wingtip system comparing very poorly in terms of control deflection magnitudes. This is caused by the experimental system's having only aileron control, with any state space movement corresponding to ordinary yawing/rudder movements available only from the yaw coupling response due to excessive aileron control. This result is certainly consistent with expectations, given no aerodynamic yawing control independent of the roll controls.

4) Lateral/Directional Vector 2 (Figures D13 through D16)

The LES baseline aircraft remains the best and the aileron-only experimental aircraft again fares very poorly, so much so that it violates linearity restrictions for control magnitudes.

Experimental Control System Evaluation

This study shows that the experimental wingtip control system

provides only marginal longitudinal control and totally inadequate lateral/directional control. This problem is initially predictable from the small magnitudes of the FLEXSTAB-computed elevator and aileron control power derivatives, $C_{m\delta_E}$ and $C_{l\delta_A}$, as shown in Table A.III, compared with the corresponding baseline LES control powers. The problem is also quantitatively demonstrated in the direct comparison tests just mentioned above. Due to the FLEXSTAB symmetry restrictions, wingtip rudder power has not been accurately modeled, but in light of the wingtips' correctly-modeled yet very poor elevator and aileron power, the rudder power is certainly expected to be equally poor with respect to the baseline LES aircraft. With no known software available to model nonsymmetrical rudder deflections, there is no method to quantitatively verify this expectation. The only way to improve the yaw control capability of the experimental aircraft so that FLEXSTAB could correctly model its control characteristics is to add a conventional fin and rudder on the aircraft's centerline. However, this is essentially a conventional control system except for unusual placement of the elevons. Wind tunnel testing appears to be the only way of gathering data for any asymmetrical aircraft/control deflection geometry.

Method Evaluation

The software used in this study does an excellent job of modeling linear aerodynamics of an arbitrary (symmetric) aircraft geometry, then translating the aerodynamics into a state space linear dynamic system suitable for analysis by a user-selected linear systems analysis program - GRAMOP in the case of this study.

However, there are some restrictions which must be observed. The first, FLEXSTAB's symmetry restriction, has been described already so will not be further repeated here.

Second, the linearity restriction of all software must be understood. Reference 1 and Chapters III and IV describe the linearity assumptions used to derive the three programs used. Focusing on the GRAMOP program, it is necessary to understand the implications of linearity to this particular optimal control problem in order to correctly interpret its solution. The constraint equation (34), used in the optimal control analysis, contains matrices A and B which are derived using these linearity/small perturbation assumptions:

- 1) linear potential theory in FLEXSTAB aerodynamic paneling;
- 2) small perturbations around reference flight condition to simplify the equations of motion. Thus the matrices A and B are a valid physical model of the aircraft only for those aircraft and control motions $\bar{x}(t)$ and $\bar{u}(t)$ which remain within the region of small perturbations with respect to the selected equilibrium flight condition. Therefore, the only physically valid GRAMOP-computed optimal state and control trajectories are those which also remain in the region of small perturbations with respect to initial state and control vectors.

Although linearity is assumed during the formulation of every software algorithm in this project, several cases have been noted where control and/or state variable magnitudes have violated these perturbation limits. These results are caused by the combination of two effects - constant A and B matrix elements and poor controllability.

First, the elements of both the A and B matrices are constant

since they represent the combined effect of all stability and control derivatives which are assumed constant over the linear/small perturbation region of both control and state variable response of the aircraft. Figure 5 provides an example. Figure 5A shows a typical C_L versus α curve, while Figure 5B shows that the small perturbation approximation adequately models Figure 5A over the

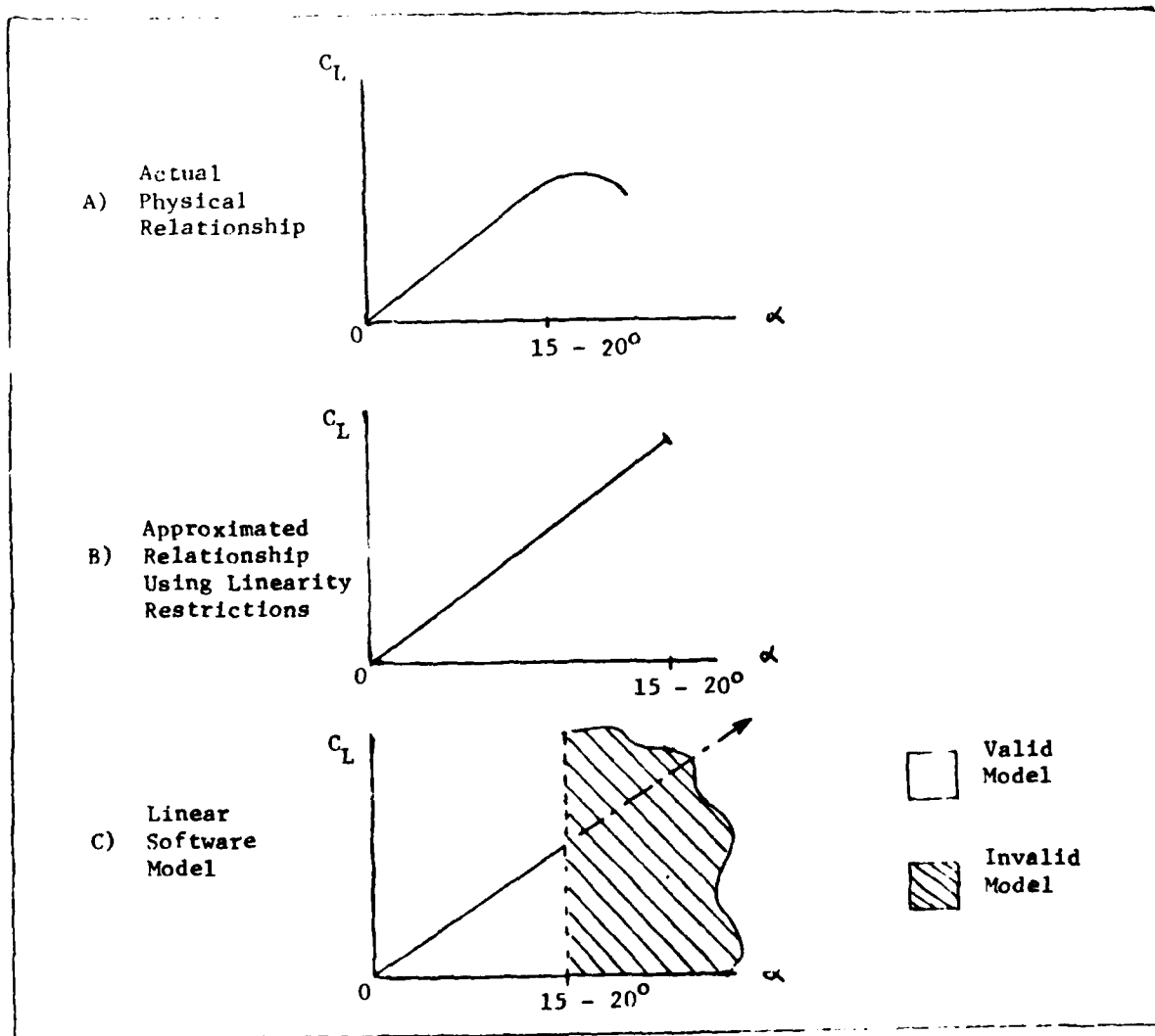


Figure 5. Linearity Restrictions

appropriately limited range of α . Figure 5C shows that the constant-value coefficient assumption erroneously allows the algorithm to extrapolate the stability and control characteristics beyond their region of physical validity.

Second, the GRAMOP algorithm makes extensive use of Σ_w , the diagonal matrix of eigenvalues of $W_c(t)$. Since the eigenvalues have no direct, physical state space meaning in terms of perturbation magnitudes, they are only limited in that they must be non-negative real numbers. But this matrix and its inverse appear in both $\bar{u}^*(t)$ and also $\bar{x}(t)$, equations (46) and (35). As described before, the relative magnitudes of the λ_i are a measure of controllability quality along each of the orthogonal eigenvector directions in state space. For even an assumed linear system, certain λ_i may be so small (i.e., those eigenvector directions \bar{v}_i may be so poorly controllable) that, when inverted in equations (46) and (35), they drive the $\bar{u}(t)$ and $\bar{x}(t)$ values beyond linearity limits.

This combination of poor controllability and extrapolated equations of motion results in the invalid, nonlinear output data shown. The correct interpretation of this situation is that GRAMOP cannot always compute the physically correct $\bar{u}^*(t)$ and $\bar{x}(t)$ outputs to reach every possible $\bar{x}(t_f)$. This problem exists even for $\bar{x}(t_f)$'s which are themselves within small perturbation limits, e.g., if this final state lies in a nearly uncontrollable subspace. The data in such cases is still usable qualitatively, rather than quantitatively. Violation of small perturbations in the output means that the physical system cannot reach the given $\bar{x}(t_f)$ when constrained within only the "linear region of motion." This is a valid, although only qualitative,

measure of aircraft controllability. It is certainly possible that this $\bar{x}(t_f)$ could be reached using larger perturbations in $\bar{u}^*(t)$ and $\bar{x}(t)$, but this type of motion is beyond the scope of both FLEXSTAB and GRAMOP. In order to acquire valid numerical data from this software, the magnitude of the "linearly accessible" $\bar{x}(t_f)$ should be scaled as small as necessary until the largest values in the resultant $\bar{u}^*(t)$ and $\bar{x}^*(t)$ trajectories also satisfy the linearity constraints. That scaled $\bar{x}(t_f)$ then represents the maximum-magnitude of the "linearly controllable" response in that particular subspace of (R^n) .

The third restriction is that all solutions to this optimal control problem depend directly on the user-input control weighting matrix, R . Even if all constraint matrices A and B and all other optimal conditions \bar{x}_f and t_f are identical, resulting $\bar{x}^*(t)$ and $\bar{u}^*(t)$ trajectories and $J^*(\bar{u}(t))$ will differ case-by-case with each different R matrix used.

Recall that the R matrix form adopted in this study is diagonal with non-negative diagonal elements. This choice of R yields a performance functional as the weighted sum of squares

$$J(\bar{u}(t)) = \frac{1}{2} \int_0^t \left(\sum_{i=1}^m u_i^2 R_{ii} \right) dt$$

The numerical values for each R_{ii} directly measure the relative control energy "penalty" that the user wishes to attach to each u_i . Each R_{ii} establishes a deflection magnitude $| \delta u_i | = \delta_i$, which is regarded as costing one "unit of equivalent control energy". The quantity $u_i' = u_i / \delta_i$ then expresses u_i as a "normalized" u_i' , in terms of "equivalent control energy" units, instead of physical units (e.g., degrees of control surface deflection). The cost functional

then becomes

$$J(\bar{u}(t)) = \frac{1}{2} \int_0^t \left(\sum_{i=1}^m u_i'^2 \right) dt = \frac{1}{2} \int_0^t \left(\sum_{i=1}^m \frac{u_i^2}{\Delta_i^2} \right) dt \quad (60)$$

Thus, $R_{11} = (1/\Delta_1)^2$, or the square of the arbitrary, user-defined physical-to-equivalent energy units conversion factor. The larger R_{11} becomes, the heavier the user is weighting (penalizing) the use of control u_1 , as measured by $J(\bar{u}(t))$. R allows the user to define equivalent control energies for controls which differ physically. The R matrix used in this study equated the control energies between angular control surface deflections, measured in degrees, and throttle movements, measured in percent of aircraft weight. The author arbitrarily chose:

1) 5 degree control surface deflection to be one unit of control surface energy

2) 10% of aircraft weight to be one unit of throttle energy.

Thus, since $R_{ii} = (1/\Delta_i)^2$,

$$R = \begin{bmatrix} 0.04 & 0.0 \\ 0.0 & 100 \end{bmatrix} \quad (61)$$

$$\text{for } \bar{u} = \begin{bmatrix} \delta_e \\ \delta_r \end{bmatrix} \quad (62)$$

For the lateral/directional cases, where only control surfaces (and no throttle) are used, R was left as the identity matrix, since the same Δ_1 was assumed for all u_1 's in these cases.

VI. Conclusions and Recommendations

Conclusions

The specific conclusions reached during this study are:

1) A quantitative measure of linear system controllability characteristics has been developed using the concept of control energy, as defined by

$$J(\bar{u}(t)) = \frac{1}{2} \int_0^t \bar{u}^T(\tau) R \bar{u}(\tau) d\tau$$

This quadratic functional is used as the performance index in the linear-constraint optimization problem; find the $\bar{u}(t)$ which minimizes

$$J(\bar{u}(t)) = \frac{1}{2} \int_0^t \bar{u}^T(\tau) R \bar{u}(\tau) d\tau$$

subject to the constraint, $\dot{\bar{x}} = A\bar{x} + B\bar{u}$, with $\bar{x}(0) = \bar{0}$ and both t_f and $\bar{x}(t_f)$ specified. The controllability Gramian

$$W_c(t) = \int_0^t \Phi(\tau) B B^T \Phi^T(\tau) d\tau$$

appears in both $\bar{u}^*(t)$ and $\bar{x}(t)$ solutions for the optimization problem. When $W_c(t)$ is expressed by its unique singular value decomposition form within the $\bar{u}^*(t)$ and $\bar{x}(t)$ expressions, it gives a ranking of the controllability quality, i.e., control energy $J(\bar{u}(t))$, required to drive the linear system along each of the n unique, time-varying, mutually orthogonal directions in state space described in Chapters I and IV.

2) Computer software program GRAMOP has been developed which analyzes any input linear system according to its controllability quality by the above process 1). Specific program options include:

a) Calculate and display the time histories of all n orthogonal, ranked response directions at any given final time;

b) Calculate optimal control and corresponding state variable response trajectories to reach any input final state $\bar{x}(t_f)$ at the specified final time.

3) GRAMOP has been successfully used on two basic aircraft/flight condition combinations which were compared by first calculating longitudinal and lateral/directional controllability characteristics using option 2a above. Second, optimal control and state response trajectories were then calculated to achieve selected $\bar{x}(t_f)$'s along each ranked response direction, using option 2b above. See Chapter V for details of these results.

4) All linearity assumptions inherent in the constraint equation (34) must be carried throughout the interpretation of any output data. In these aircraft test cases, the small perturbation assumption restricts physically valid output data to those same small perturbation limits. Any "large" output data is correctly interpreted as showing the aircraft's inability to reach the desired $\bar{x}(t_f)$ when using only "small" control inputs and state variable responses. Once either control or state variable output magnitudes exceed this region, the linear dynamics model is an invalid representation of the physical aircraft system. In such cases, the magnitude of the desired $\bar{x}(t_f)$ should be scaled down until linear/small perturbation constraints are met by all control and state output data.

5) As implemented on the particular LES 230-Y aircraft, the experimental wingtip control system was unsuccessful. This was proven quantitatively by:

a) very low FLEXSTAB-computed values for control power

derivatives;

b) poor relative performance in a "head-to-head" comparison with the baseline aircraft;

c) frequent violation of linearity restrictions throughout the controllability analysis. The control system symmetry limitation in FLEXSTAB also precluded accurate modeling of the rudder characteristics of the wingtips.

Recommendations

These recommendations center around changes in the physical system being analyzed, and also possible modifications to the GRAMOP algorithm.

First, this study looked at only the "raw" stability and control derivatives of the basic aircraft tested. A useful extension of this analysis would be to modify the A, B matrix representation of the aircraft by including the dynamics of additional physical control system equipment, such as the transfer functions for servos, stability augmentation systems, etc.

Second, different cost functionals could be studied. The present $J(\bar{u}(t))$ penalizes only the magnitude of $\bar{u}(t)$, and allows any $\dot{\bar{u}}(t)$ rates with no penalty. Better aircraft-related analysis might result from including some control rate penalty. Similarly, penalties for $\bar{x}(t)$ and $\dot{\bar{x}}(t)$ could also be added. This would make the cost functional

$$J'(\bar{u}, \dot{\bar{u}}, \bar{x}, \dot{\bar{x}}, t_1) = \frac{1}{2} \int_0^{t_f} [\bar{u}^T R \bar{u} + \dot{\bar{u}}^T S \dot{\bar{u}} + \bar{x}^T Q \bar{x} + \dot{\bar{x}}^T P \dot{\bar{x}}] dt$$

Third, other software changes could be made to FLEXSTAB. A routine could be added to produce linearized state equations. A most

challenging computer/aerodynamic project would be to replace FLEXSTAB's existing aerodynamic paneling code with other more advanced paneling schemes.

Bibliography

1. AFFDL-TR-77-55. A Method for Predicting the Stability Characteristics of an Elastic Airplane. Vol I. FLEXSTAB 3.01.00 Theoretical Description. Seattle, Washington: Boeing Commercial Airplane Co., 1977.
2. AFFDL-TR-77-55. A Method for Predicting the Stability Characteristics of an Elastic Airplane. Vol II. FLEXSTAB 3.02.00 User's Manual. Seattle, Washington: Boeing Commercial Airplane Co., 1977.
3. ASD Computer Center. ASD Computer Center Calcomp Plotter Guide (Revision D). Wright-Patterson AFB, Ohio: ASD Computer Center, 1978.
4. ASD Computer Center. ASD Computer Center CDC NOS/BE User's Guide (Revision F). Wright-Patterson AFB, Ohio: ASD Computer Center, 1979.
5. Bowlin, W.R. et al. Military Airplane Aeroelastic Cycle Study (Document #D180-25038-1). Seattle, Washington: Boeing Co., 1979.
6. Control Data Corporation. Fortran Extended Version 4 Reference Manual (Revision B). Sunnyvale, California: Control Data Corporation, 1976.
7. Control Data Corporation. Intercom Version 4 Reference Manual (Revision B). Sunnyvale, California: Control Data Corporation, 1976.
8. Fortmann, T.E. and K.L. Hitz. An Introduction to Linear Control Systems (Control and Systems Theory Vol 5). New York: Marcek Dekker Inc., 1977.
9. Kleinman, D.L. Computer Programs Useful in Linear Systems Studies. Cambridge, Massachusetts: Systems Control, Inc., 1971.
10. Kleinman, D.L. Description of Computer Programs for Use in Linear Systems Studies. Dept. of Electrical Engineering and Computer Science, University of Connecticut, Storrs, Connecticut, 1977.
11. Luenberger, D.G. Optimization by Vector Space Methods. New York: Wiley, 1969.
12. Moore, J.T. Elements of Linear Algebra and Matrix Theory. New York: McGraw-Hill Book Co., 1968.
13. Ogata, K. State Space Analysis of Control Systems. Englewood Cliffs, New Jersey: Prentice-Hall Inc., 1976.

14. Roskam, J. Flight Dynamics of Rigid and Elastic Airplanes.
Part 1. Lawrence, Kansas: Roskam Aviation and Engineering Corp.,
1976.
15. Stewart, G.W. Introduction to Matrix Computations. New York:
Academic Press, 1973.

Appendix A: Aircraft Specifications and FLEXSTAB Results

This Appendix contains all geometric specifications, trim parameters for flight conditions, and resultant stability and control data for the aircraft used in this study.

Table A.I
Aircraft Data Specifications

	BOTH LES - 230Y MODELS
WING AREA (FT**2)	670
REF. CHORD (FT)	25.55
WING SPAN (FT)	34.87
AIRCRAFT WEIGHT (LB)	36970
MOMENTS OF INERTIA (SLUG-FT**2)	
Ixx	25940
Iyy	136800
Izz	155500
Ixz	11700

Table A.II
Trim Parameters

	BOEING LES	EXP'L LES
MACH NUMBER (ND)	0.80	0.80
ALTITUDE (FT)	35000	35000
VELOCITY (FT/SEC)	779	779
DYNAMIC PRESSURE (LB/FT**2)	224	224
ROLL ANGLE (DEG)	0	0
ROLL RATE (DEG/SEC)	0	0
YAW RATE (DEG/SEC)	0	0
NORMAL LOAD FACTOR (ND)	1.0	1.0
ANGLE OF ATTACK (DEG)	1.85	2.11
FLIGHT PATH ANGLE (DEG)	0	0
PITCH ATTITUDE (DEG)	1.85	2.11
THRUST (LB)	5627	2450
ELEVATOR ANGLE (DEG)	4.3	35.7
SIDESLIP ANGLE (DEG)	0	0
AILERON ANGLE (DEG)	0	0
RUDDER ANGLE (DEG)	0	0

Table A.III

FLEXSTAB Stability and Control Derivatives

	BOEING LES	EXP'L LES
C_{L_0} (ND)	0.0906	0.0661
C_{D_0} (ND)	0.0231	0.0046
C_{M_0} (ND)	0.0320	0.0386
C_{L_1} (ND)	0.2464	0.2464
C_{D_1} (ND)	0.0375	0.01633
C_{M_1} (ND)	0.0	0.0
C_{L_u} (1/RAD)	0.5446	0.5722
C_{D_u} (1/RAD)	0.0458	0.0400
C_{M_u} (1/RAD)	-0.0272	-0.0276
C_{L_α} (1/DEG)	0.0377	0.0332
C_{D_α} (1/DEG)	0.0070	0.0068
C_{M_α} (1/DEG)	-0.0009	0.0011
C_{L_q} (1/RAD)	2.1825	1.8951
C_{D_q} (1/RAD)	0.1741	0.1636
C_{M_q} (1/RAD)	-0.7779	-0.6509
$C_{y\beta}$ (1/DEG)	-0.0104	-0.0025
$C_{l\beta}$ (1/DEG)	-0.0010	0.0007
$C_{n\beta}$ (1/DEG)	0.0030	-0.0006
C_{yp} (1/RAD)	-0.1572	0.0931
C_{lp} (1/RAD)	-0.1821	-0.1276
C_{np} (1/RAD)	0.0860	-0.0277
C_{yr} (1/RAD)	0.7309	0.0200

Table A.III (continued)

	BOEING LES	EXP'L LES
C_{l_r} (1/RAD)	0.1384	0.0488
C_{n_r} (1/RAD)	-0.3679	-0.0458
C_{l_α} (1/RAD)	0.7875	1.1347
C_{D_α} (1/RAD)	0.0995	0.1304
C_{M_α} (1/RAD)	-0.2344	-0.3244
C_{y_β} (1/RAD)	-0.2187	-0.2205
C_{l_β} (1/RAD)	0.0033	0.0018
C_{n_β} (1/RAD)	-0.0037	-0.0104
$C_{L_{\delta_E}}$ (1/DEG)	0.0196	0.0031
$C_{D_{\delta_E}}$ (1/DEG)	0.0015	0.0001
$C_{m_{\delta_E}}$ (1/DEG)	-0.0071	-0.0011
$C_{Y_{\delta_A}}$ (1/DEG)	0.0018	-0.0016
$C_{l_{\delta_A}}$ (1/DEG)	0.0034	0.0009
$C_{n_{\delta_A}}$ (1/DEG)	-0.0011	0.0005
$C_{y_{\delta_R}}$ (1/DEG)	0.0044	0.0002 *
$C_{l_{\delta_R}}$ (1/DEG)	0.0009	-0.0000 *
$C_{n_{\delta_R}}$ (1/DEG)	-0.0024	-0.0001 *
* These derivatives correspond to strake deflection and are ignored in any subsequent calculations.		

Appendix B: Sample Output Data for LES-230Y

This is a collection of sample output data generated for the Boeing LES 230-Y using the original flight control system at the flight conditions outlined in Chapter V.

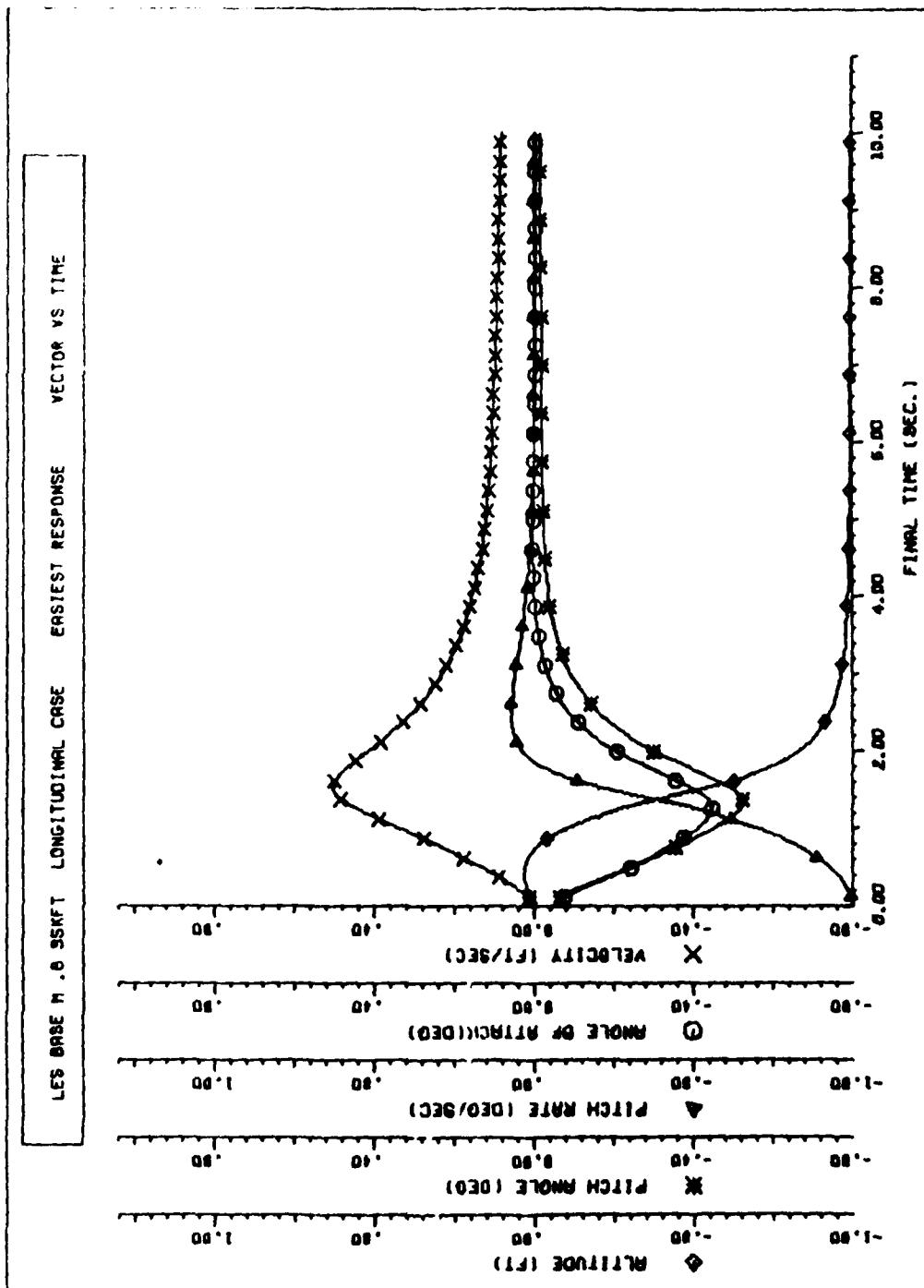


Figure B1 Baseline LES Longitudinal $\vec{V}_1(t_f)$

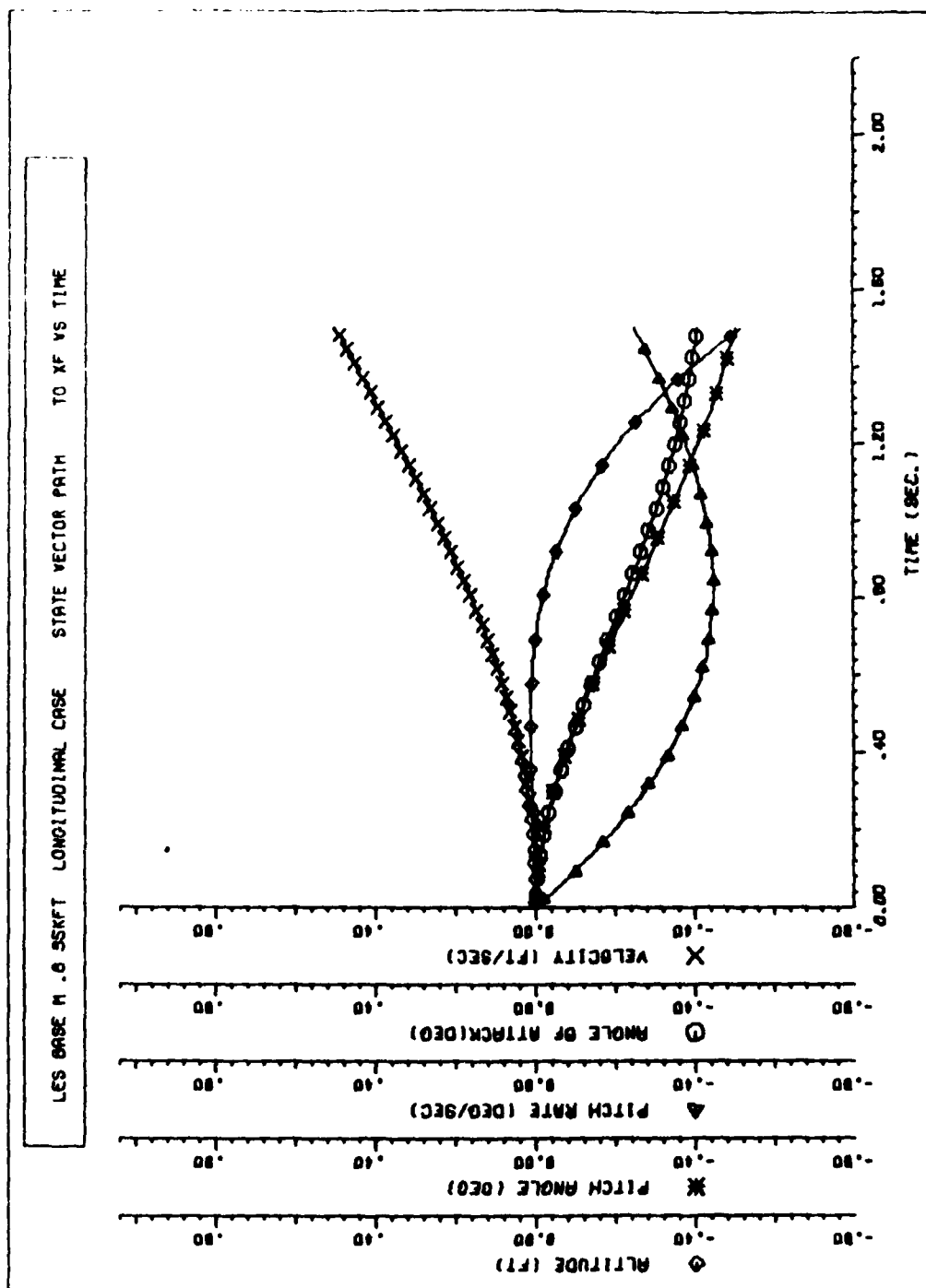


Figure B2 Baseline LES Longitudinal Response to Reach $\bar{V}_1(t_f = 1.5 \text{ Seconds})$

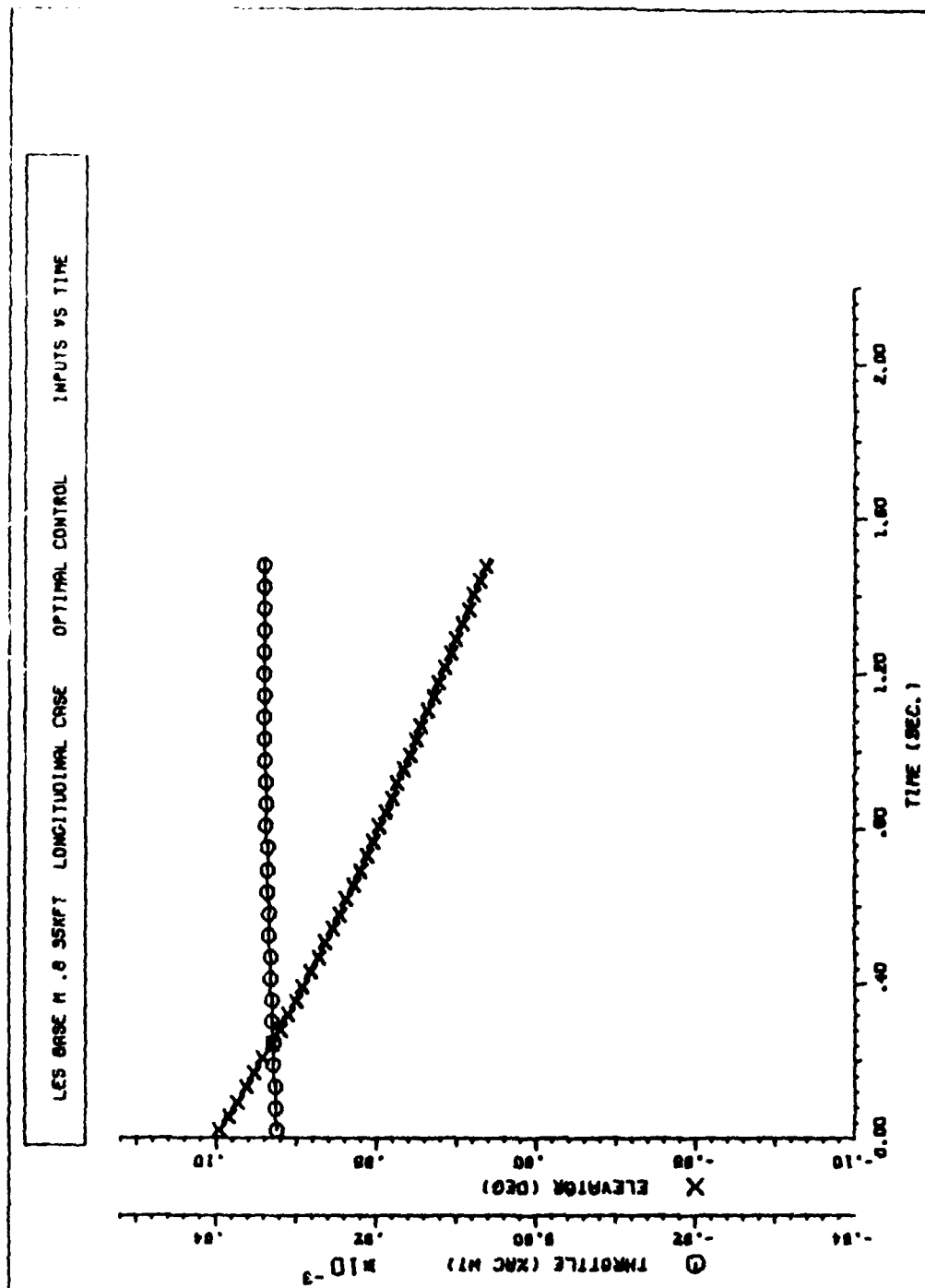


Figure B3 Baseline LES Longitudinal Controls to Reach $\bar{V}_1(t_f = 1.5 \text{ Seconds})$

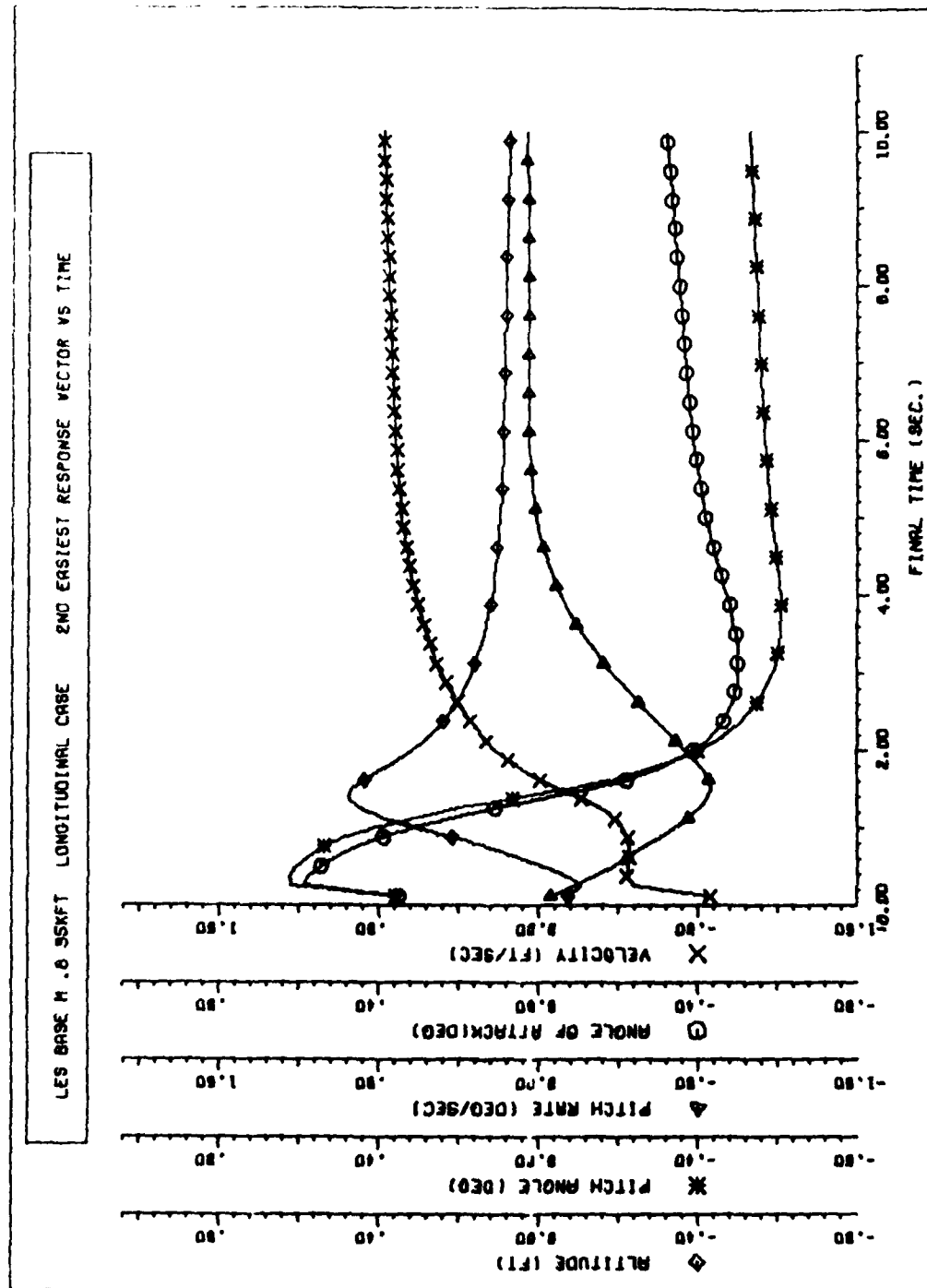


Figure B4 Baseline LES Longitudinal $\vec{U}_2(t_f)$

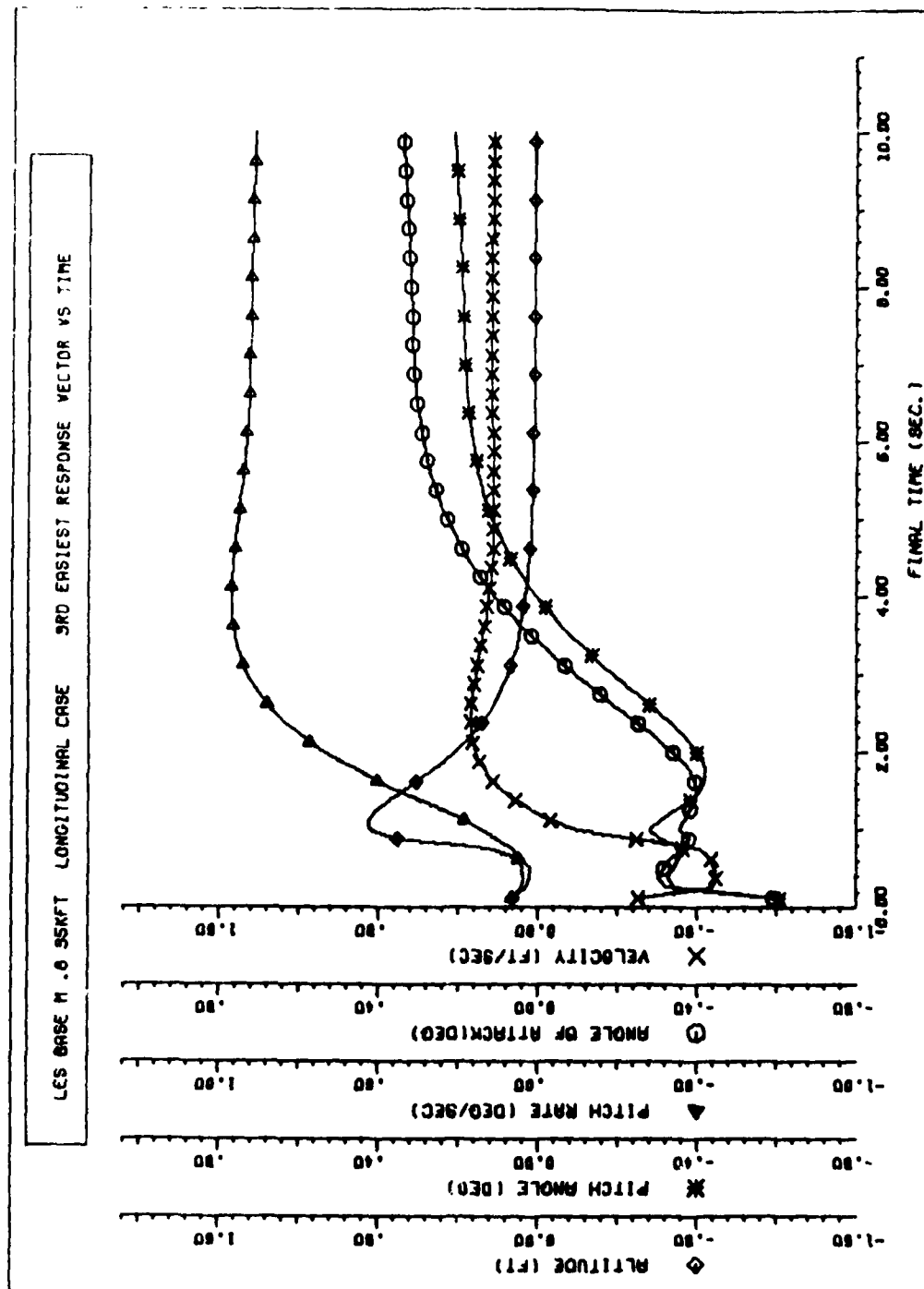


Figure B5 Baseline LES Longitudinal $\bar{u}_1(t_f)$

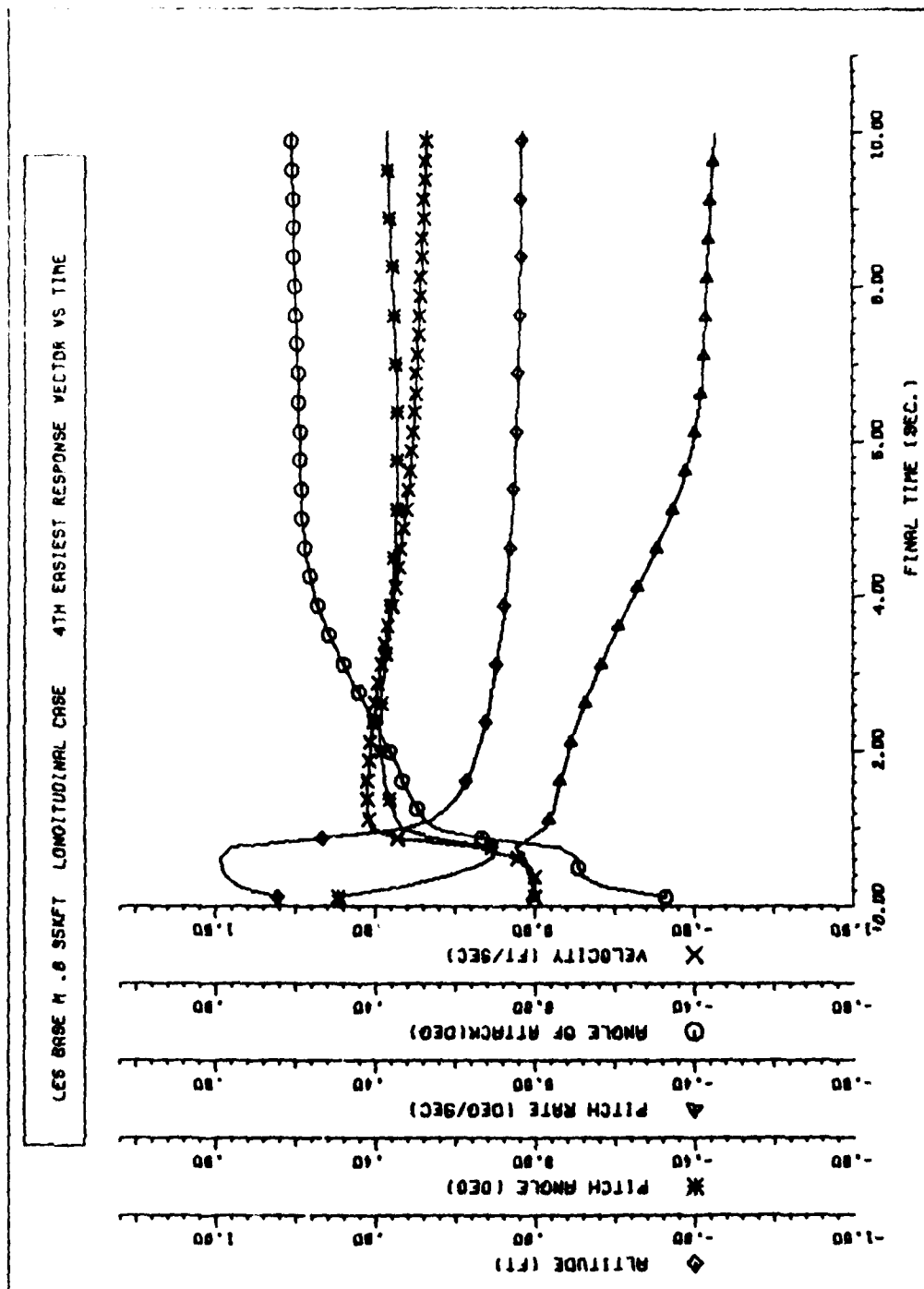


Figure B6 Baseline LES Longitudinal $\mathcal{V}_4(t_f)$

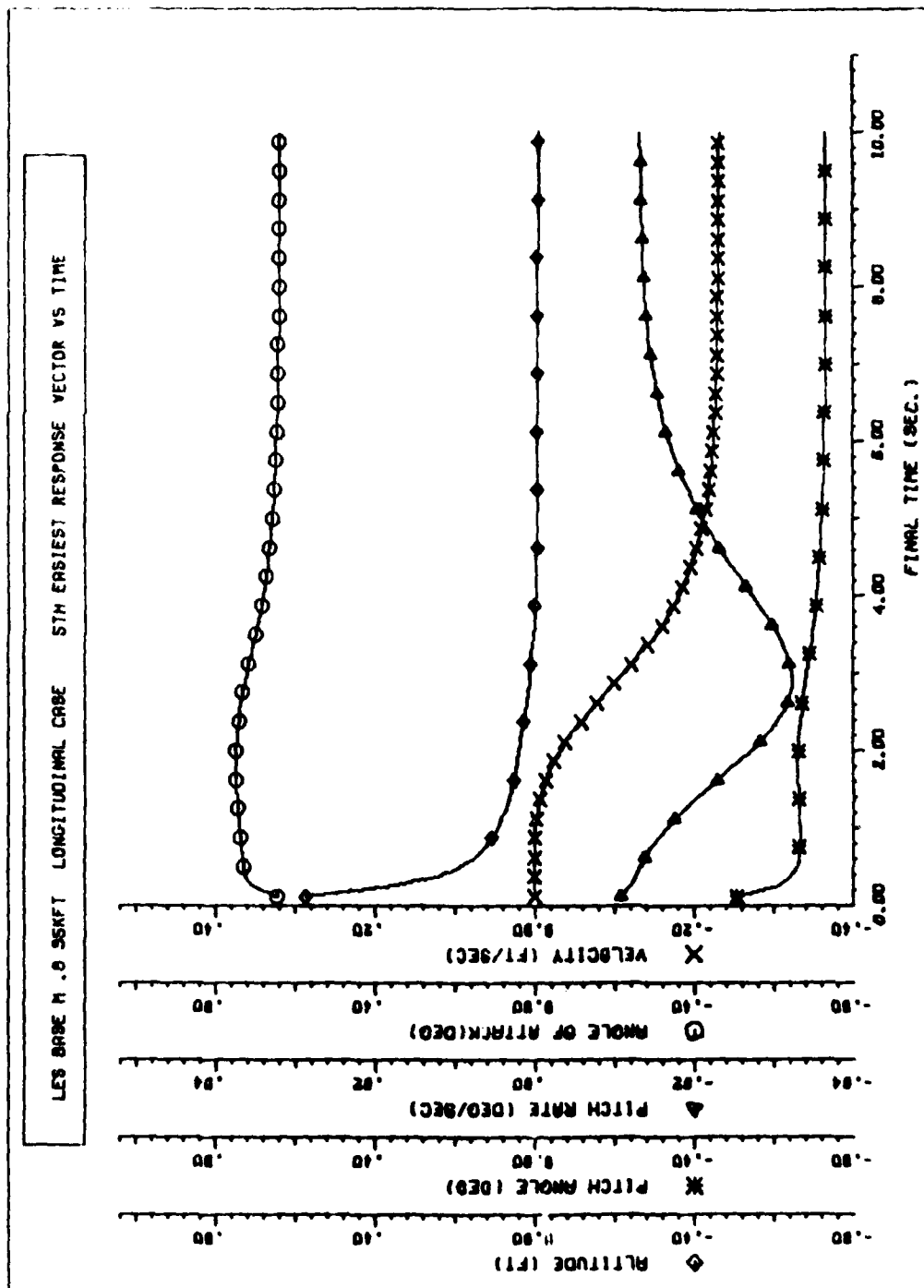


Figure B7 Baseline LES Longitudinal $\vec{v}_s(t_f)$

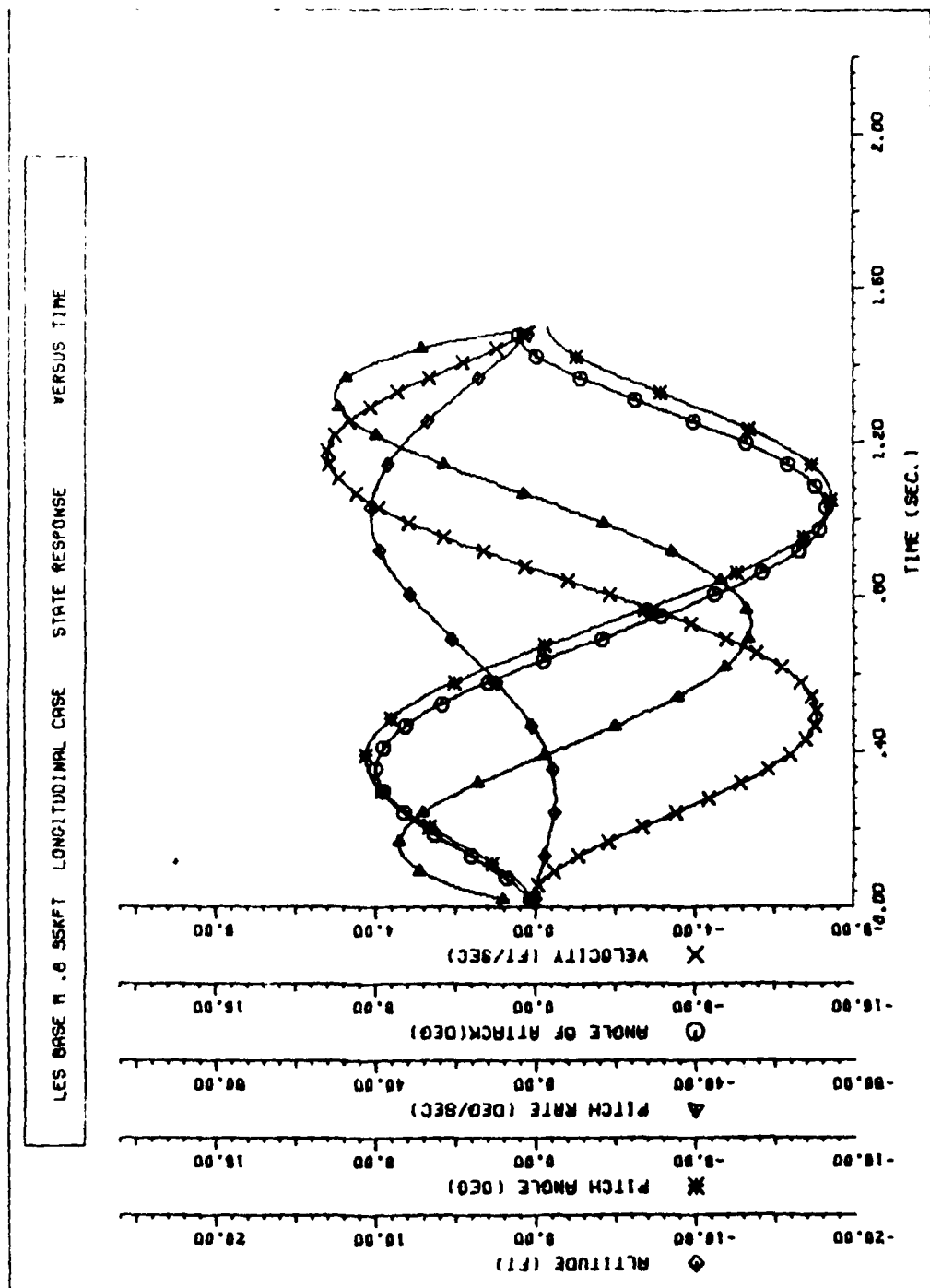


Figure B8 Baseline LES Longitudinal Response to Reach \bar{V}_E ($t_f = 1.5$ Seconds)

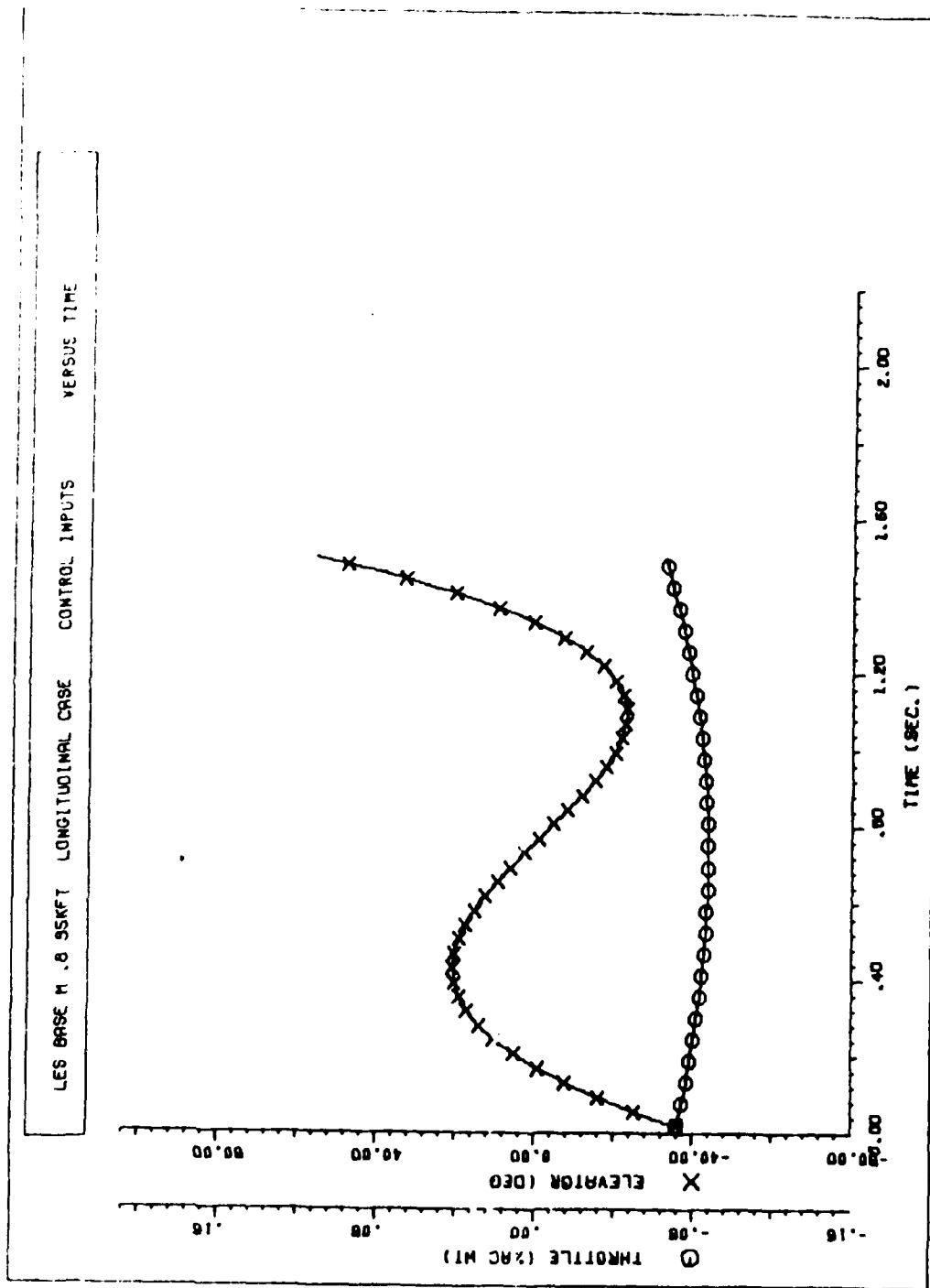


Figure B9 Baseline LES Longitudinal Controls to Reach \bar{v}_5 ($t_f = 1.5$ Seconds)

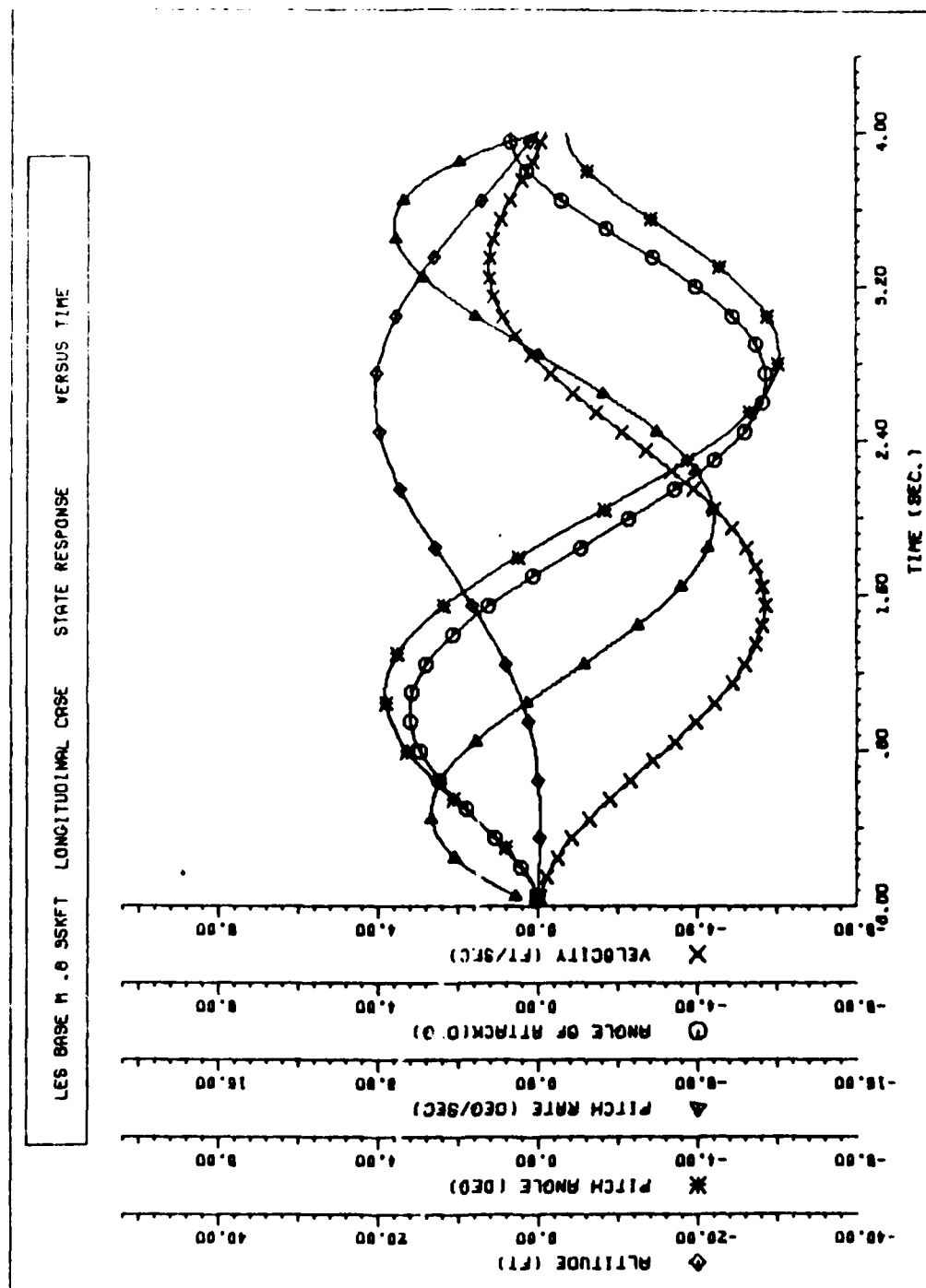


Figure B10 Baseline LES Longitudinal Response to Reach \bar{v}_s ($t_f = 4.0$ Seconds)

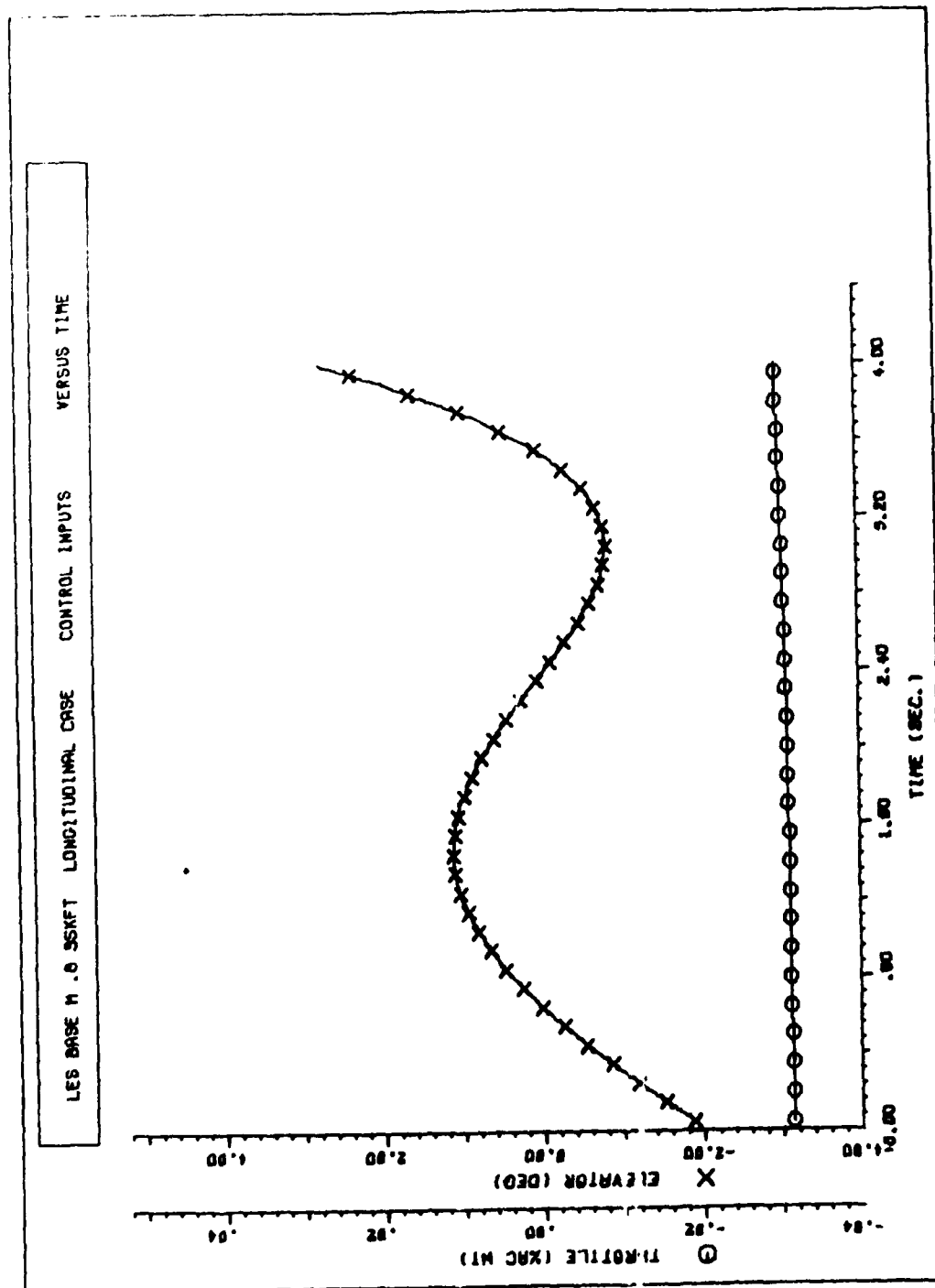


Figure B11 Baseline LES Longitudinal Controls to Reach \bar{v}_5 ($t_f = 4.0$ Seconds)

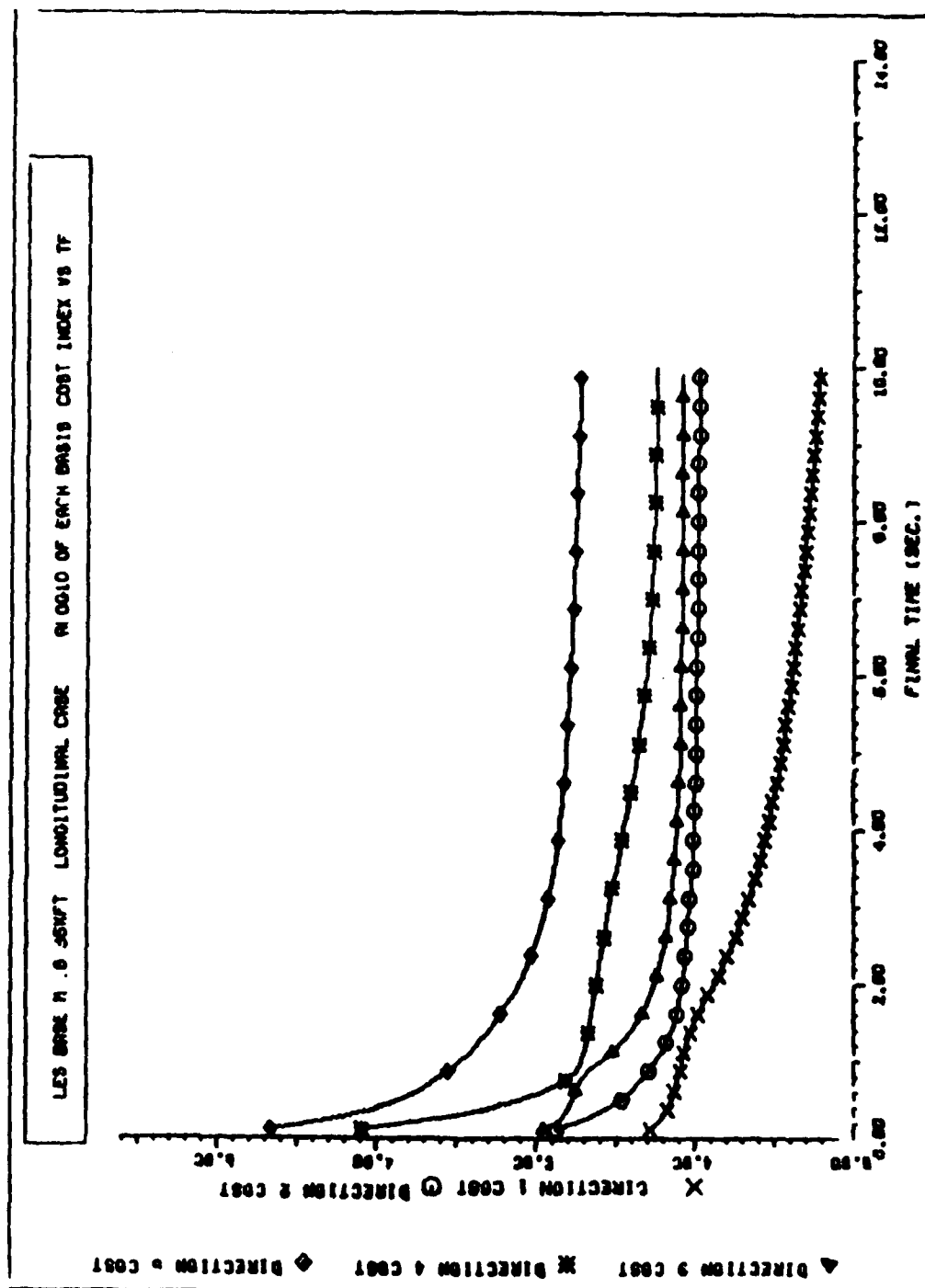


Figure B12 Log₁₀ of Baseline LES Weighted Control Costs for All Longitudinal Basis Vectors

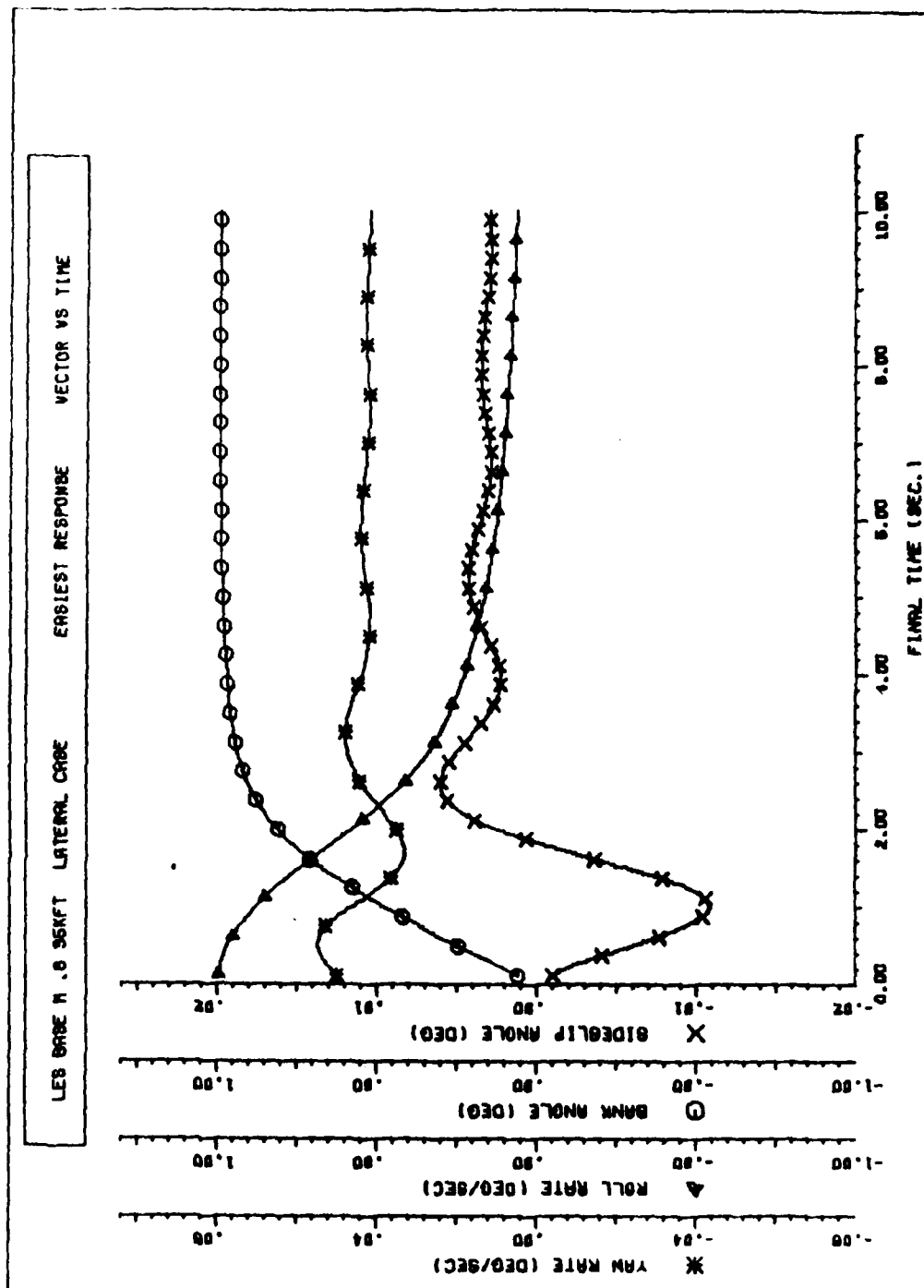


Figure B13 Baseline LES Lateral/Directional $\vec{v}_2(t_f)$

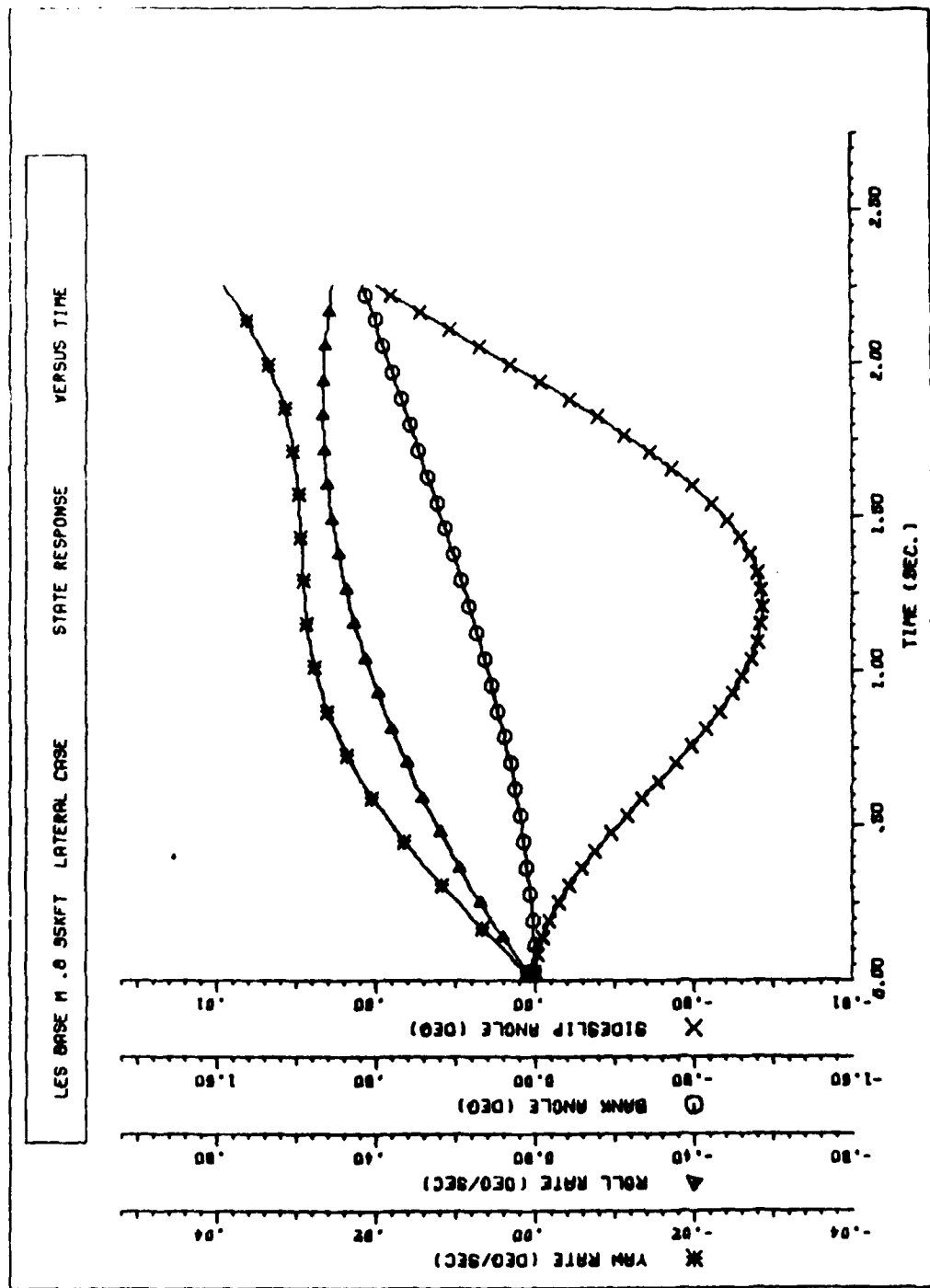


Figure B14 Baseline LES Lateral/Directional Response to Reach $\bar{U}_1(t_f = 2.25 \text{ Seconds})$

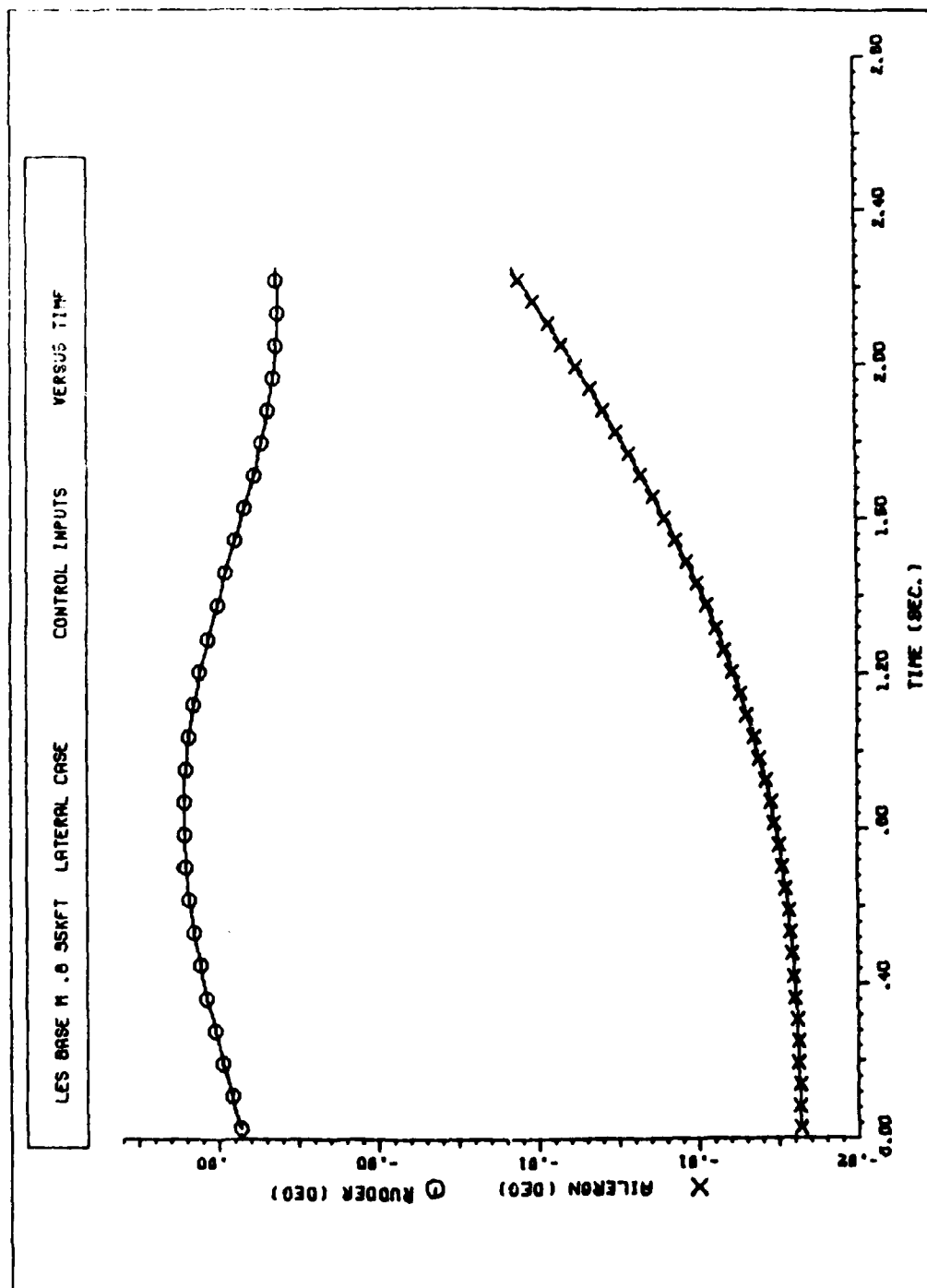


Figure B15 Baseline LES Lateral/Directional Controls to Reach \bar{v}_1 ($t_f = 2.25$ Seconds)

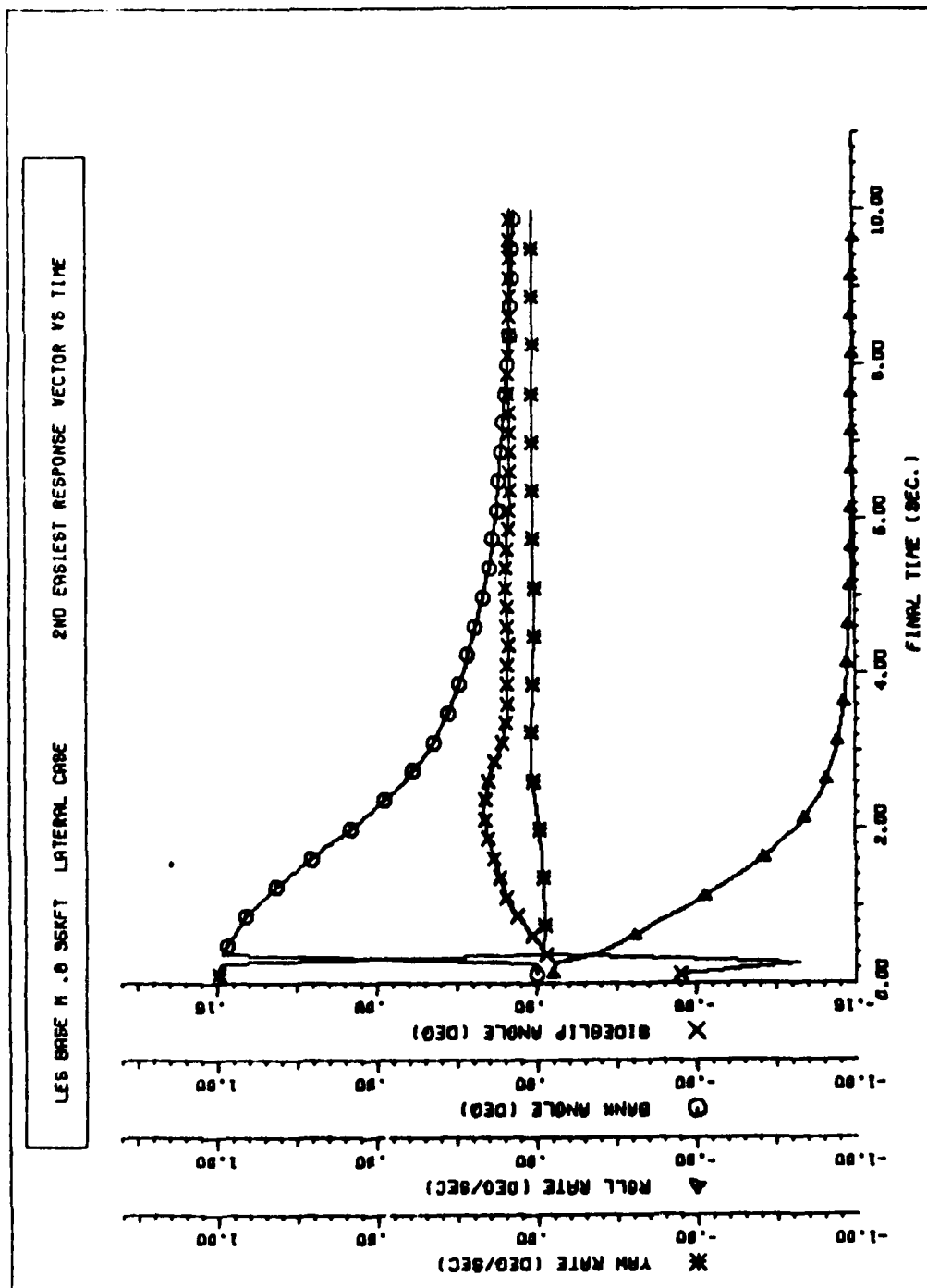


Figure B16 Baseline LES Lateral/Directional $\bar{u}_a(t_f)$

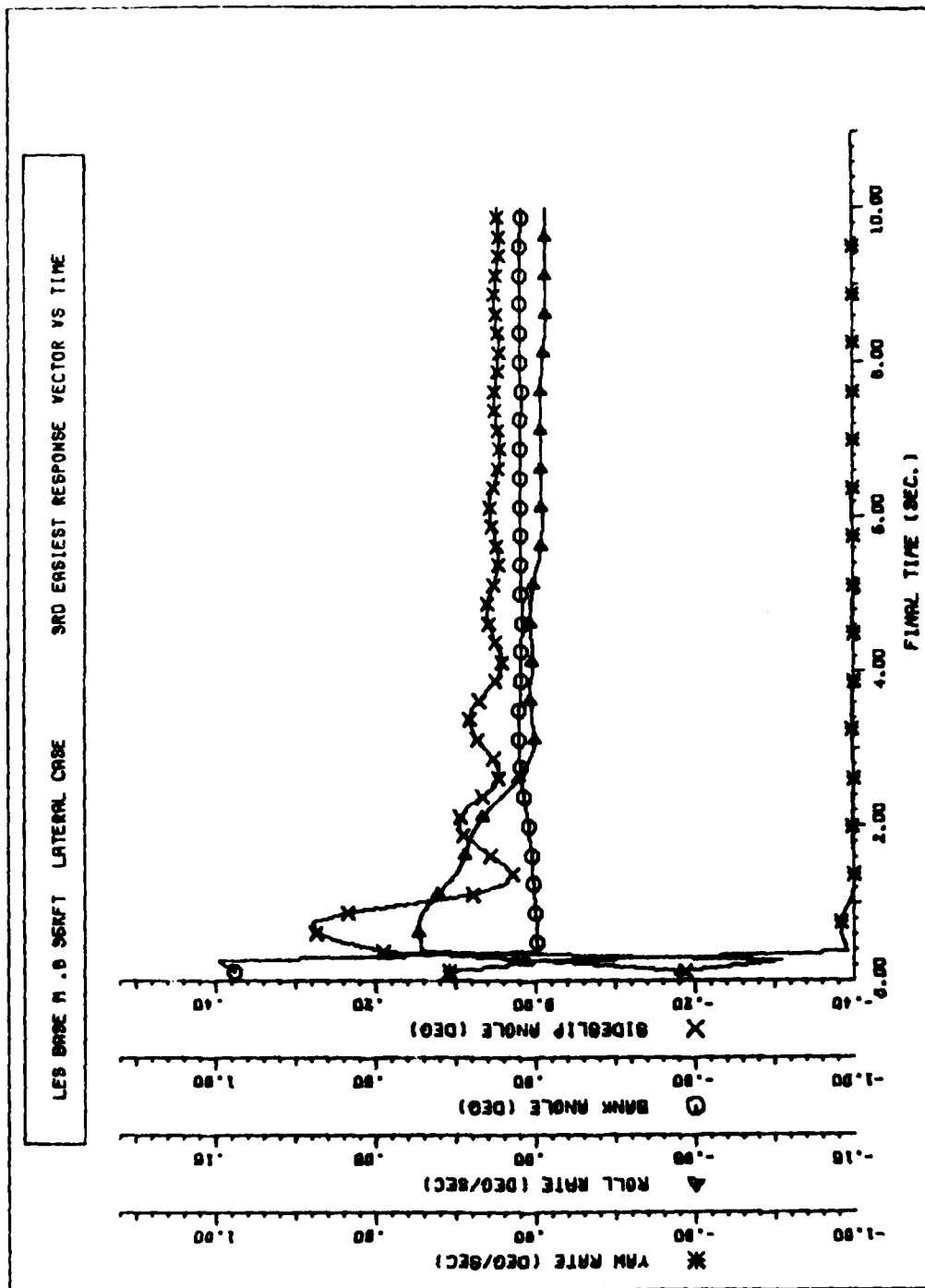


Figure B17 Baseline LES Lateral/Directional $\bar{v}_3(t_f)$

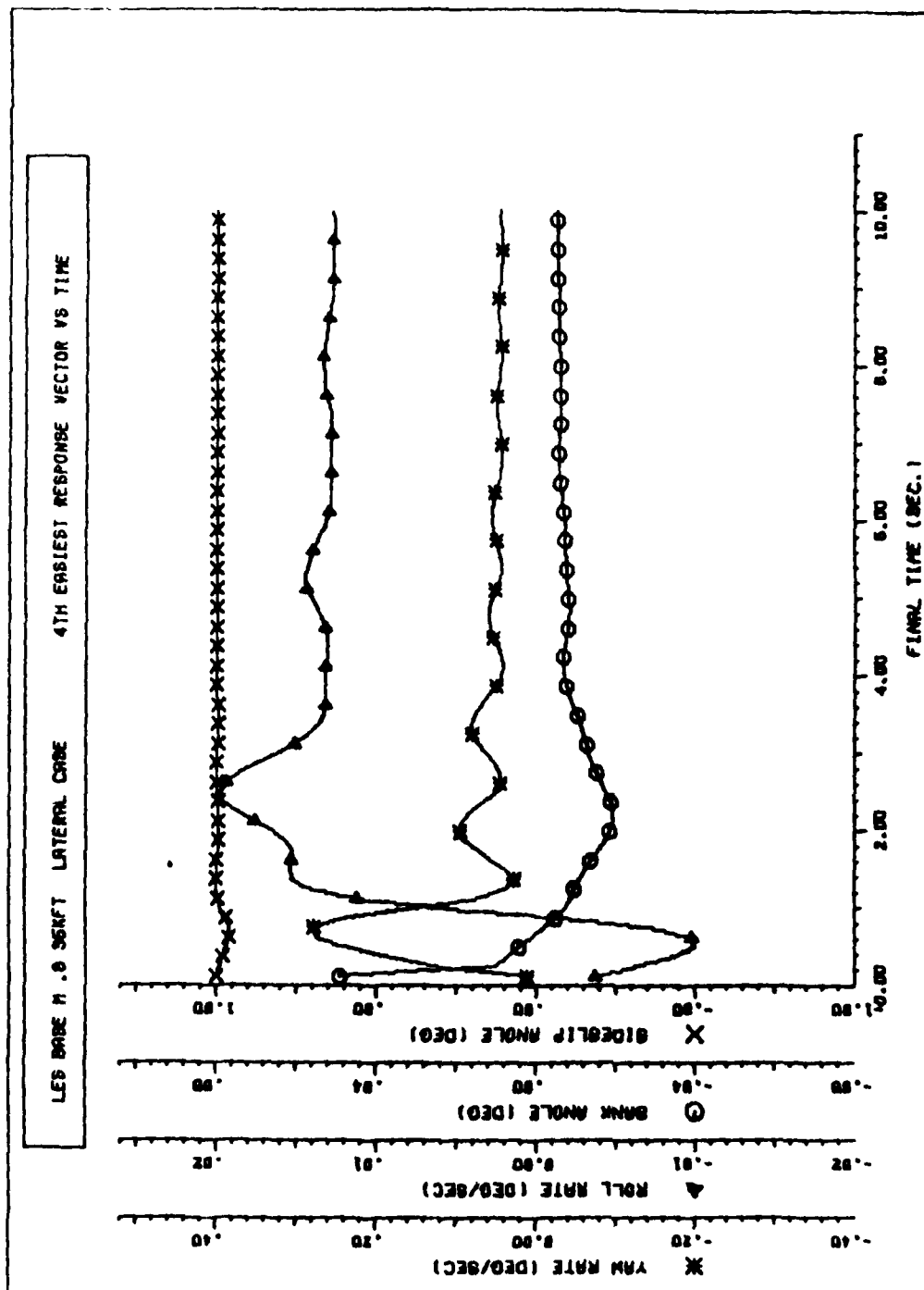


Figure B18 Baseline LES Lateral/Directional $\vec{V}_4(t_f)$

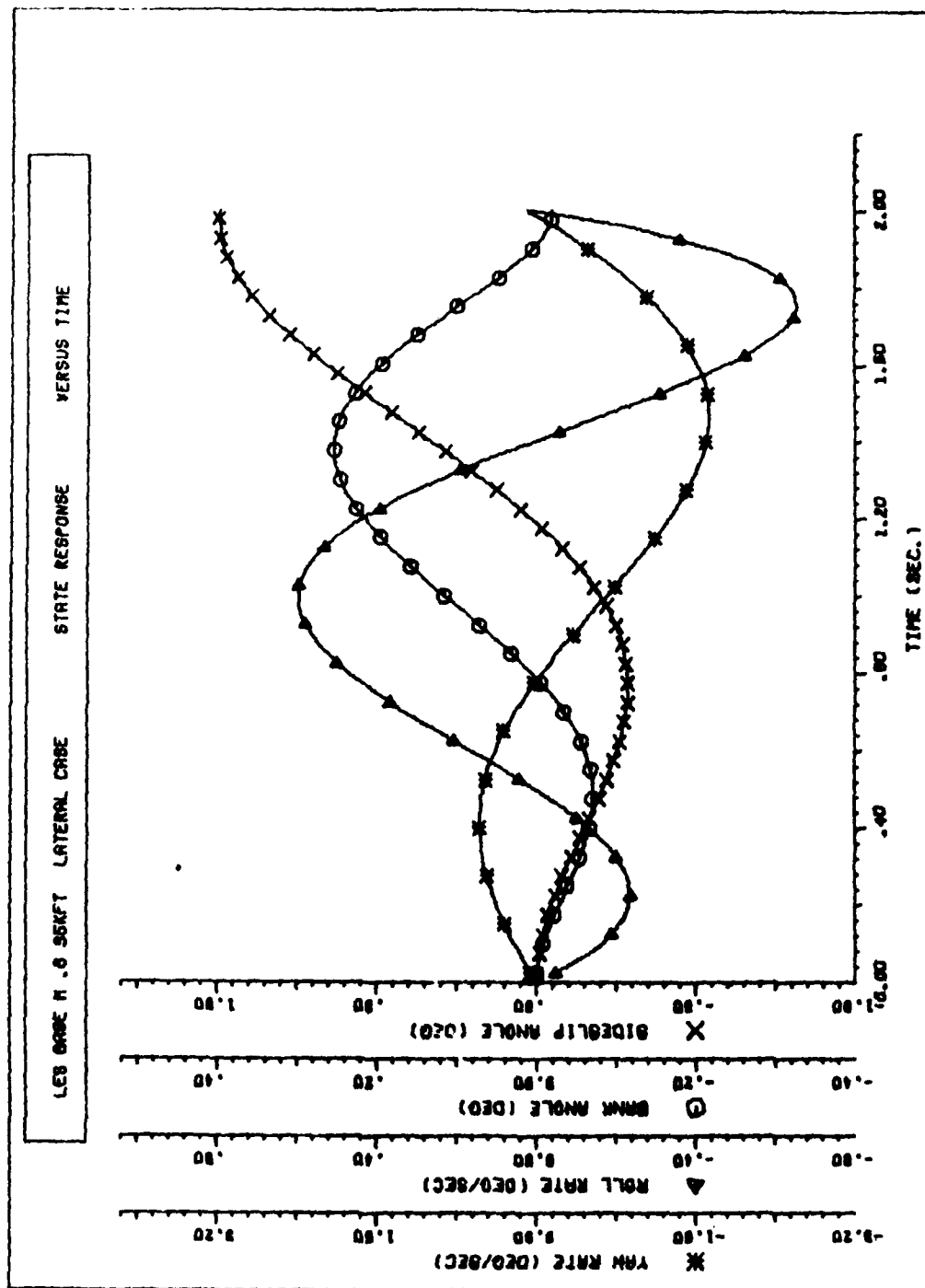


Figure B19 Baseline LES Lateral/Directional Response to Reach \bar{U}_4 ($t_f = 2.0$ Seconds)

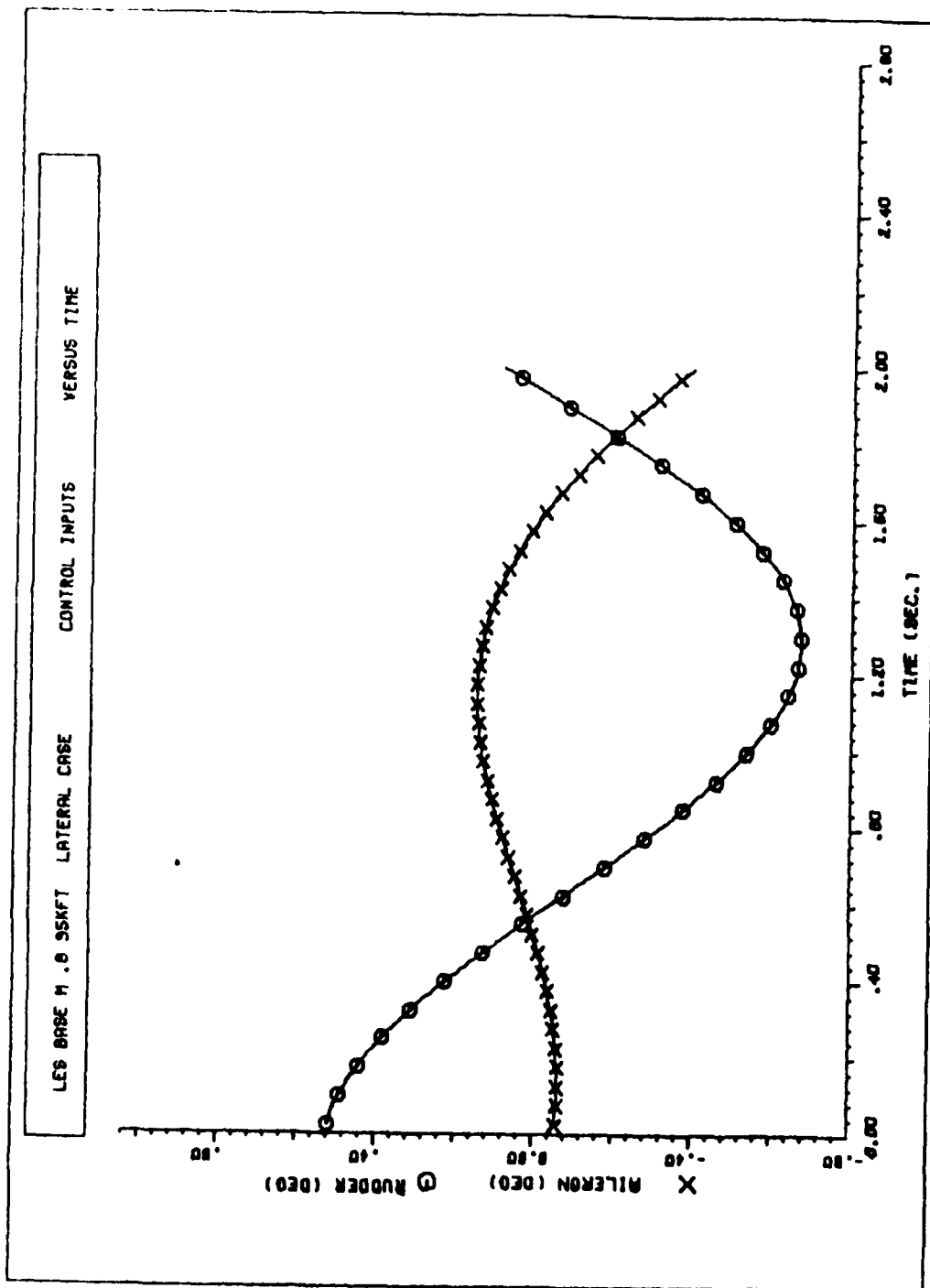


Figure B20 Baseline LES Lateral/Directional Controls to Reach \bar{v}_q ($t_f = 2.0$ Seconds)

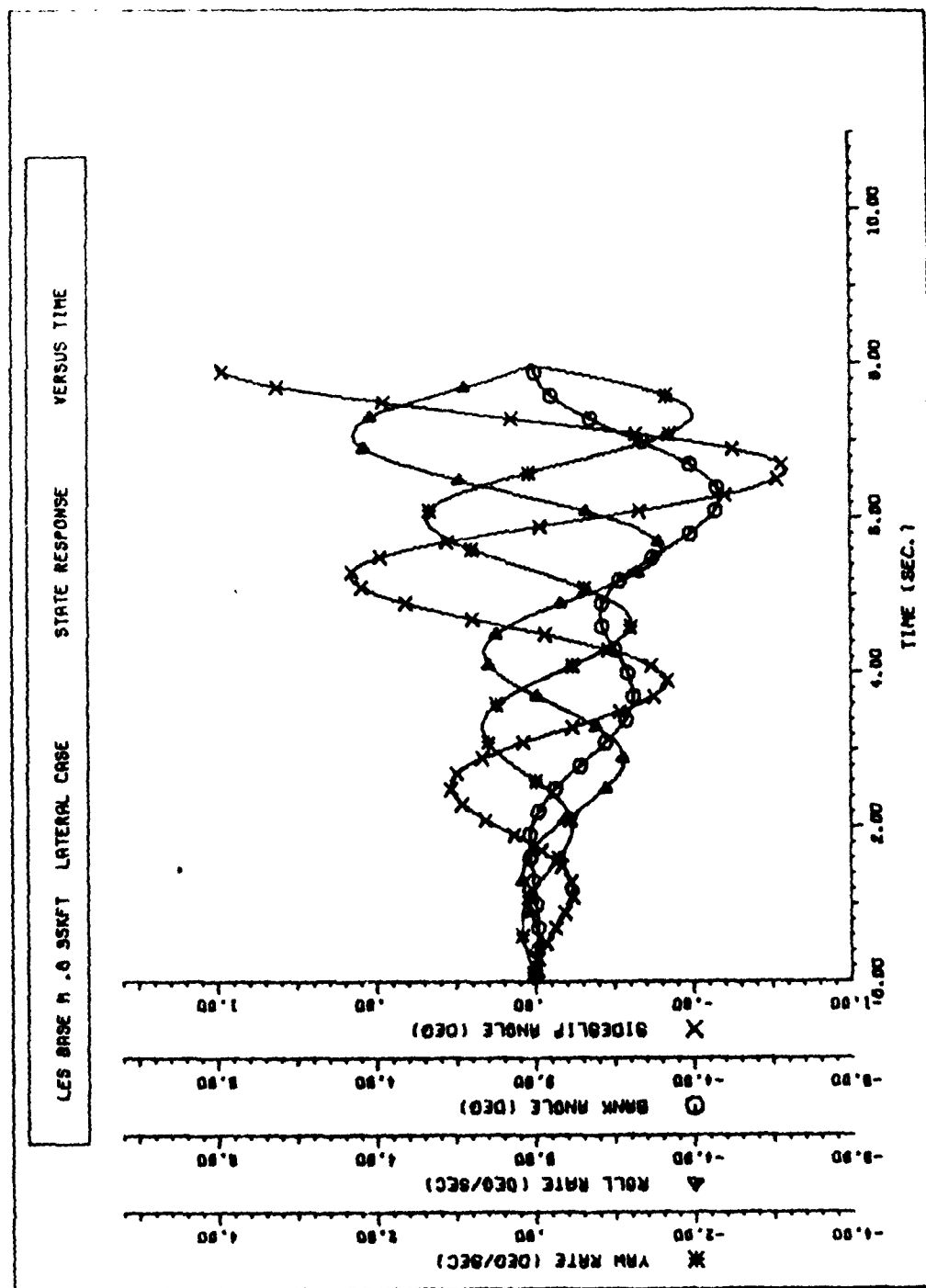


Figure B21 Baseline LES Lateral/Directional Response to Reach \bar{v}_d ($t_f = 8.0$ Seconds)

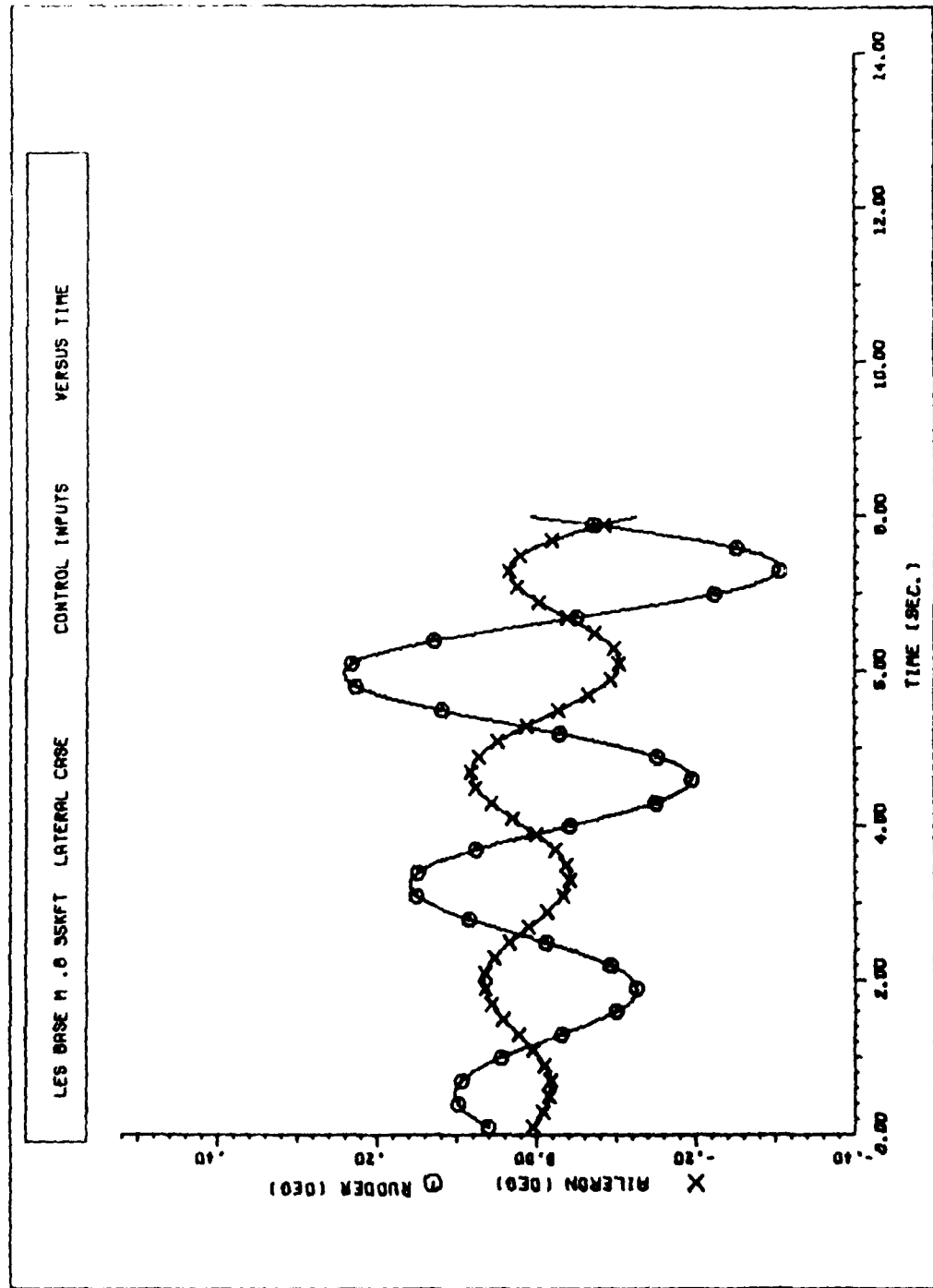


Figure B22 Baseline LES Lateral/Directional Controls to Reach \bar{v}_4 ($t_f = 8.0$ Seconds)

AD-A115 549

AIR FORCE INST OF TECH WRIGHT-PATTERSON AFB OH SCHOO--ETC F/G 20/4
CALCULATING AIRCRAFT CONTROLLABILITY QUALITY.(U)

DEC 79 J M YARGER

UNCLASSIFIED

AFIT/GAE/AA/79D-19

NL

2 2

2 2

END

DATE

FORMED

7 82

DATE

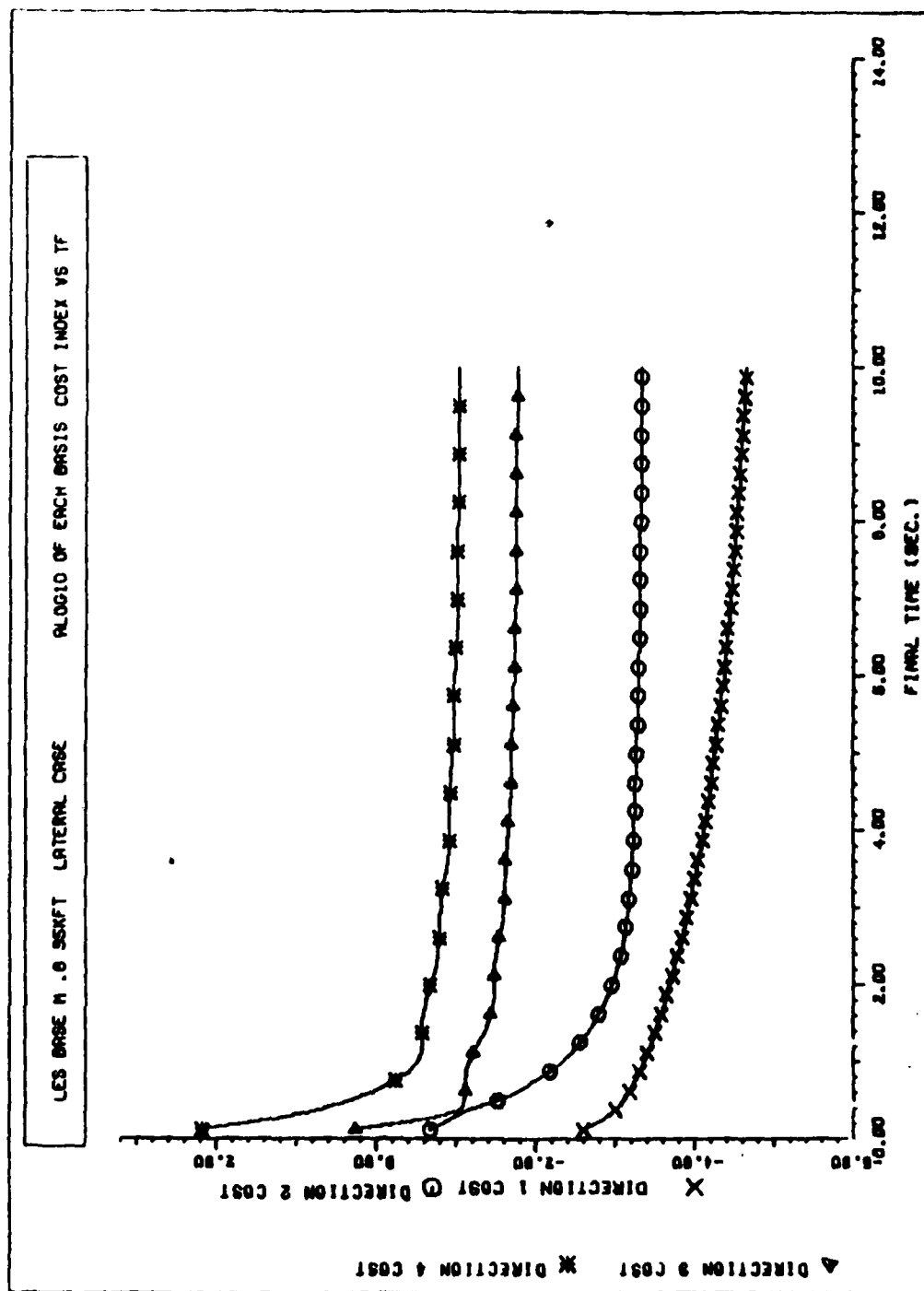


Figure B23 Log₁₀ of Baseline LES Weighted Control Costs for All Lateral/Directional Basis Vectors

Appendix C: Sample Output for Modified LES 230-Y

This is a collection of sample output data generated for the Boeing LES 230-Y using the proposed new flight control system at the flight conditions outlined in Chapter V.

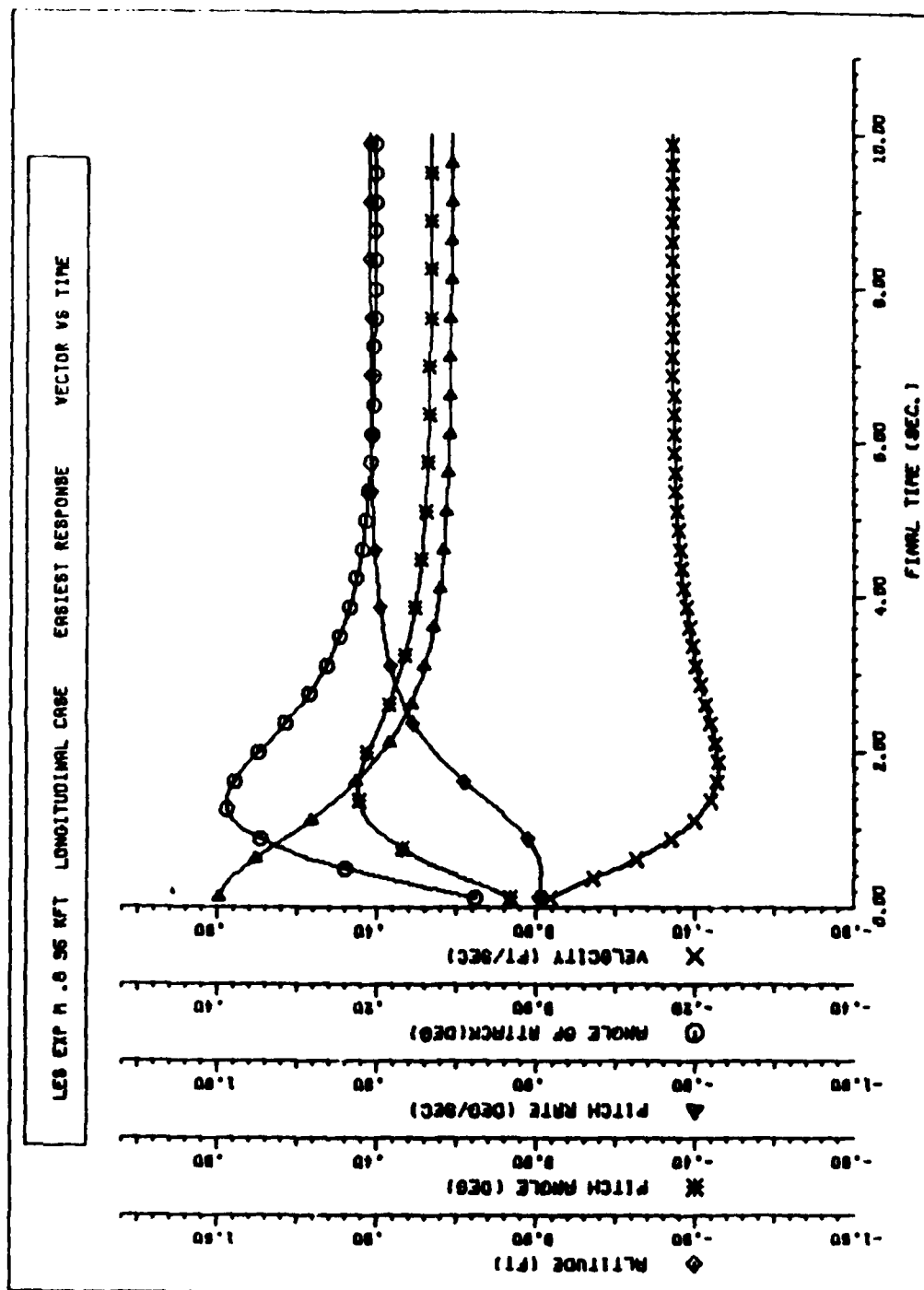


Figure C1 Experimental LES Longitudinal $\vec{v}_3(t_f)$

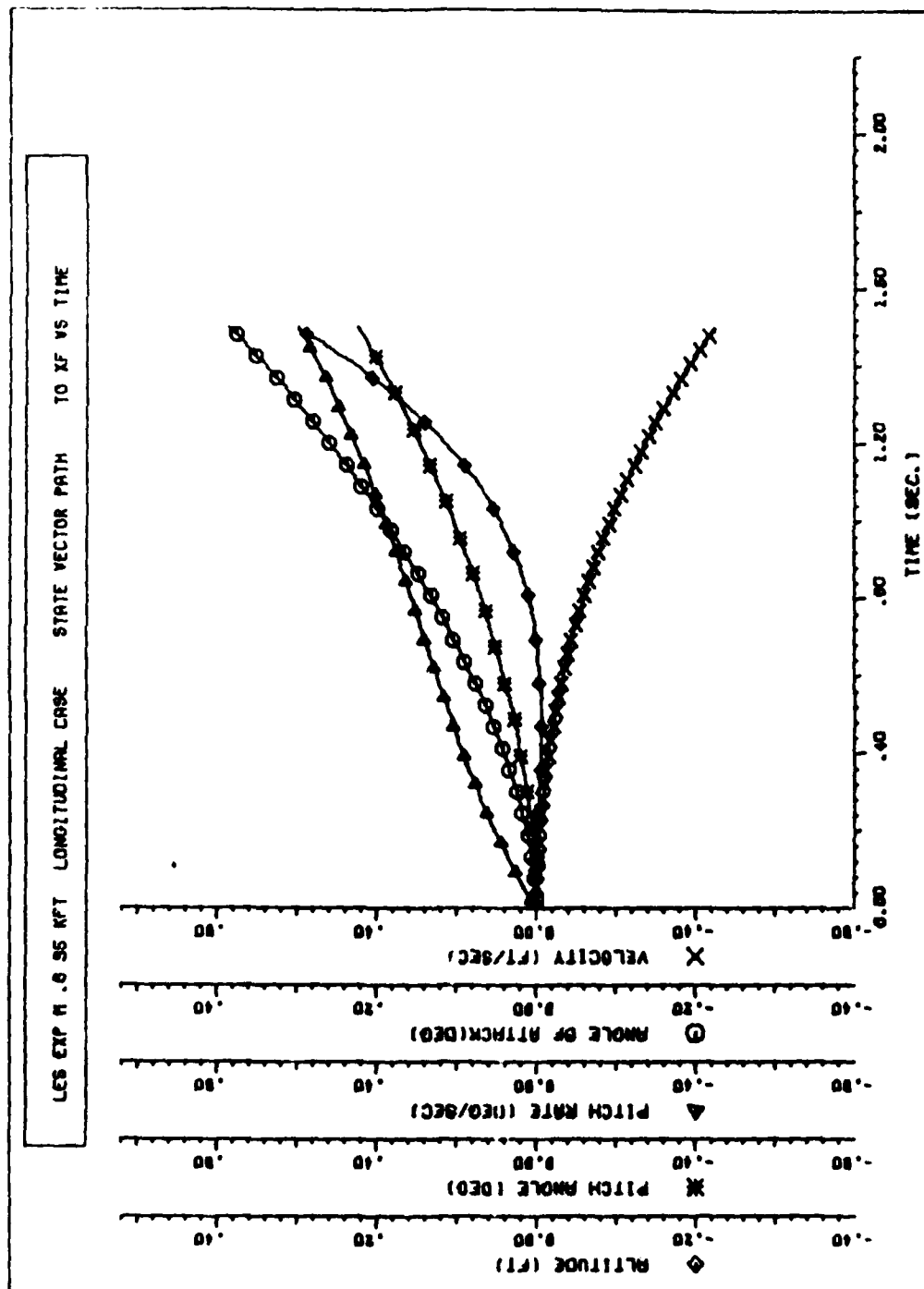


Figure C2 Experimental LES Longitudinal Response to Reach \bar{u}_1 ($t_f = 1.5$ Seconds)

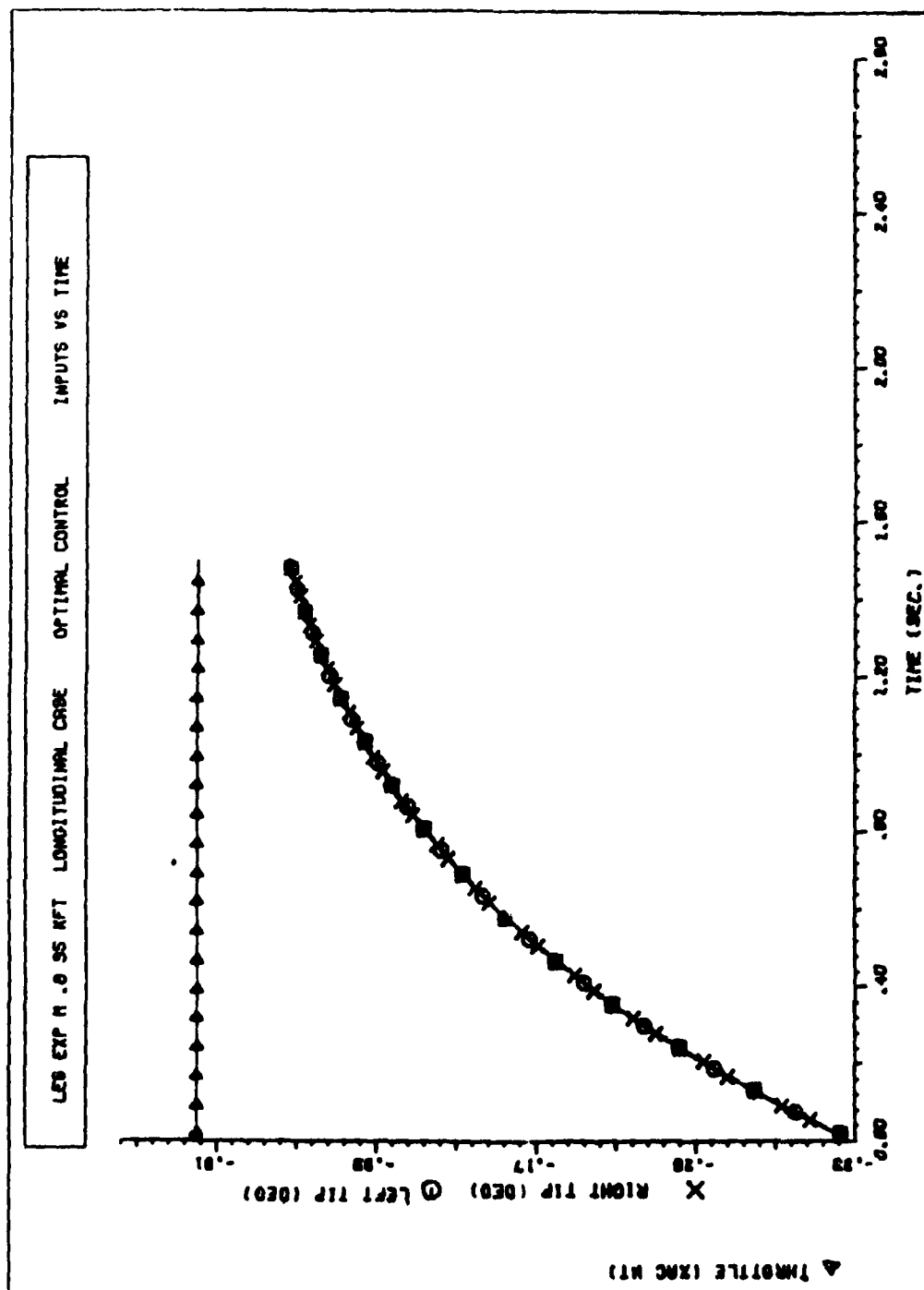


Figure C3 Experimental LES Longitudinal Controls to Reach \bar{v}_1 ($t_f = 1.5$ Seconds)

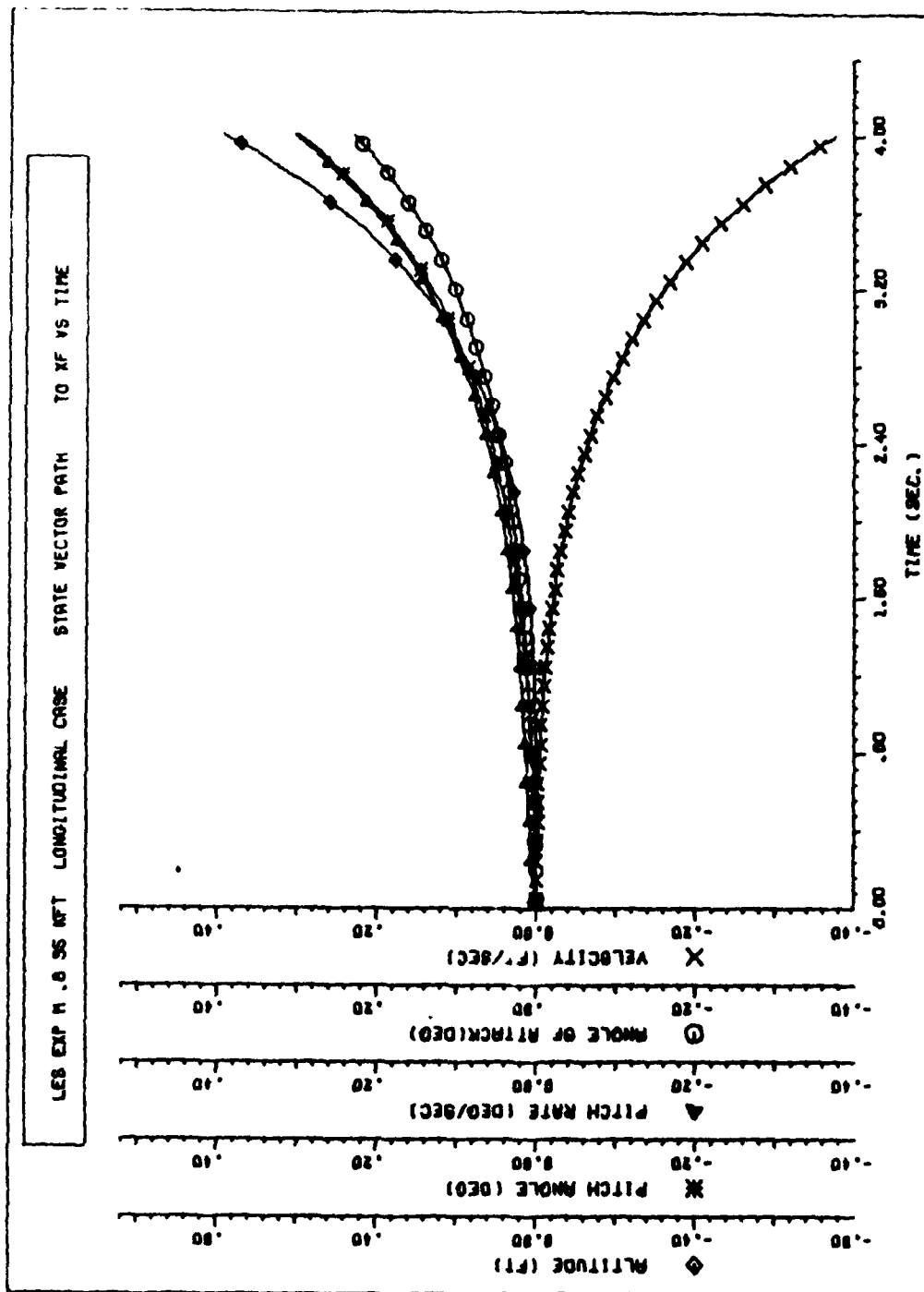


Figure C4 Experimental LES Longitudinal Response to Reach \bar{v}_1 ($t_f = 4.0$ Seconds)

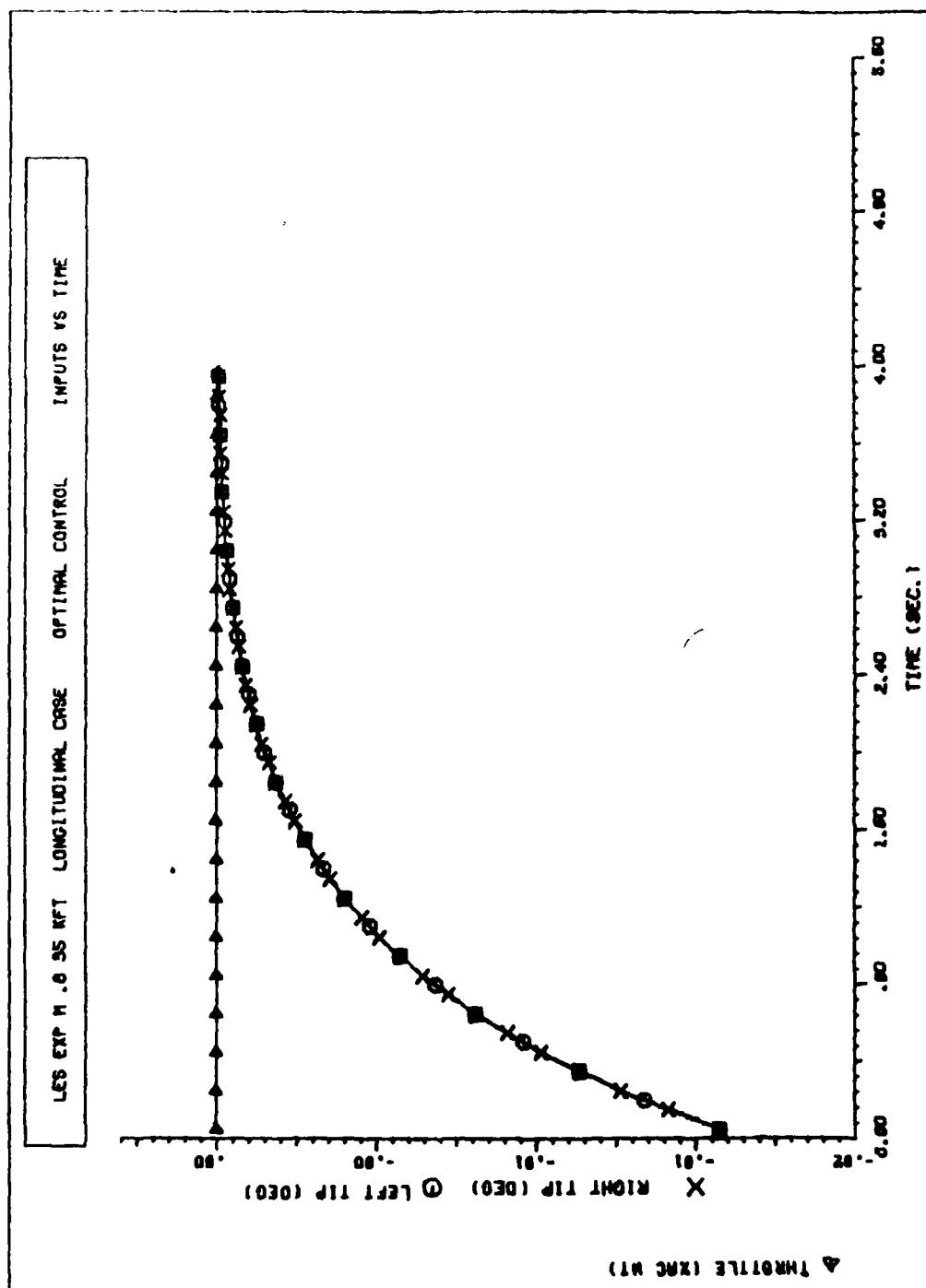


Figure C5 Experimental LES Longitudinal Controls to Reach \bar{v}_d ($t_f = 4.0$ Seconds)

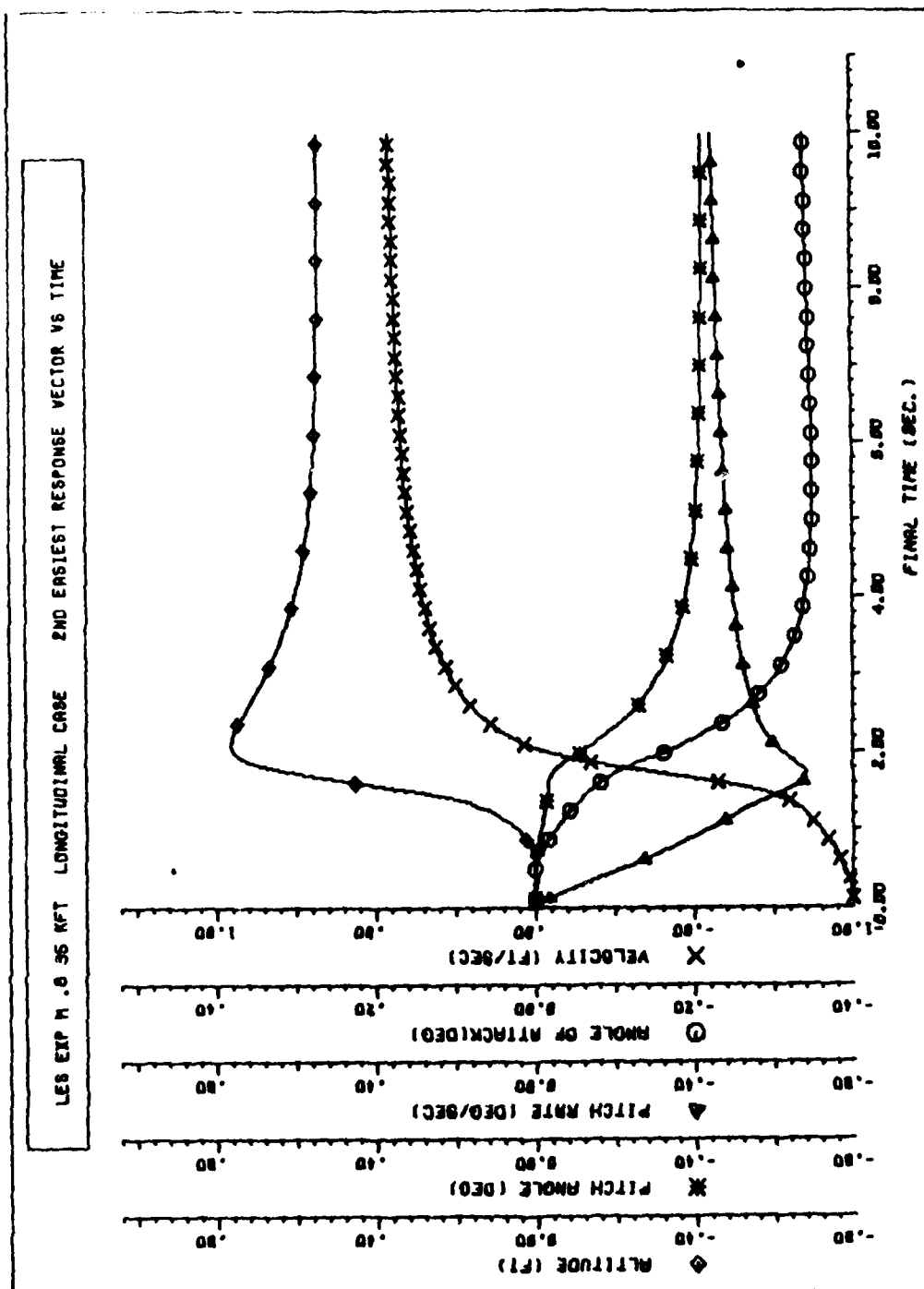


Figure C6 Experimental LES Longitudinal $\bar{v}_a(t_f)$

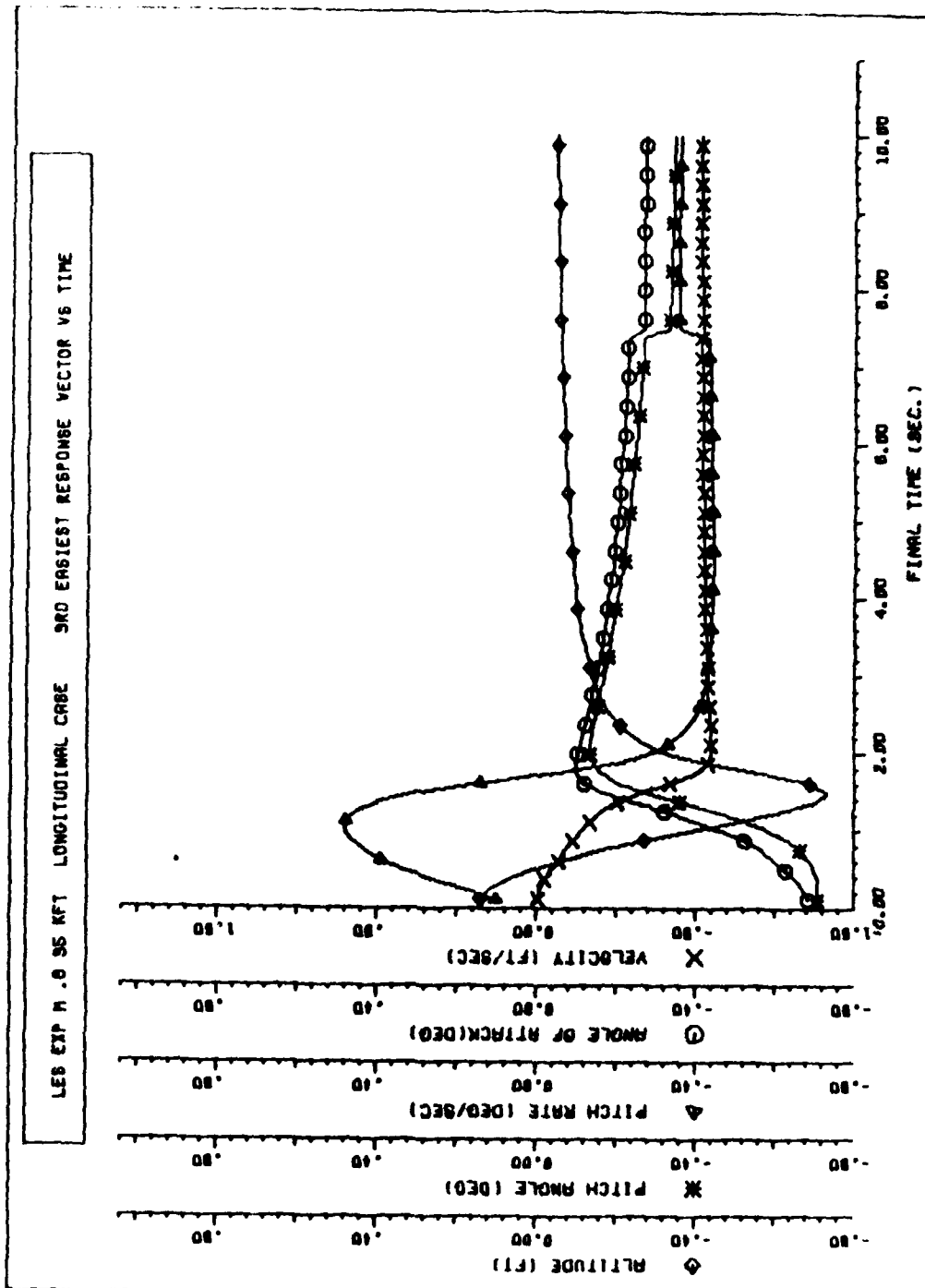


Figure C7 Experimental LES Longitudinal $\bar{v}_3(t_f)$

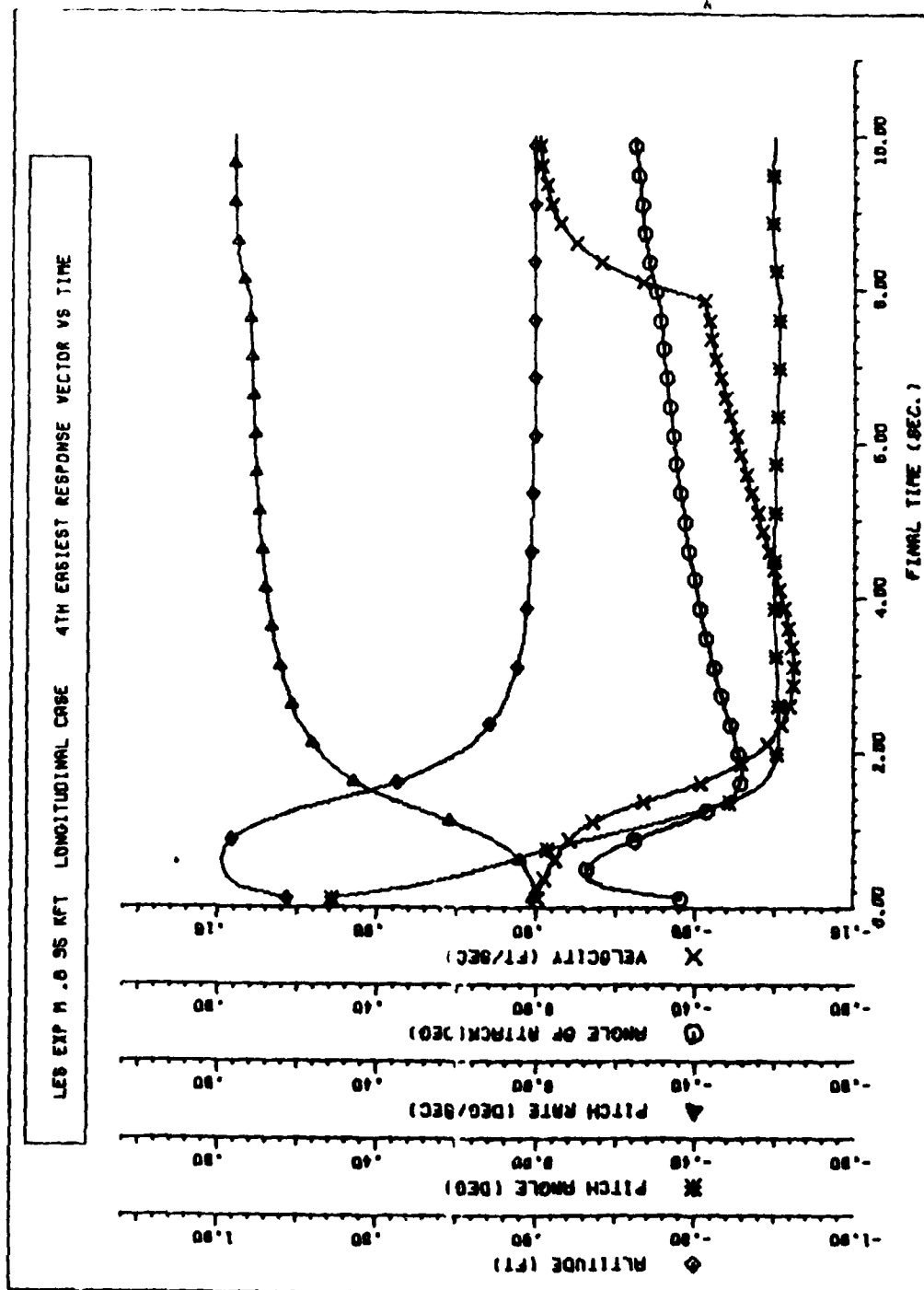


Figure C8 Experimental LES Longitudinal $\bar{v}_q(t_f)$

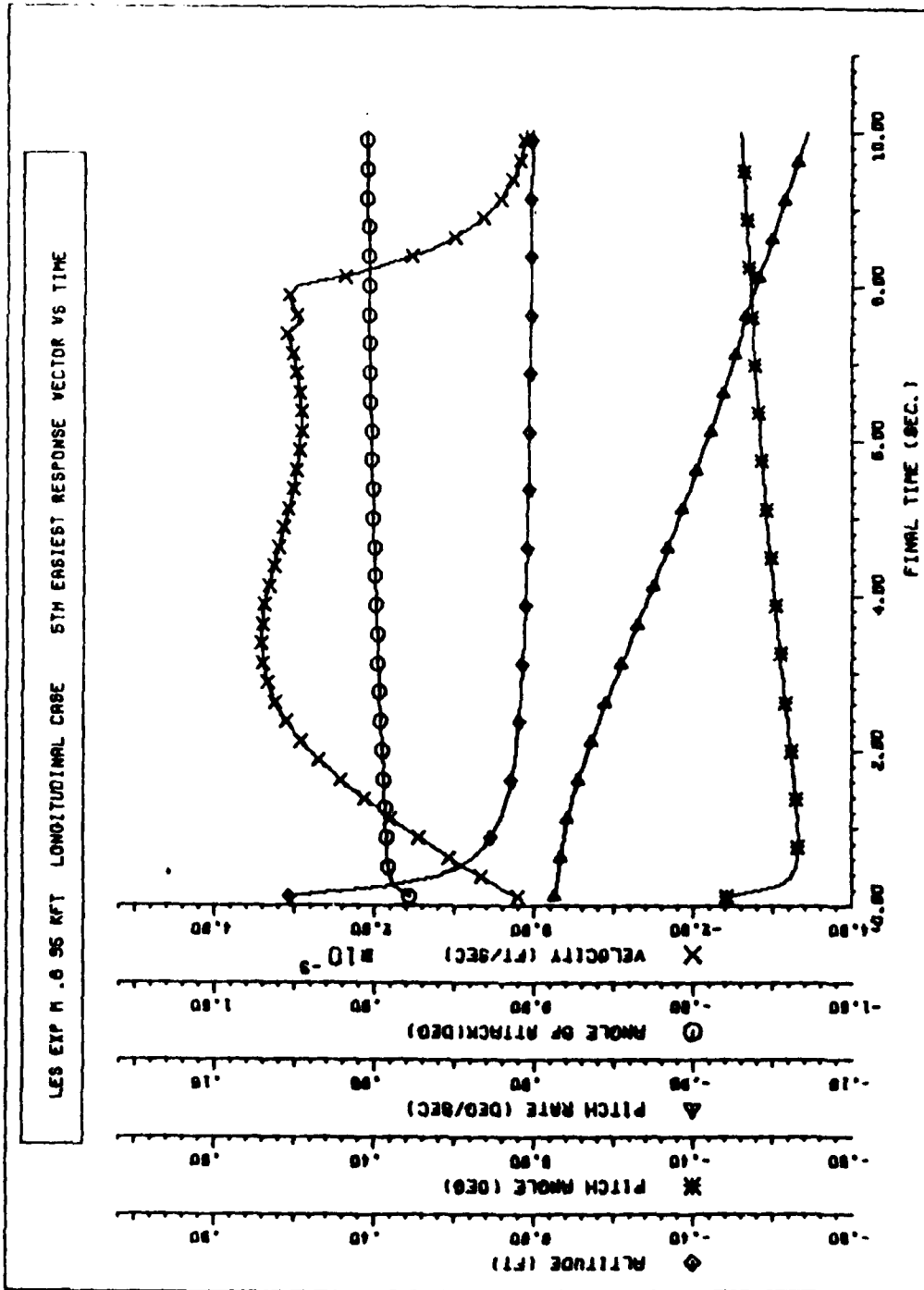


Figure C9 Experimental LES Longitudinal $\vec{v}_s(t_f)$

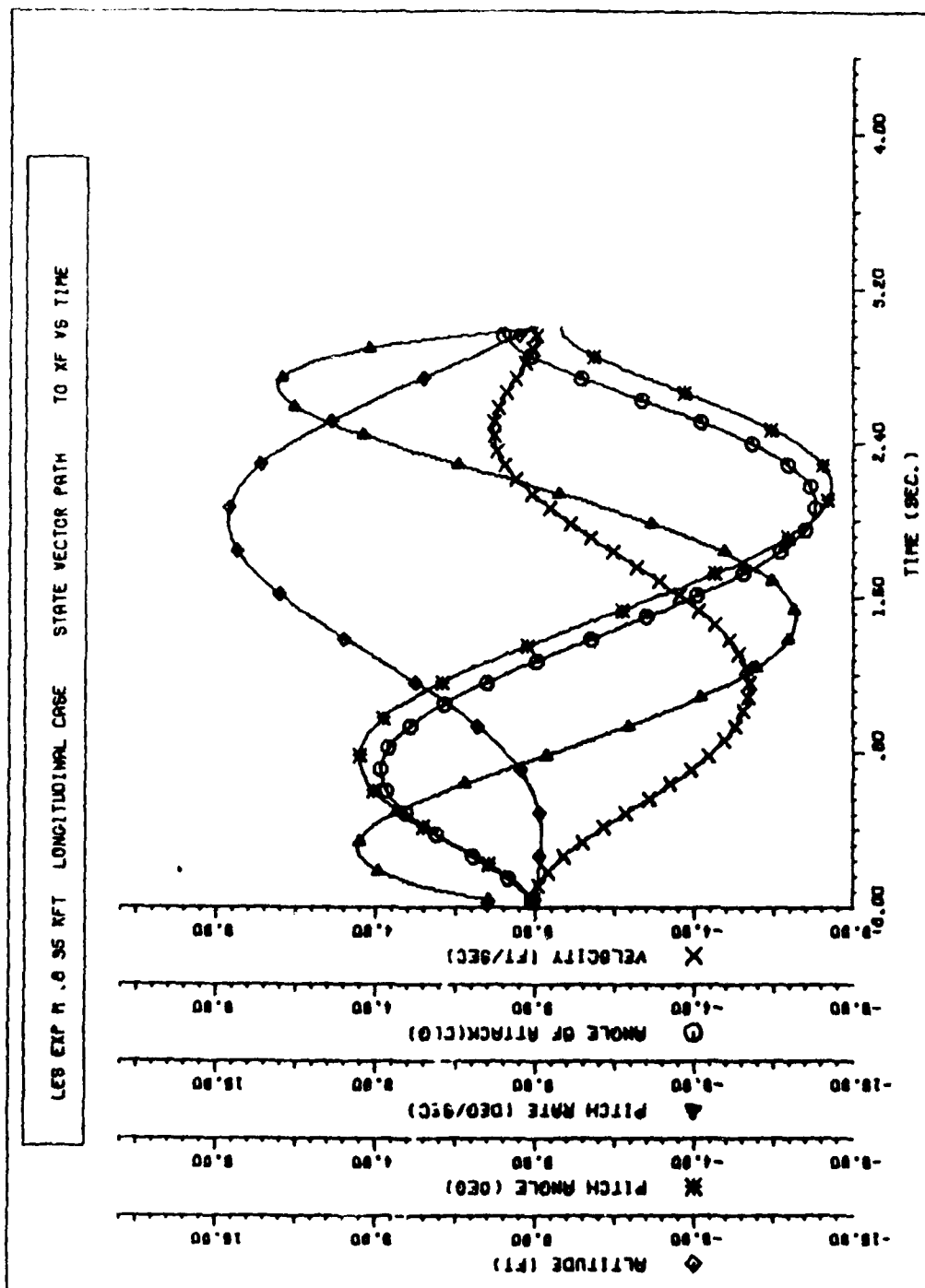


Figure C10 Experimental LES Longitudinal Response to Reach $\bar{u}_5 (t_f = 3.0 \text{ Seconds})$

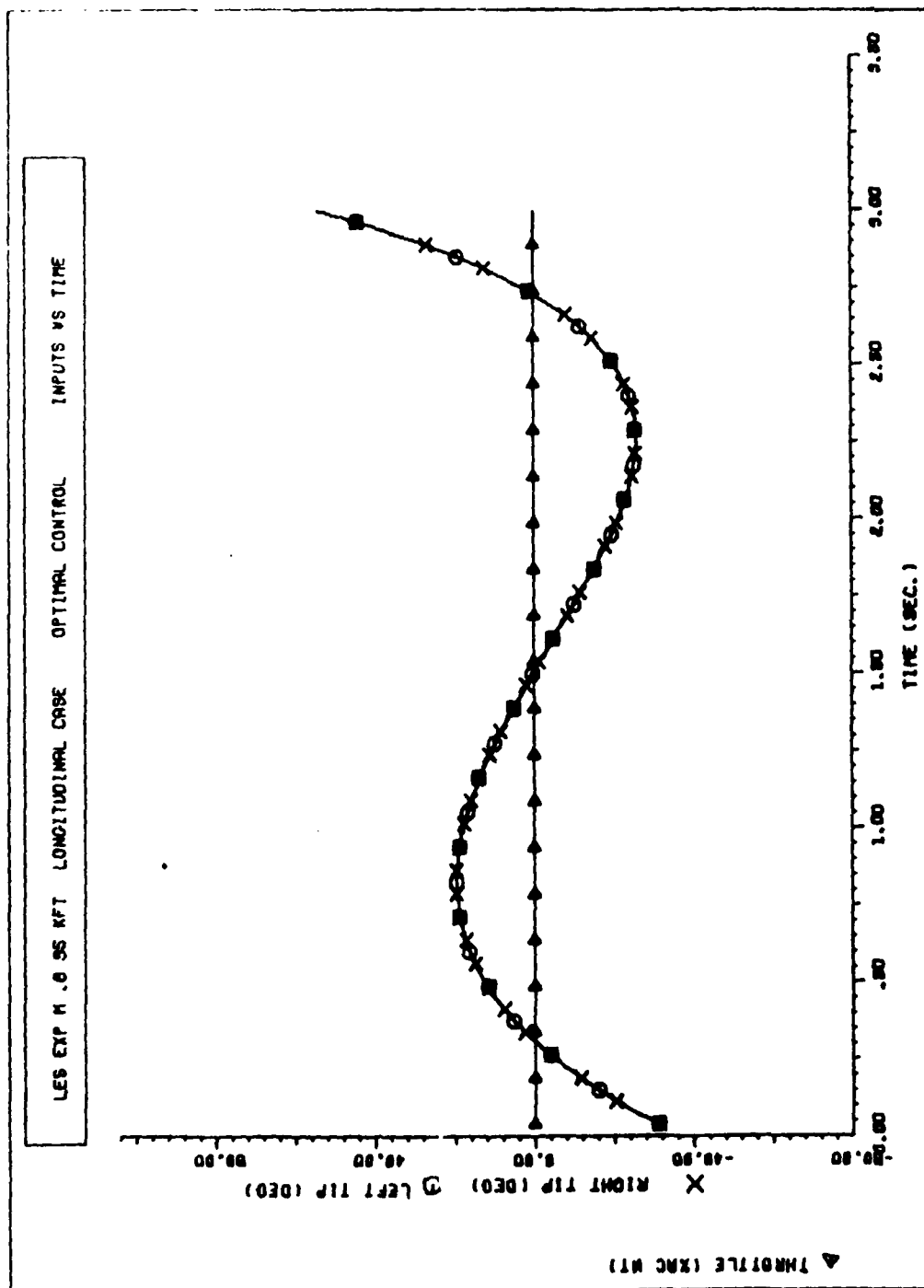


Figure C11 Experimental LES Longitudinal Controls to Reach ϑ_f ($t_f = 3.0$ Seconds)

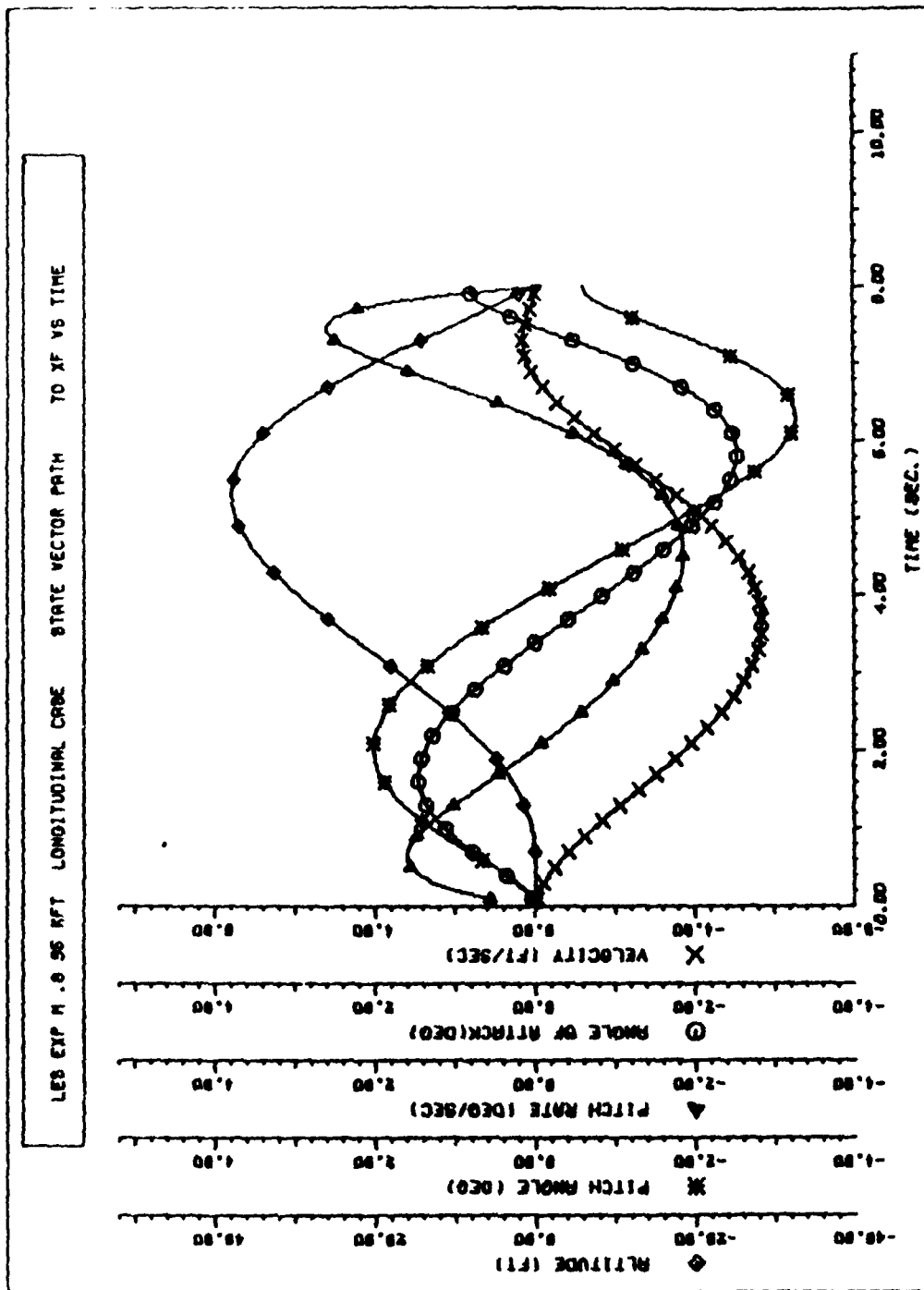


Figure C12 Experimental LES Longitudinal Response to Reach \bar{v}_x ($t_f = 8.0$ Seconds)

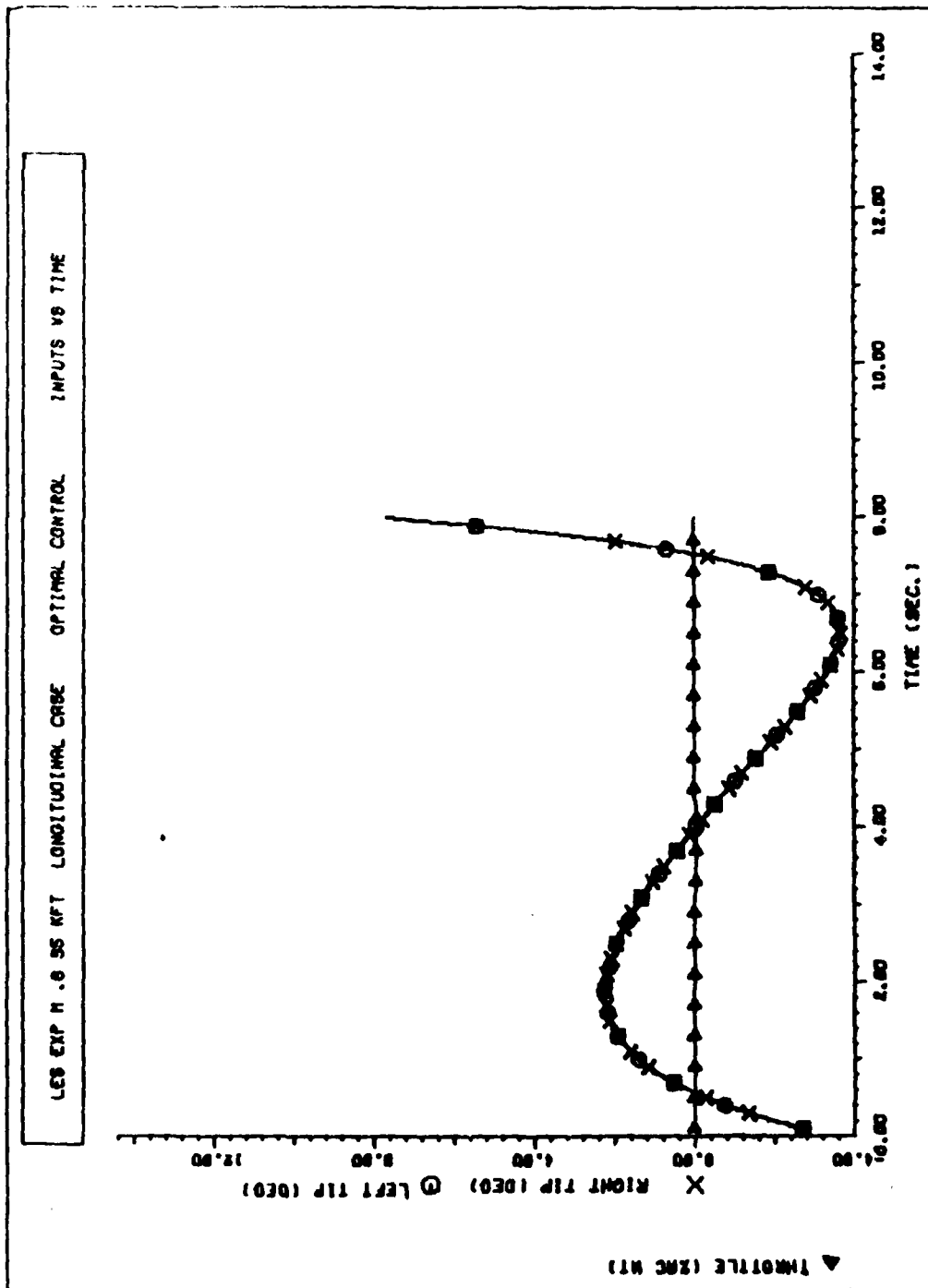


Figure C13 Experimental LES Longitudinal Controls to Reach \bar{v}_c ($t_f = 8.0$ Seconds)

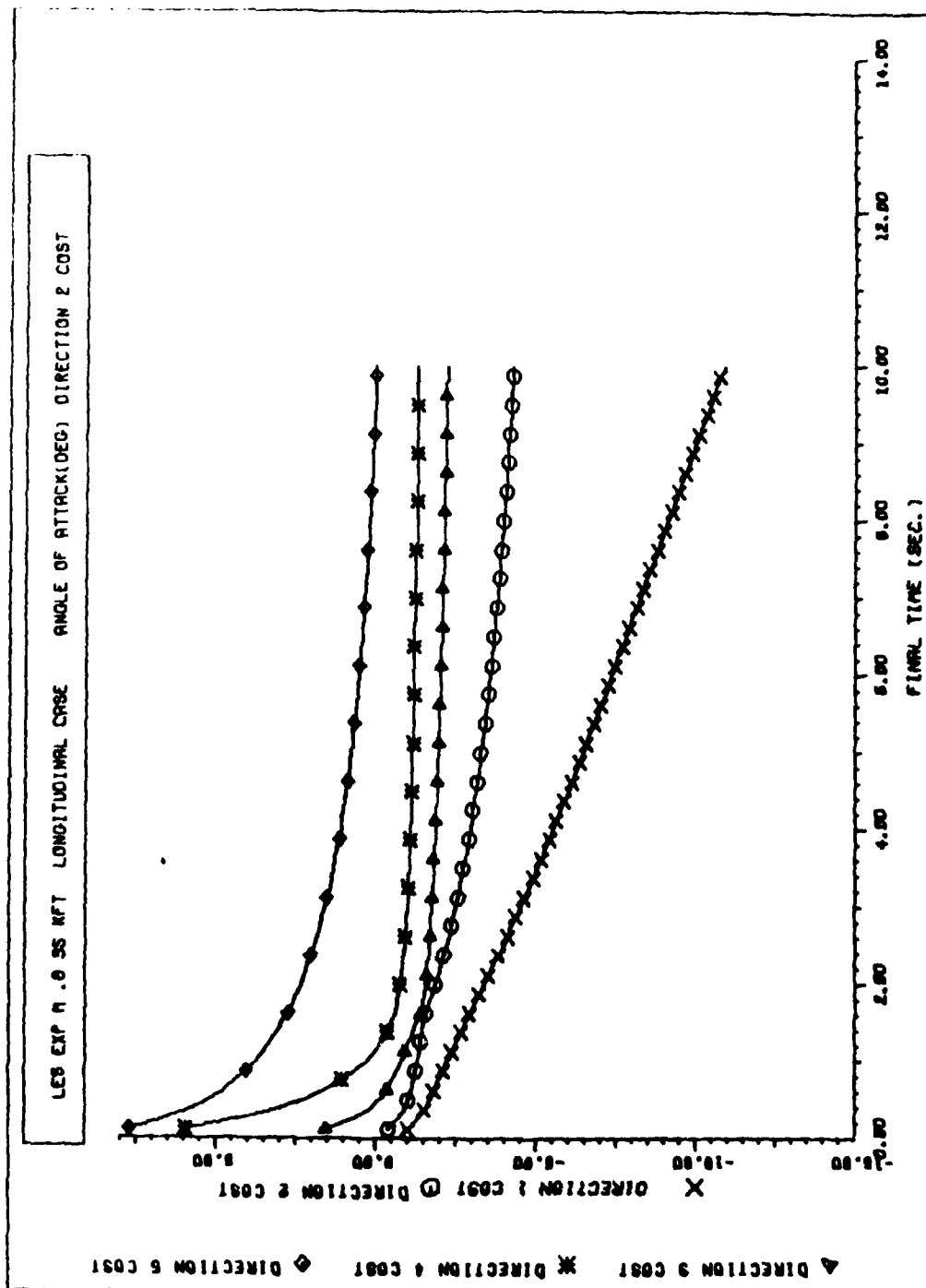


Figure C14 \log_{10} of Experimental LES Weighted Control Costs for All Longitudinal Basis Vectors

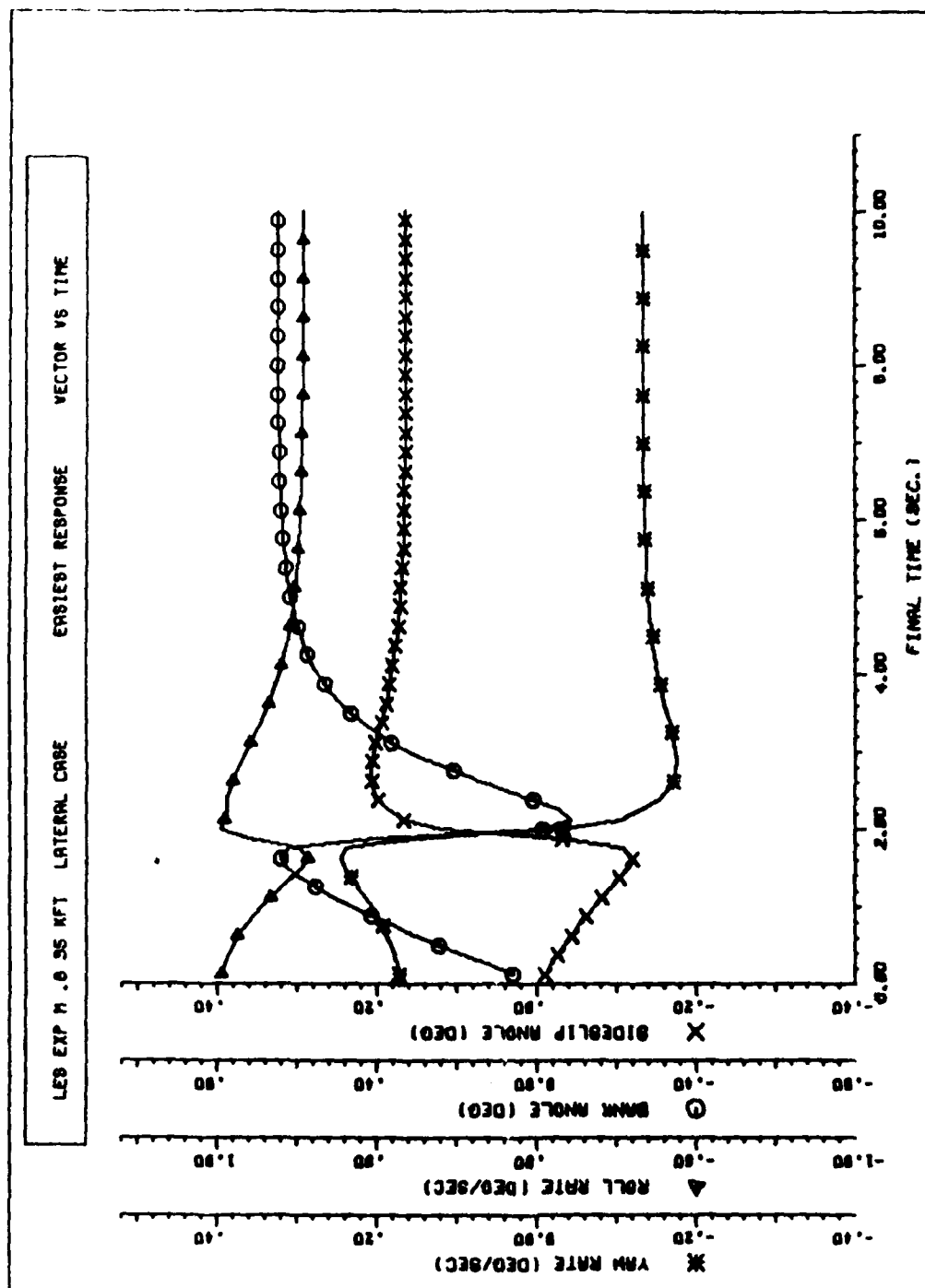


Figure C15 Experimental LES Lateral/Directional $\vec{v}_1(t_f)$

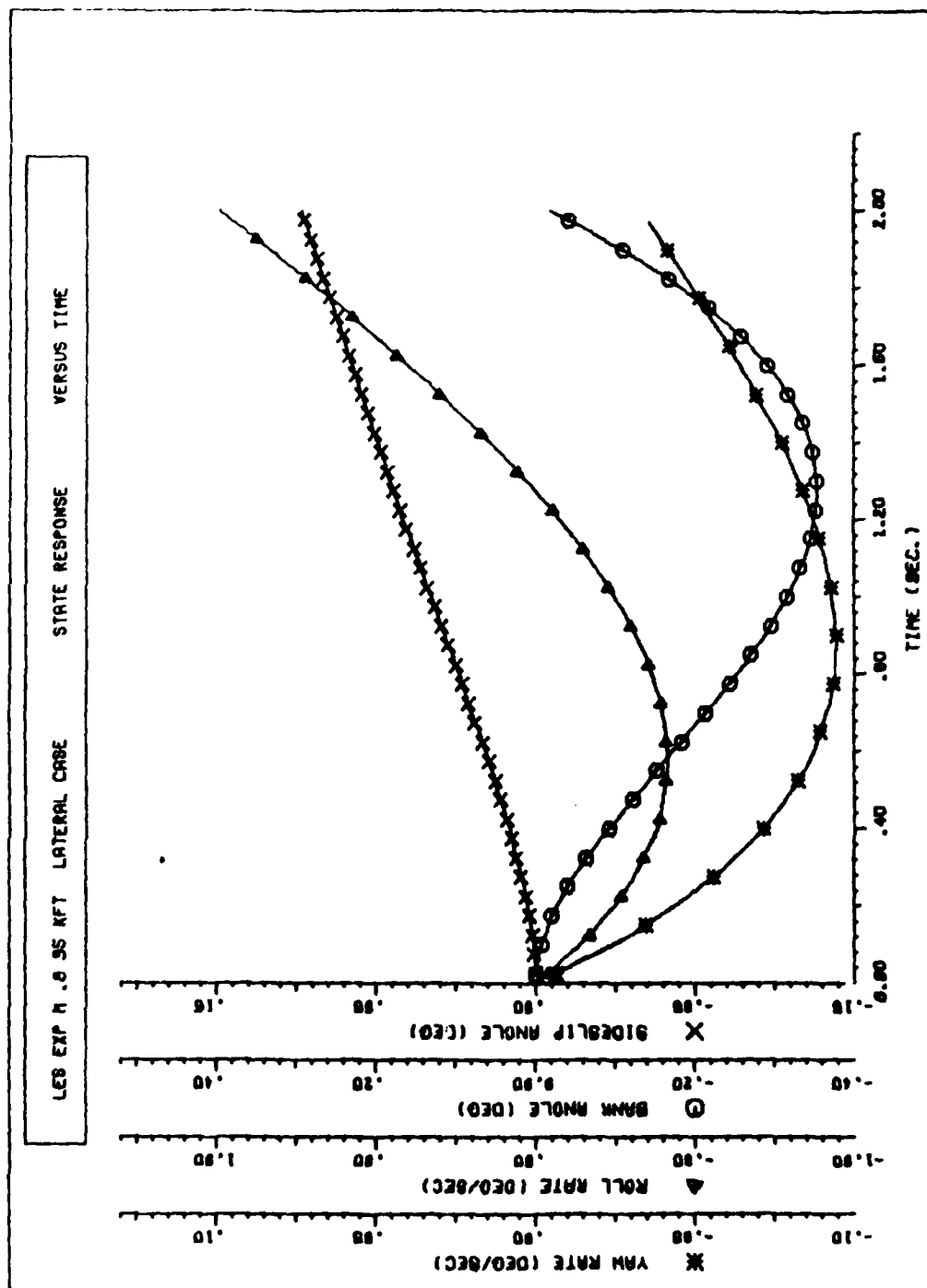


Figure C16 Experimental LES Lateral/Directional Response to Reach \bar{u} , ($t_f = 2.0$ Seconds)

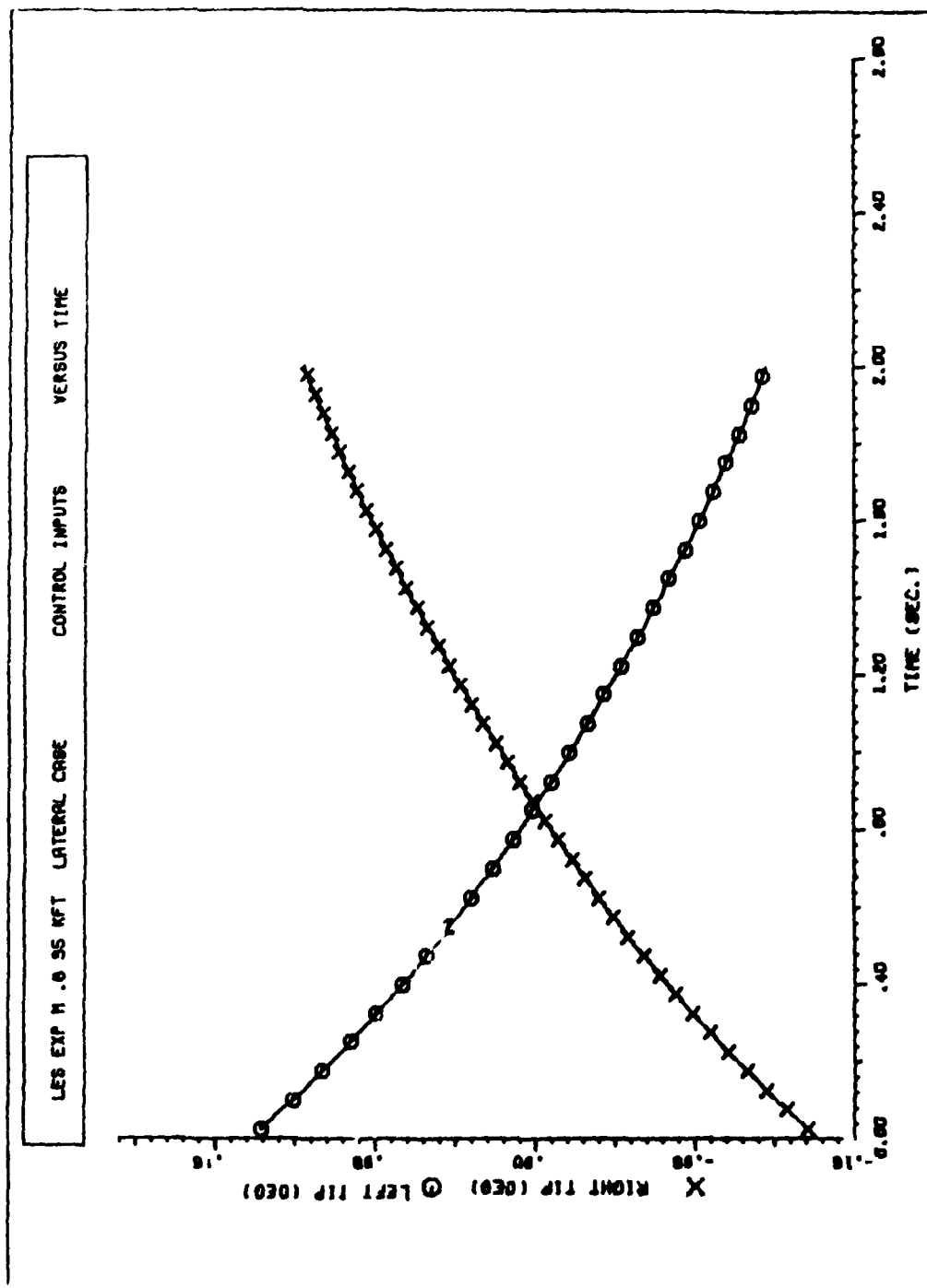


Figure C17 Experimental LES Lateral/Directional Controls to Reach $\bar{\theta}_1$ ($t_f = 2.0$ Seconds)

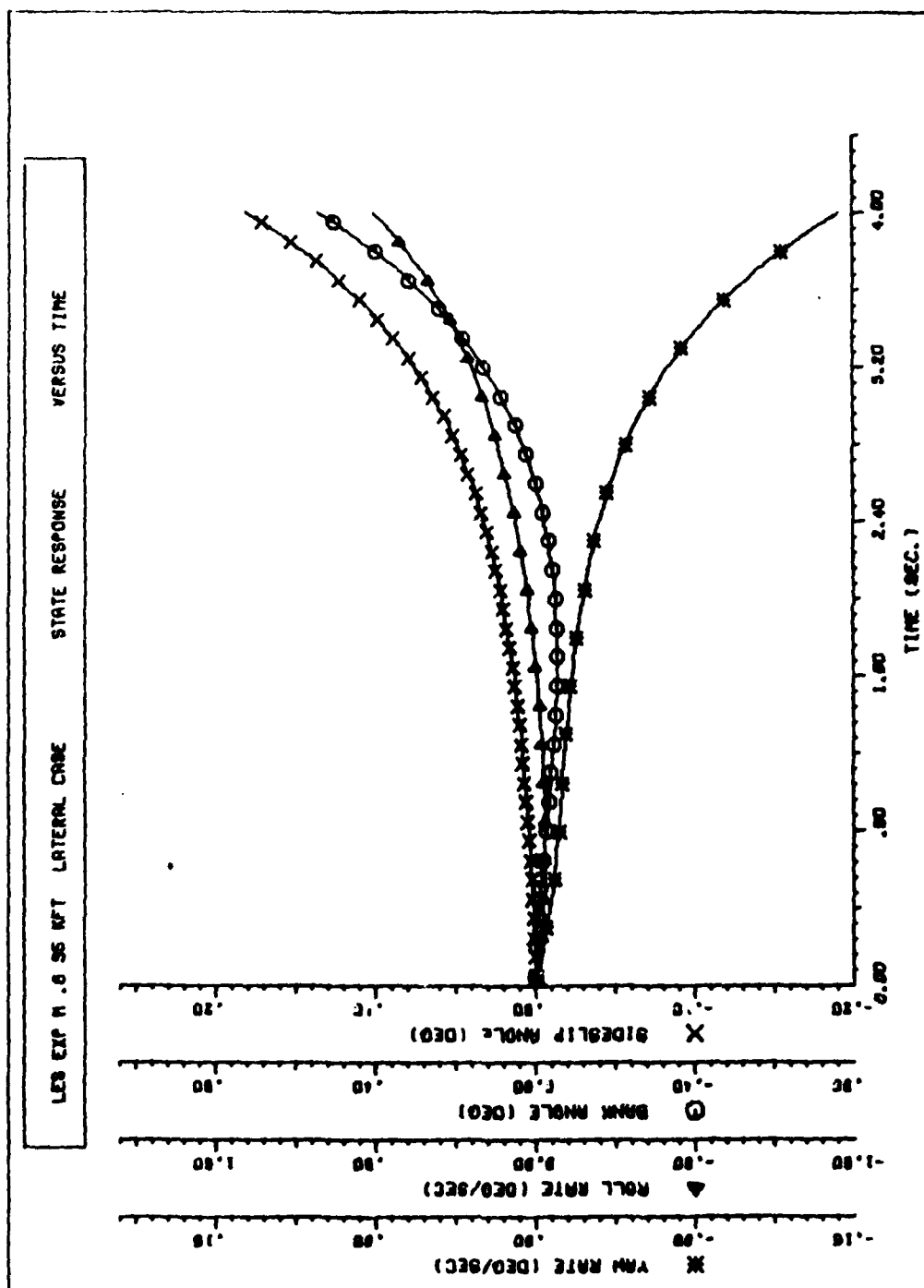


Figure C18 Experimental LES Lateral/Directional Response to Reach \bar{v}_i ($t_f = 4.0$ Seconds)

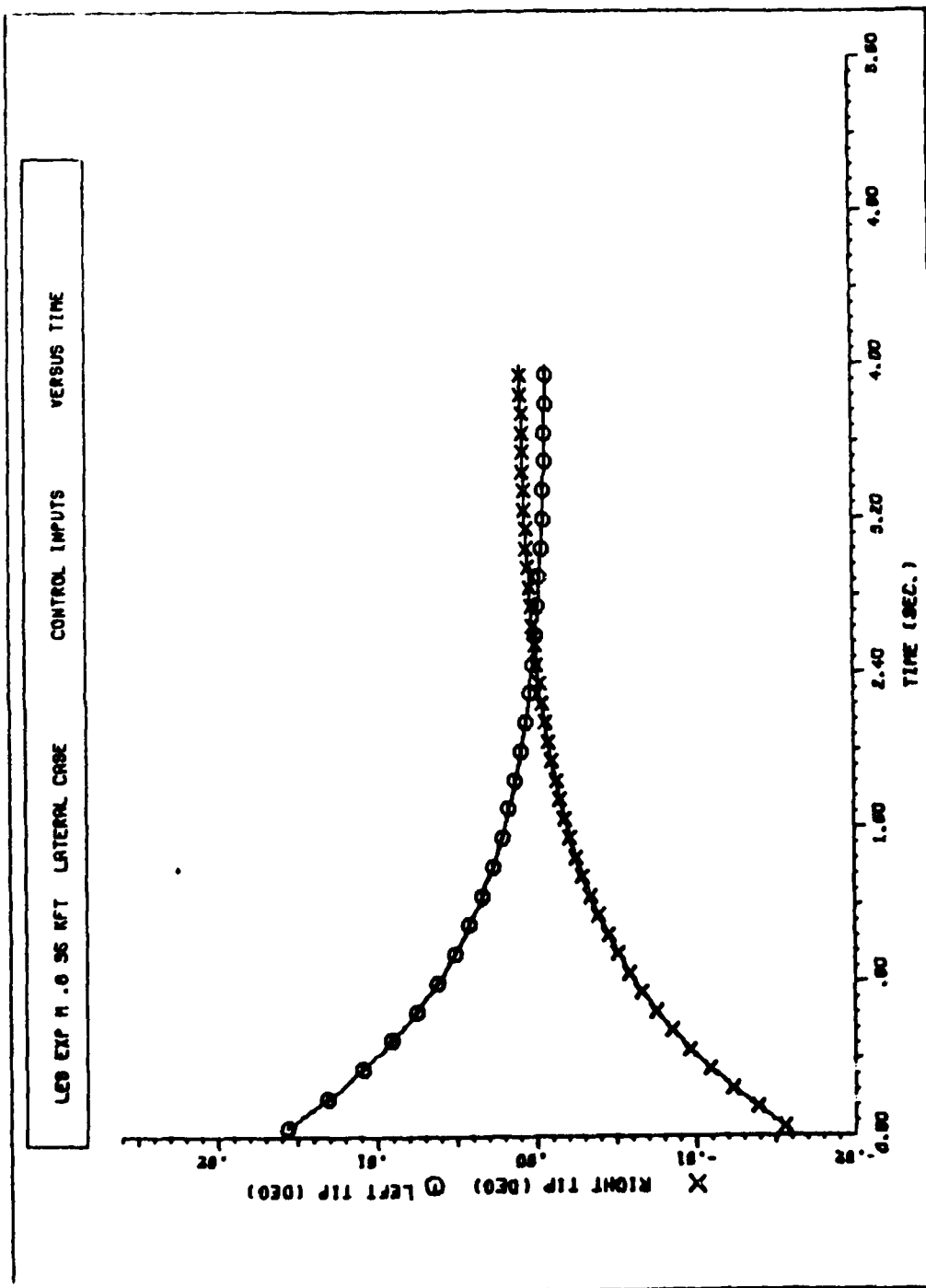


Figure C19 Experimental LES Lateral/Directional Controls to Reach \bar{v}_1 ($t_f = 4.0$ Seconds)

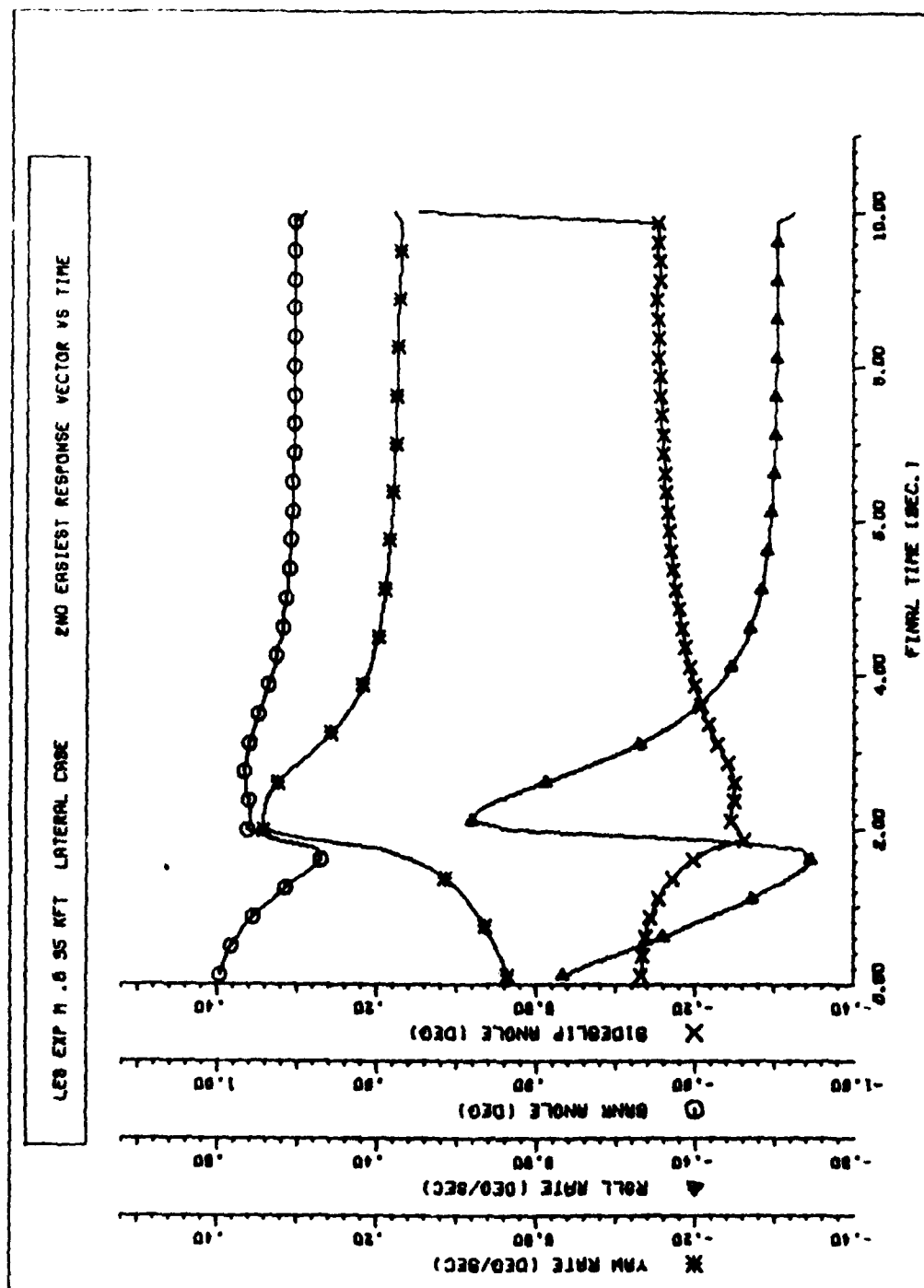


Figure c20 Experimental LES Lateral/Directional $\vec{v}_2(t_f)$

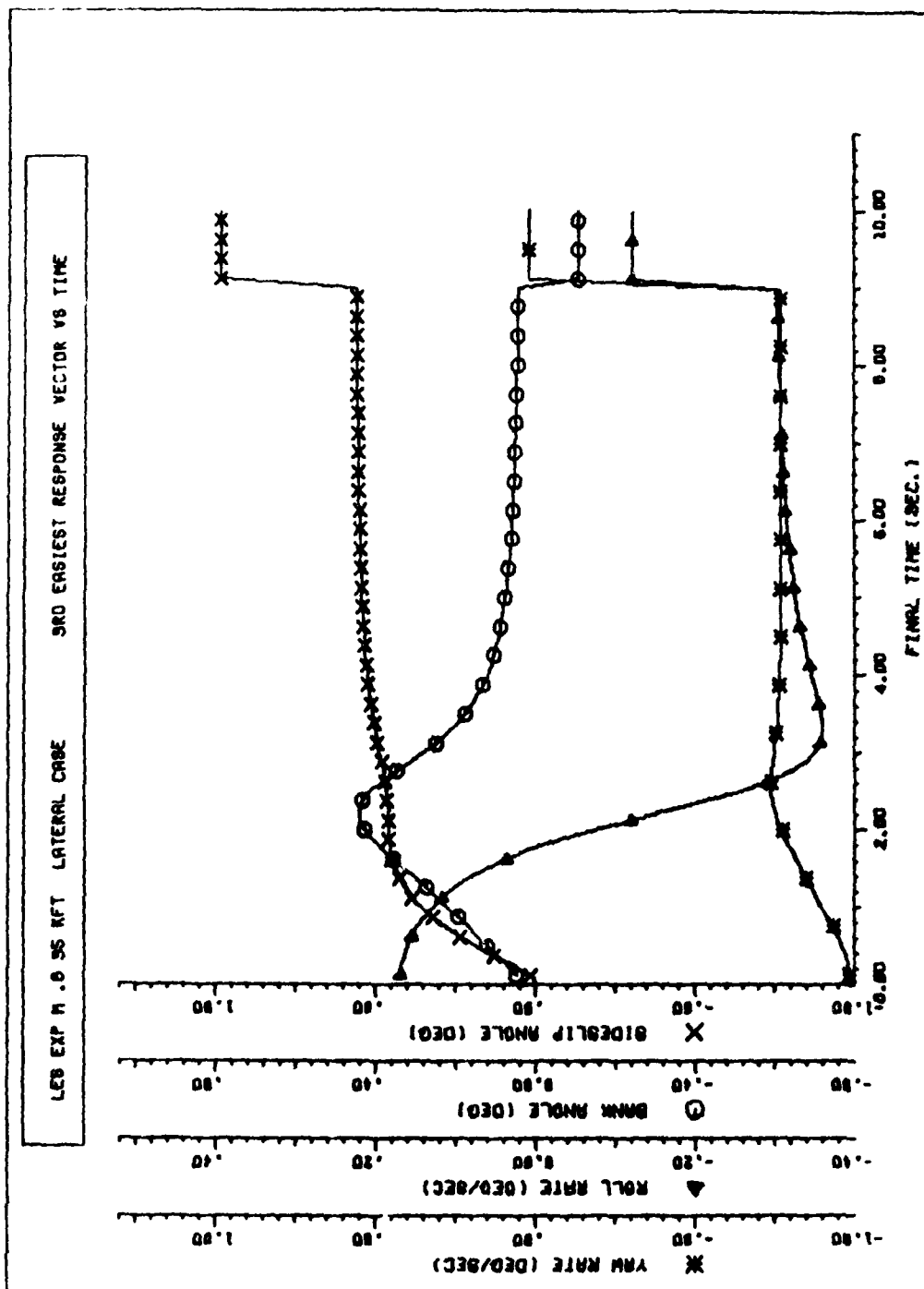


Figure c21 Experimental LES Lateral/Directional $\bar{U}_3(t_f)$

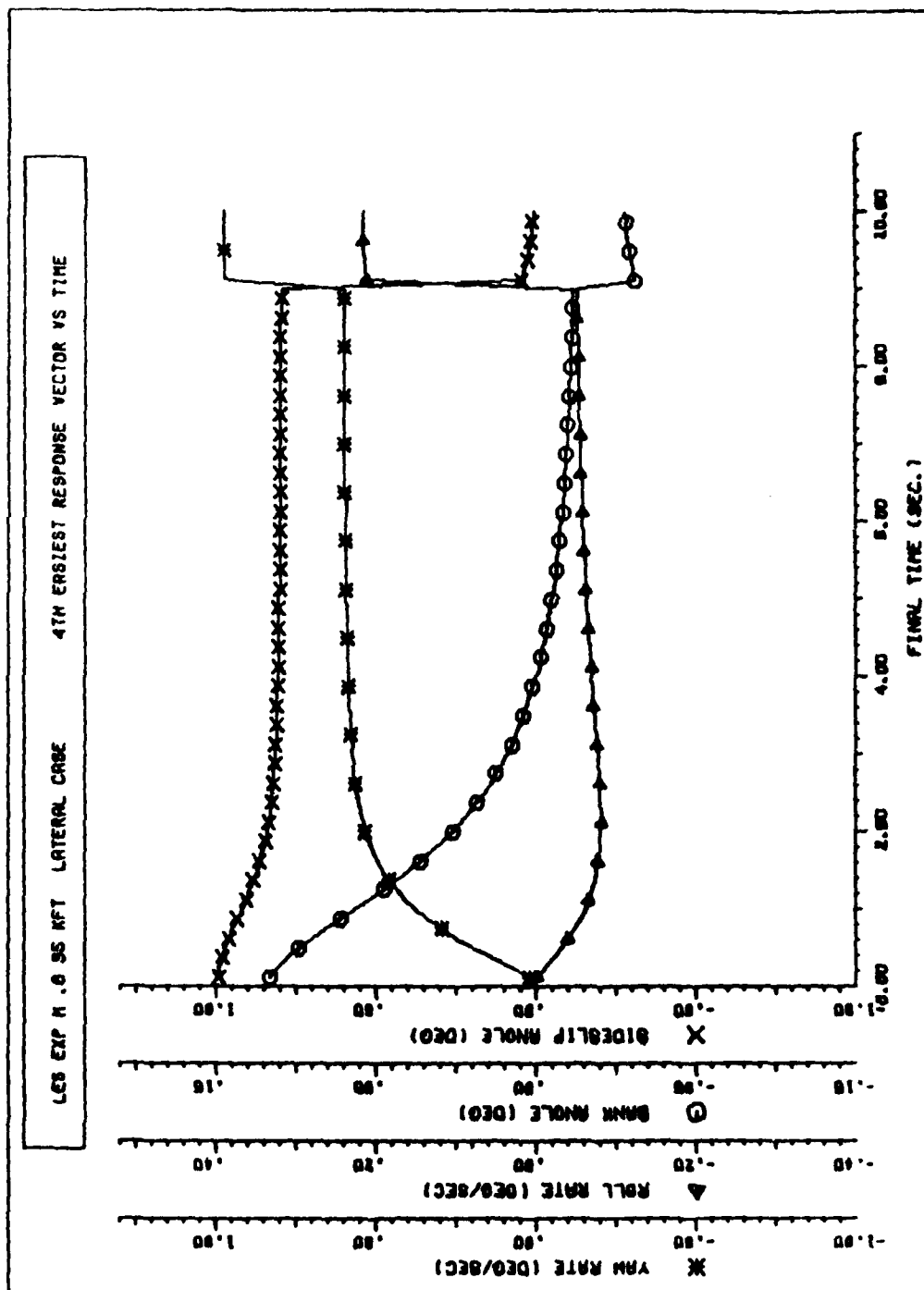


Figure 022 Experimental LES Lateral/Directional $\bar{V}_4(t_f)$

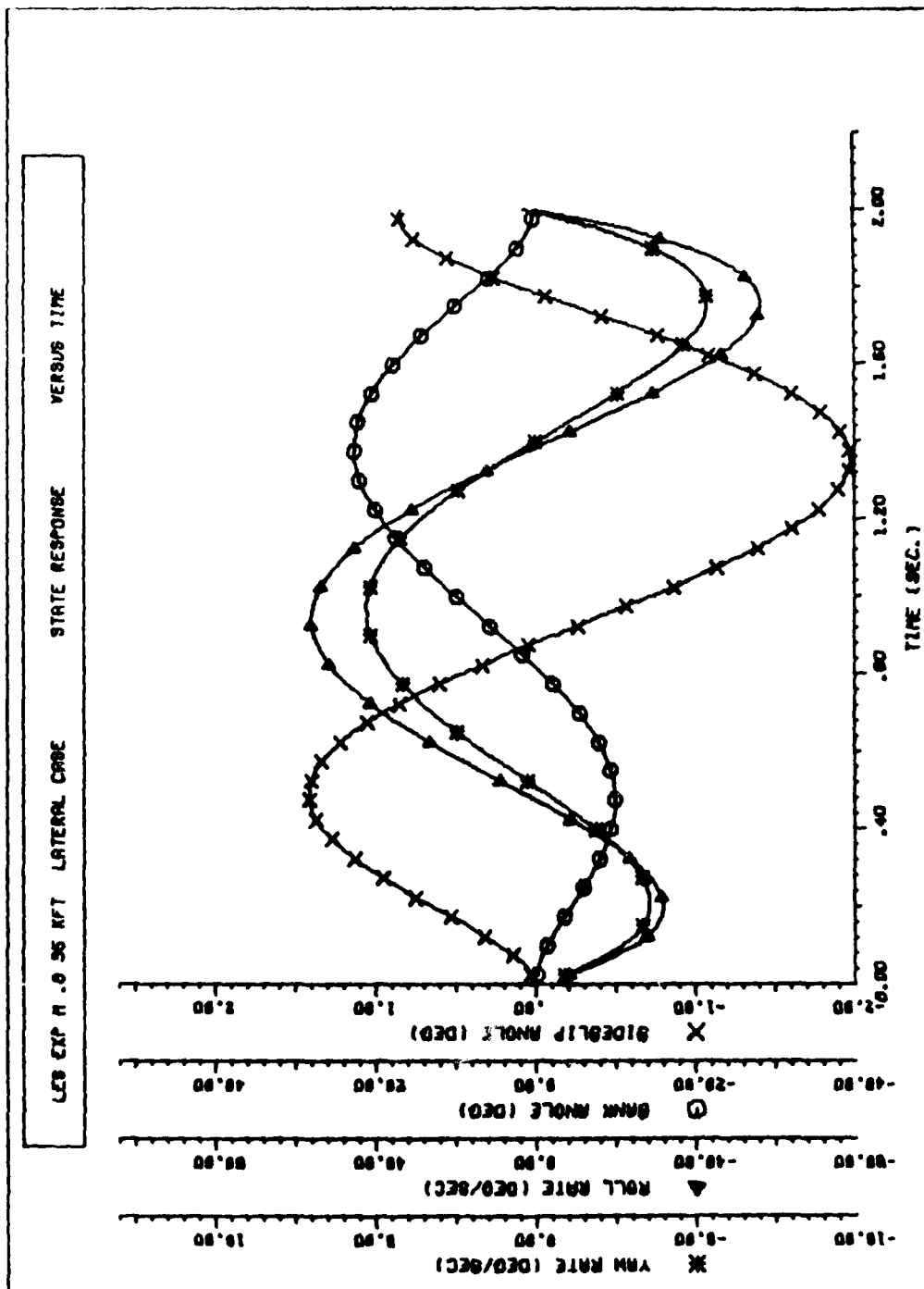


Figure C23 Experimental LES Lateral/Directional Response to Reach \bar{v}_4 ($t_f = 2.0$ Seconds)

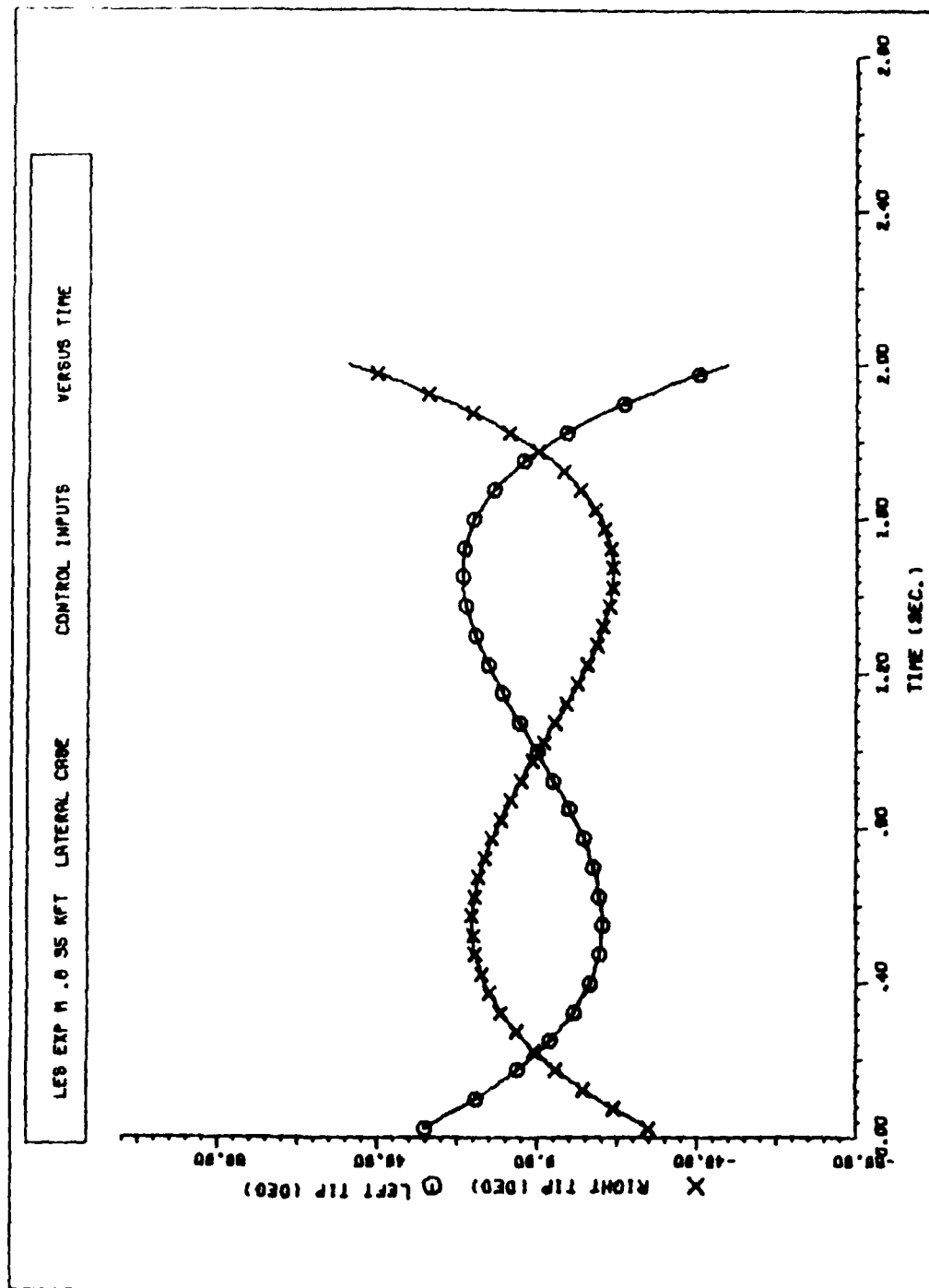


Figure C24 Experimental LES Lateral/Directional Controls to Reach \bar{v}_4 ($t_f = 2.0$ Seconds)

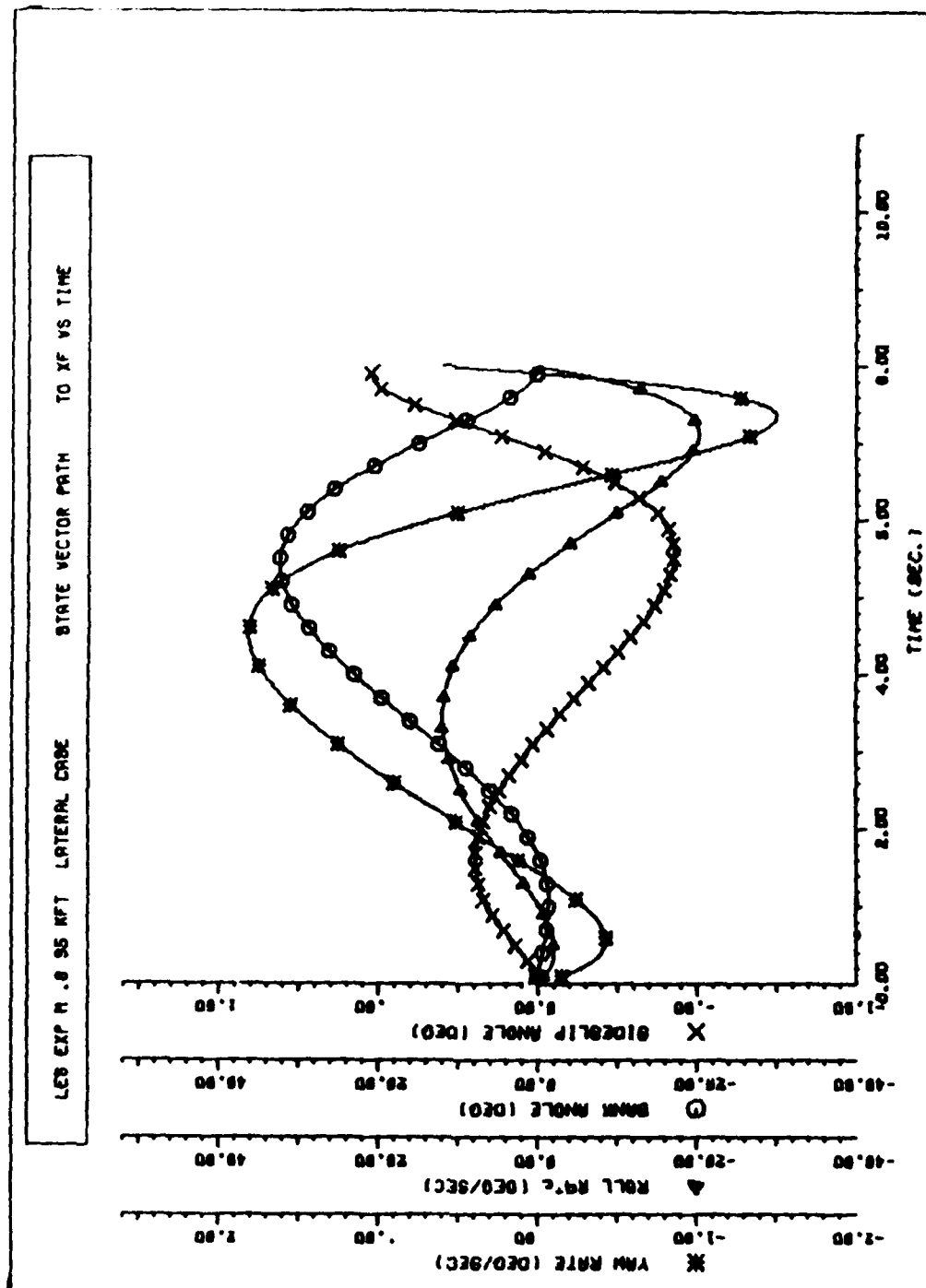


Figure C25 Experimental LES Lateral/Directional Response to Reach $\bar{v}_x(t_f = 2.0 \text{ Seconds})$

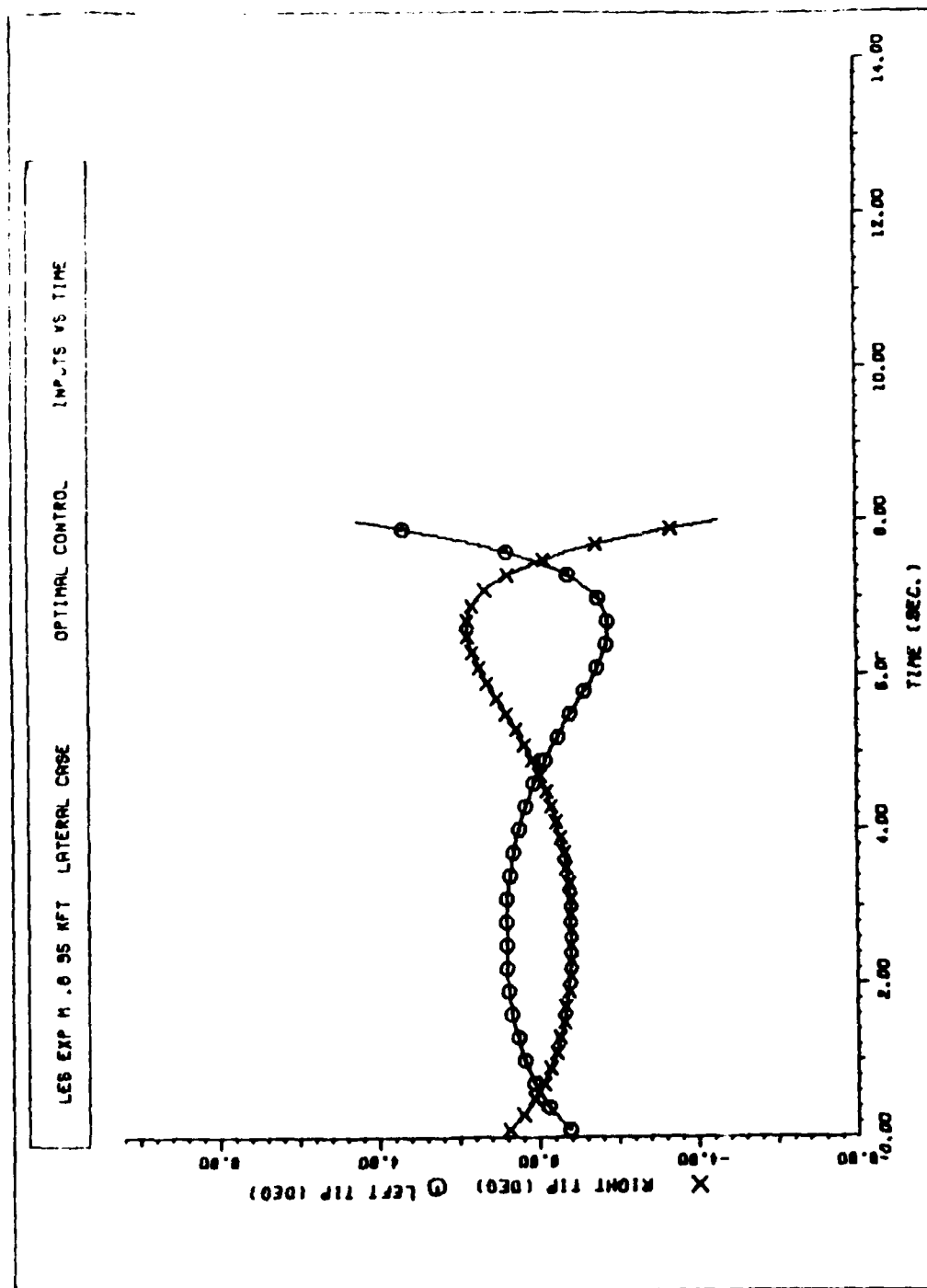


Figure C26 Experimental LES Lateral/Directional Controls to Reach \bar{v}_4 ($t_f = 8.0$ Seconds)

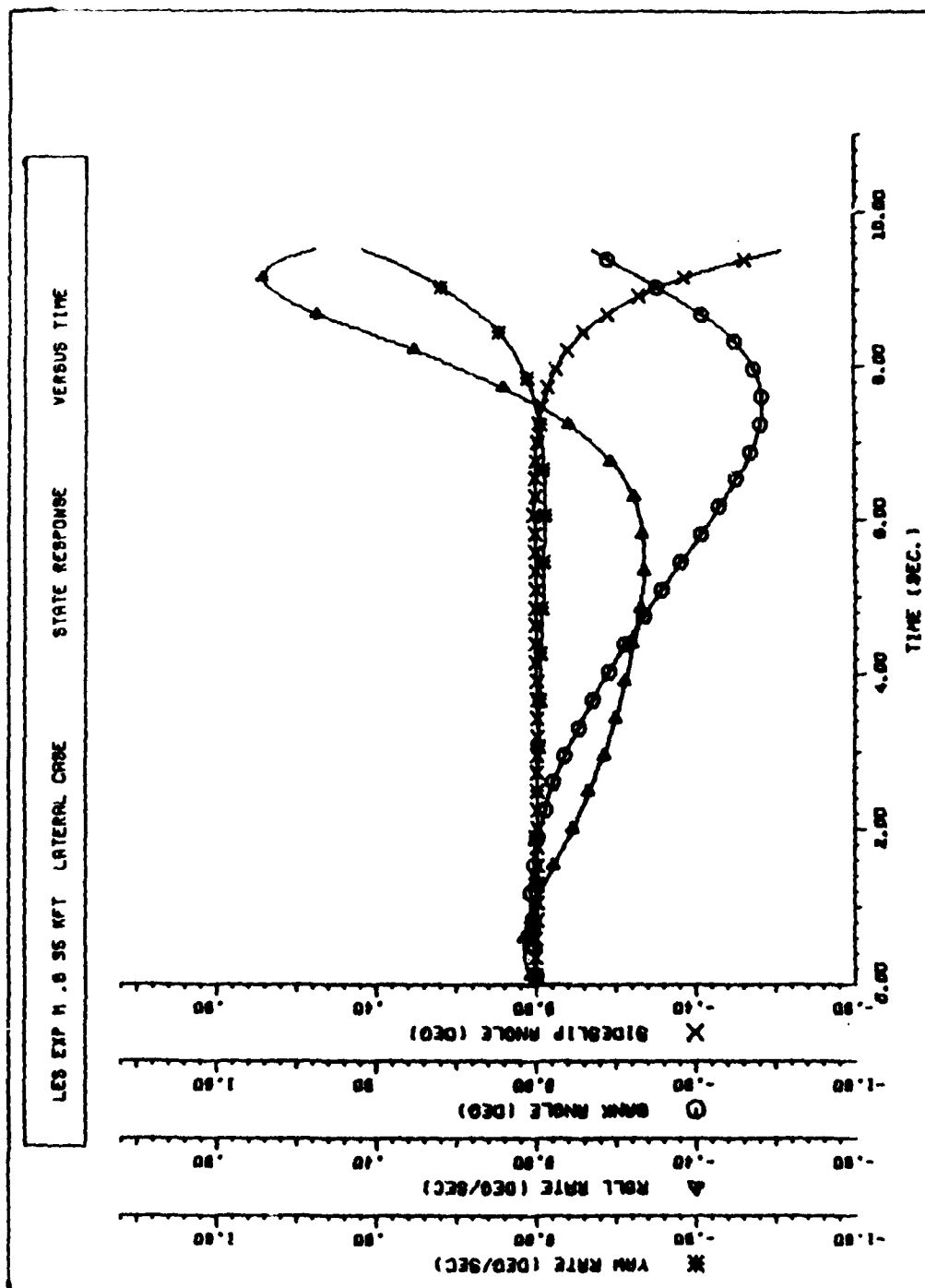


Figure C27 Experimental LES Lateral/Directional Response to Reach \bar{U}_4 ($t_f = 9.5$ Seconds)

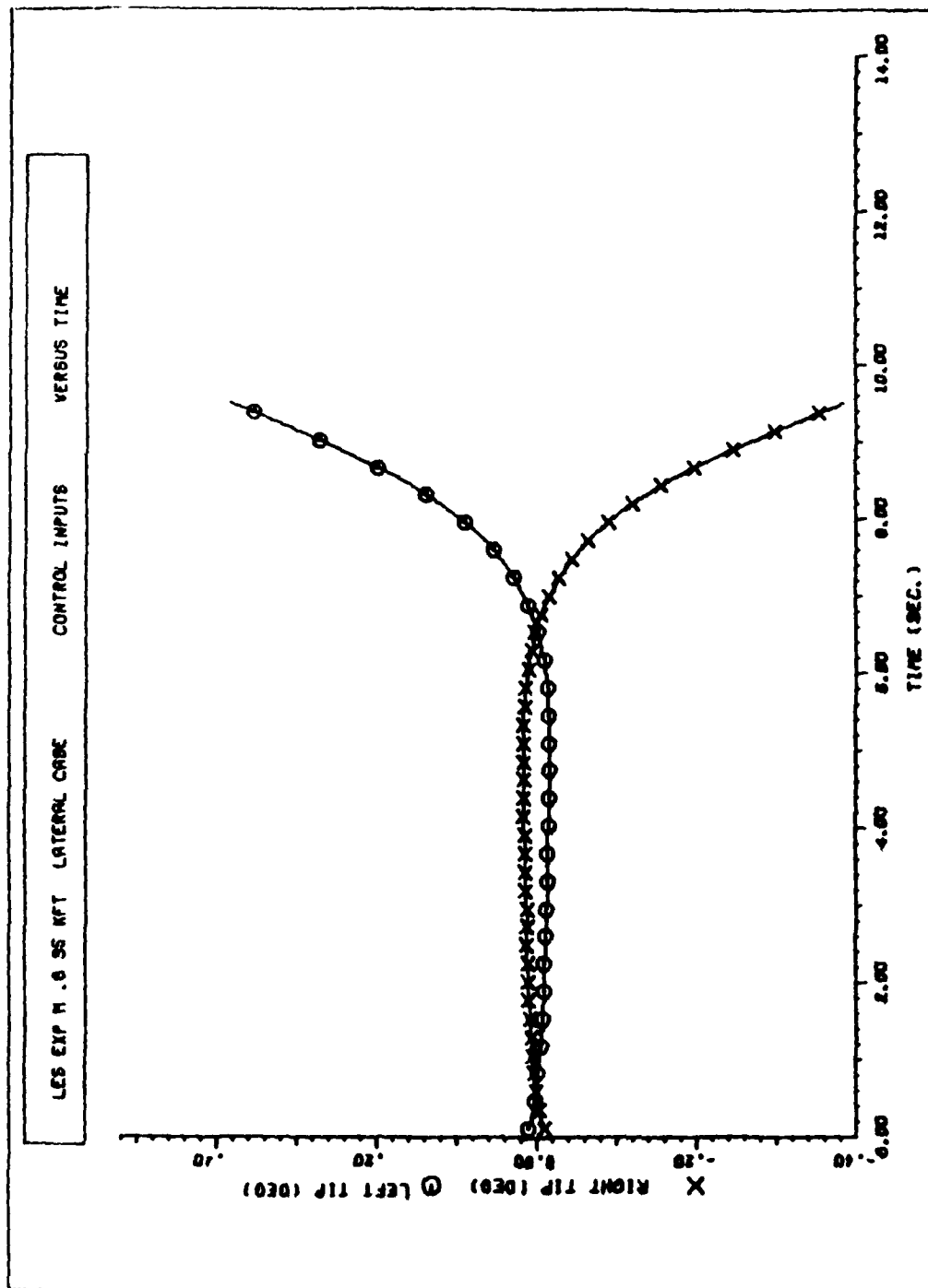


Figure C28 Experimental LES Lateral/Directional Controls to Reach \bar{u}_4 ($t_f = 9.5$ Seconds)

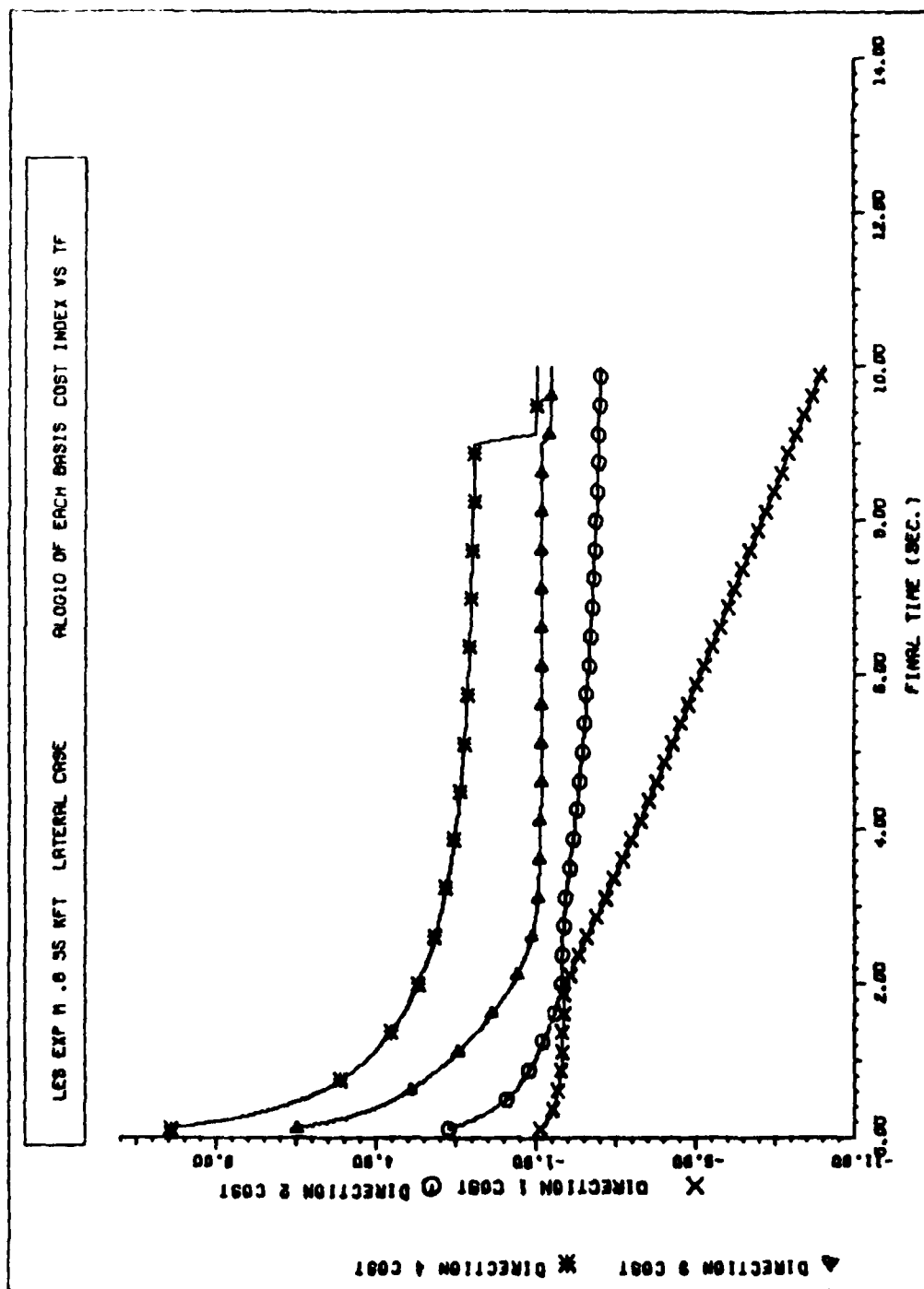


Figure c29 Log₁₀ of Experimental LES Weighted Control Costs for All Lateral/Directional Basis Vectors

Appendix D: Sample Data for Direct Aircraft Comparison

This collection of data shows a direct comparison between all three aircraft. They were each flown to the same arbitrary set of two longitudinal and two lateral/directional final state vectors, as outlined in Chapter V.

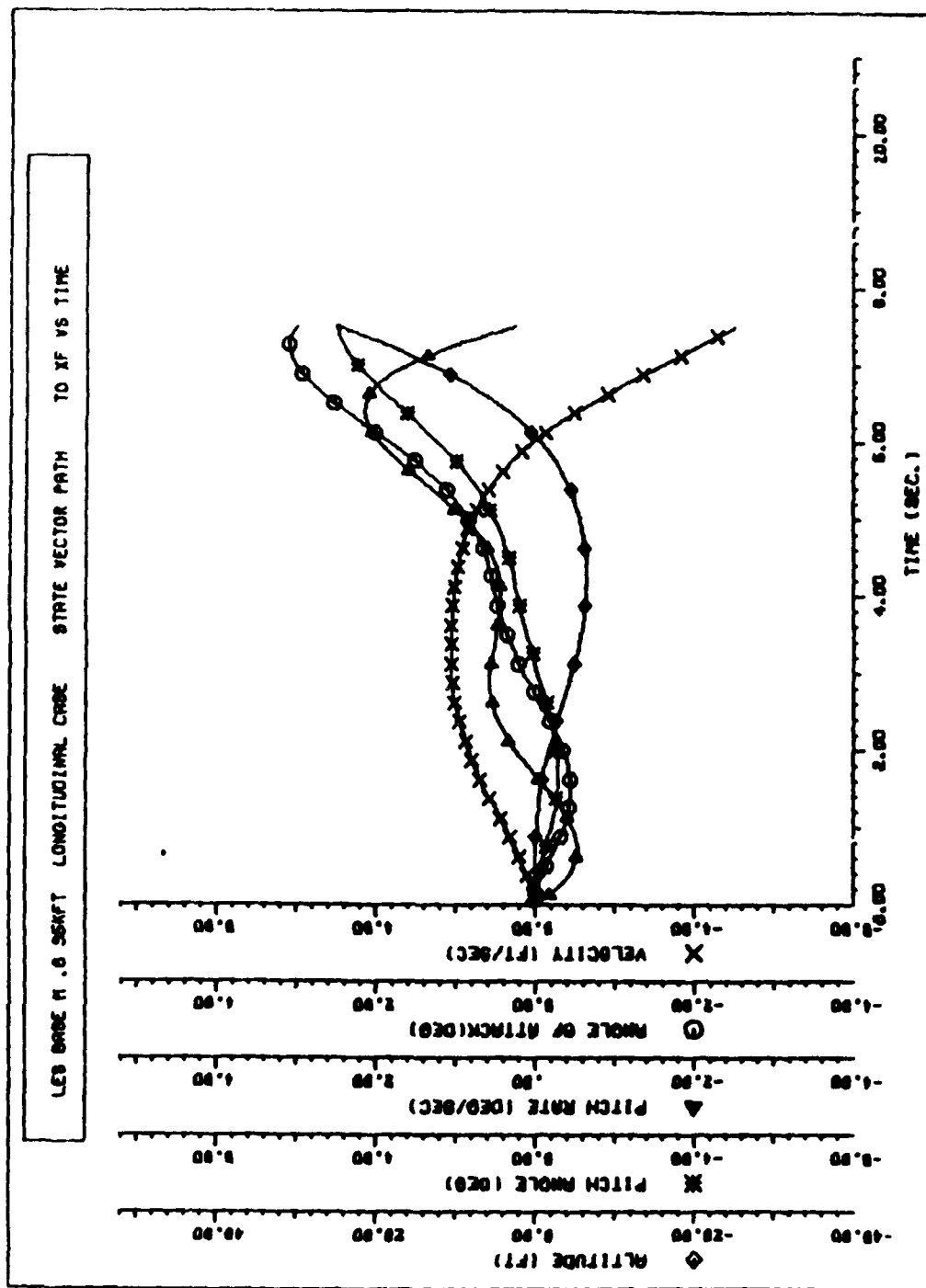


Figure D1 Baseline LES Longitudinal Response to Reach Longitudinal Vector

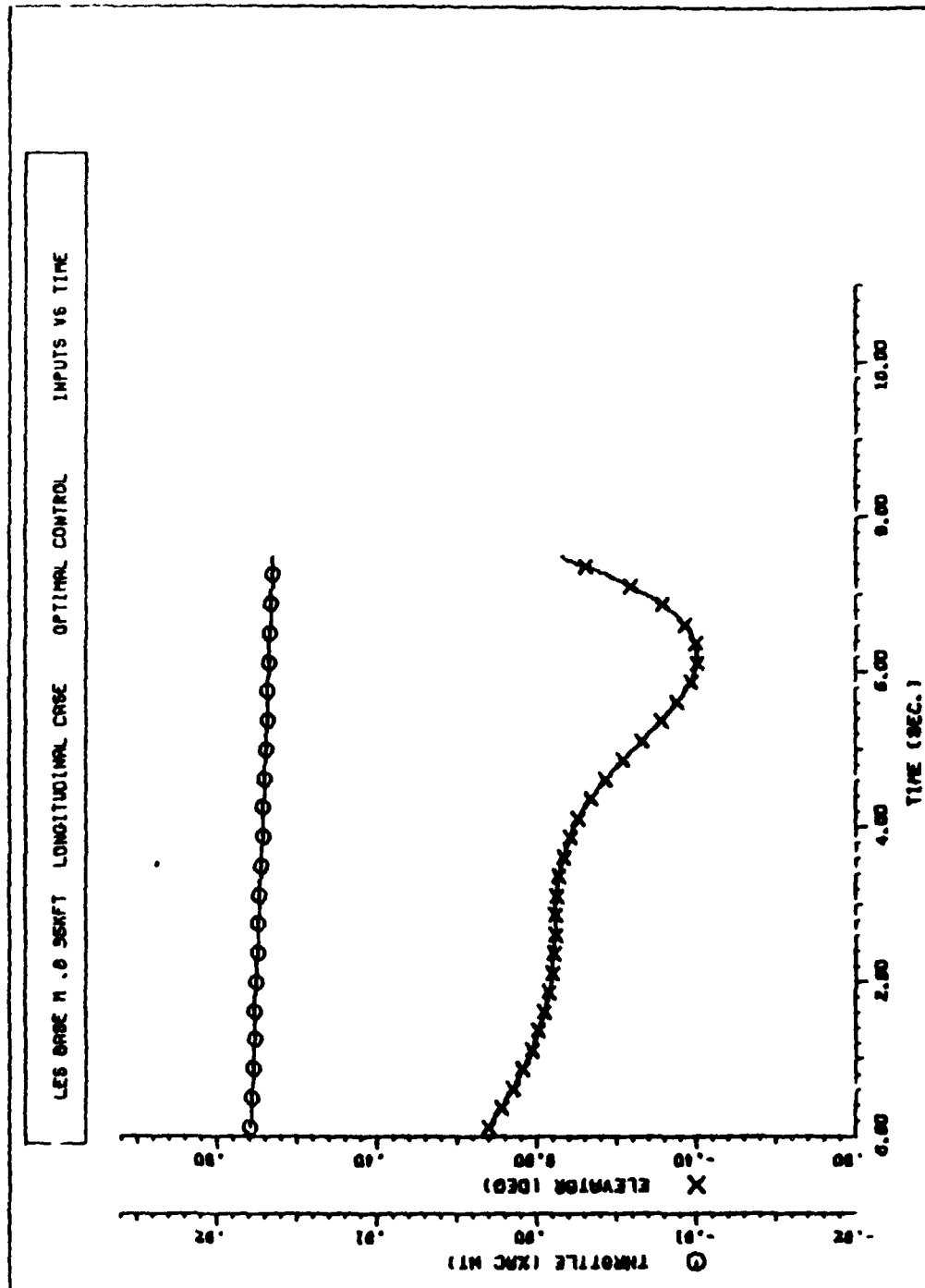


Figure D2 Baseline LES Longitudinal Controls to Reach Longitudinal Vector I

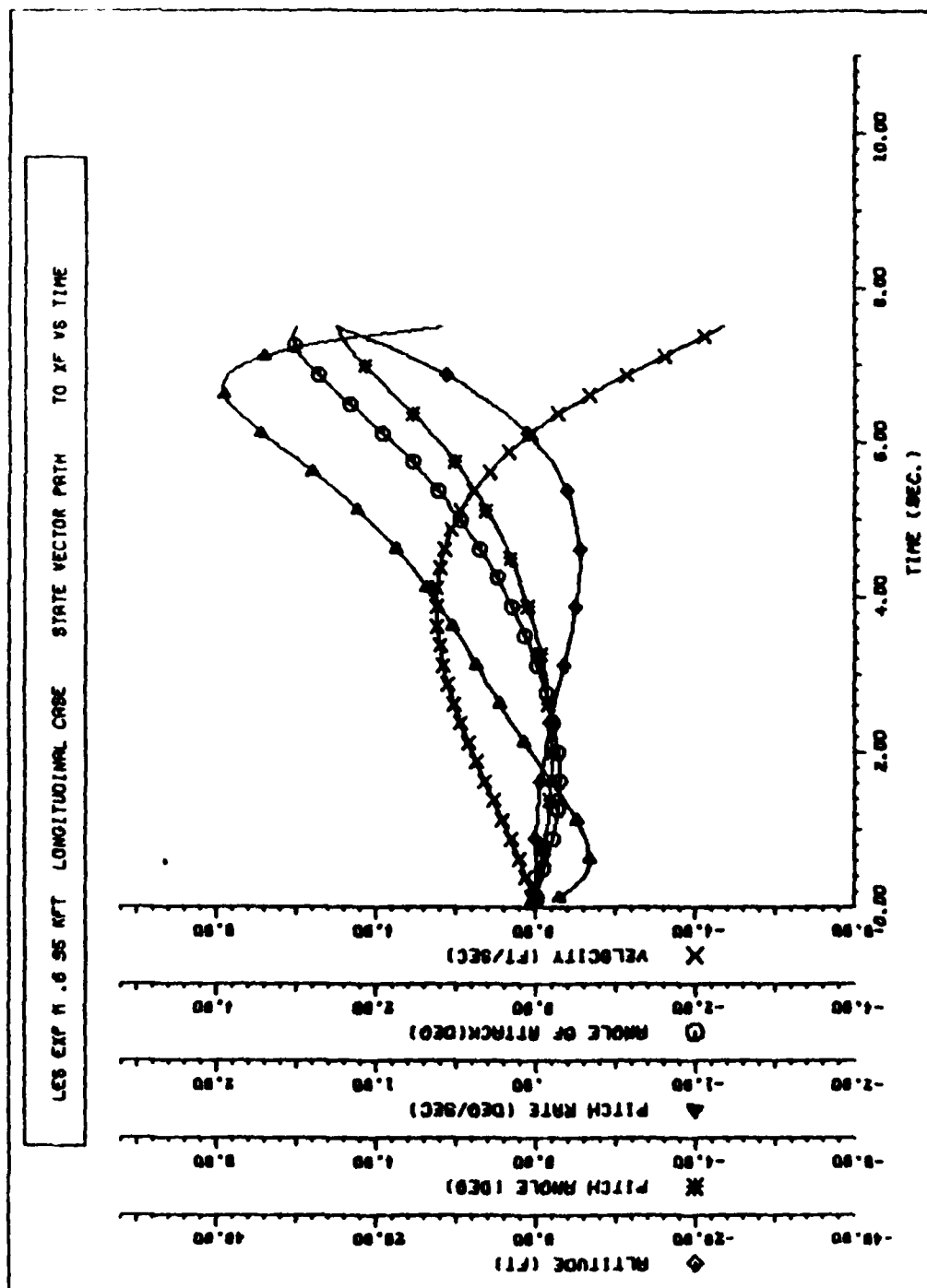


Figure D3 Experimental LES Longitudinal Response to Reach Longitudinal Vector 1

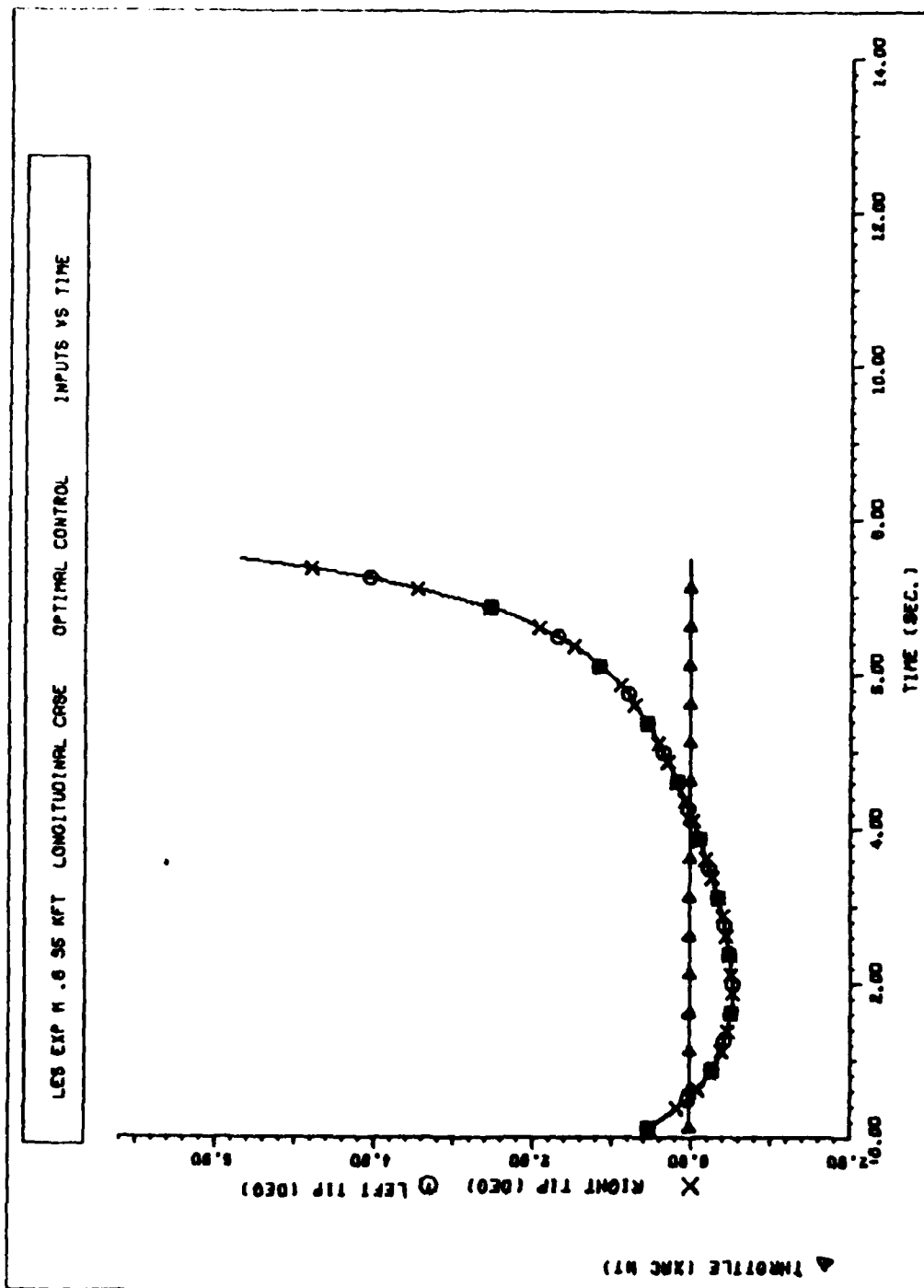


Figure D4 Experimental LES Longitudinal Controls to Reach Longitudinal Vector I

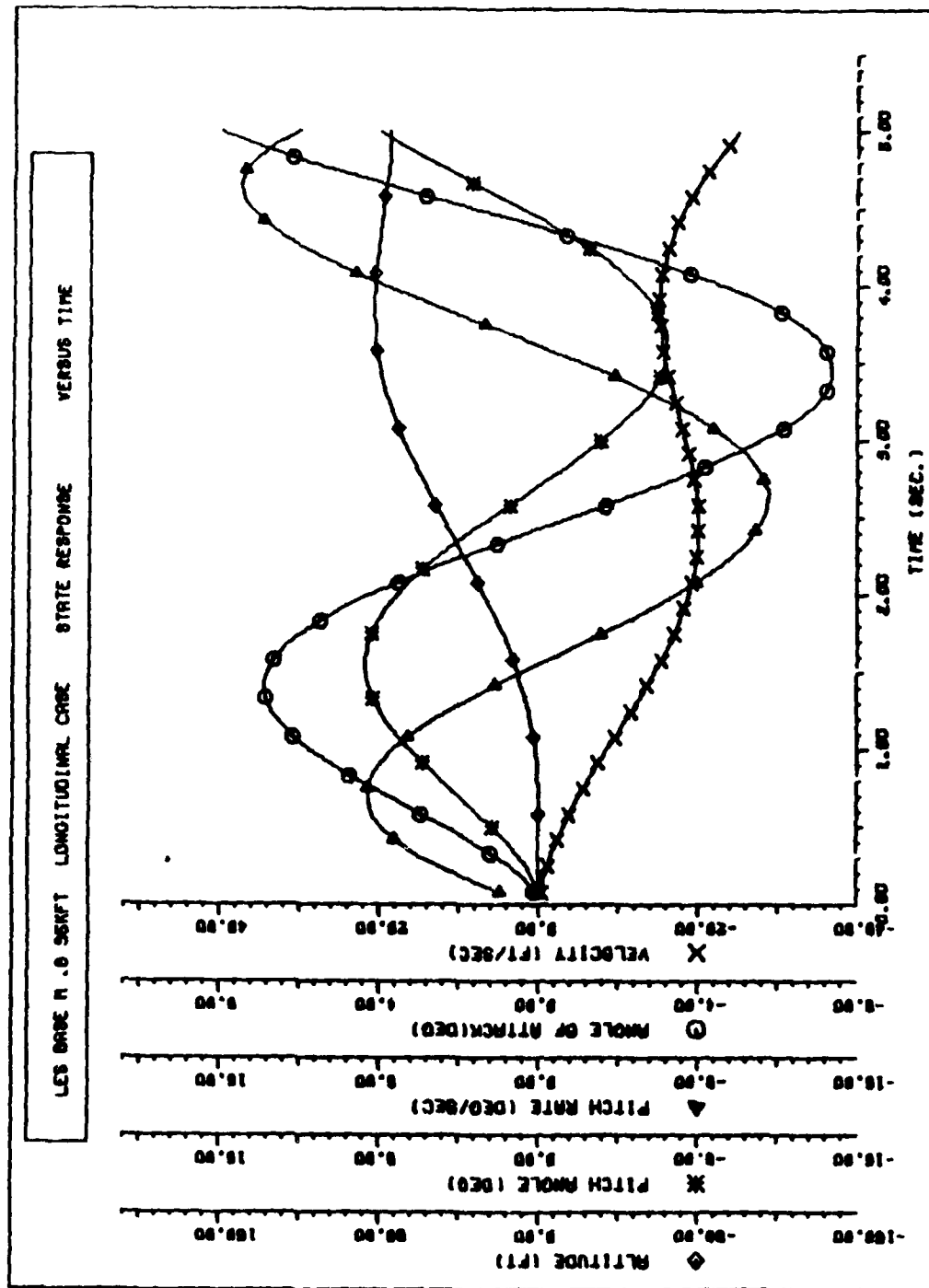


Figure D5 Baseline LES Longitudinal Response to Reach Longitudinal Vector 2

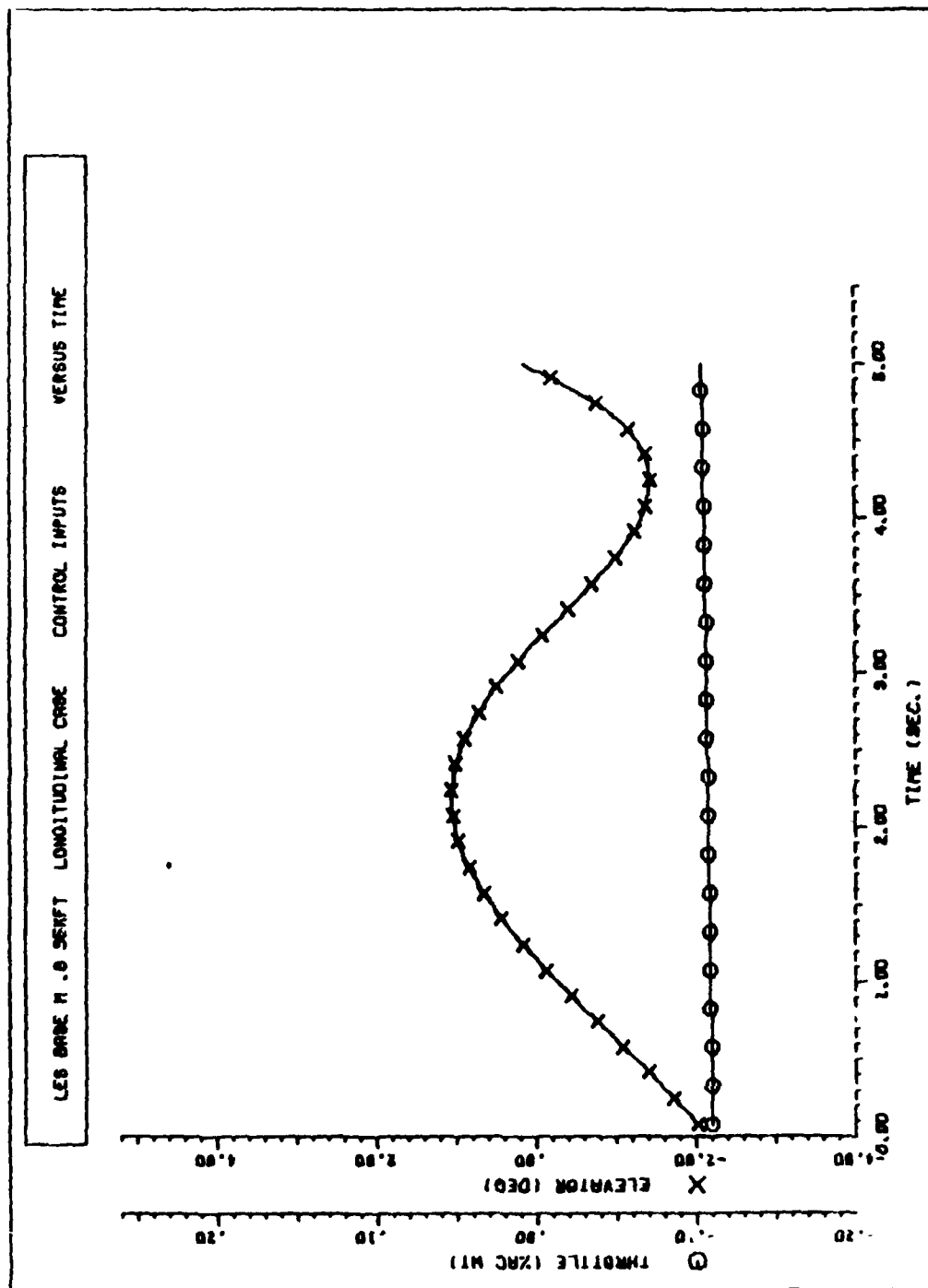


Figure n6 Baseline LES Longitudinal Controls to Reach Longitudinal Vector 2

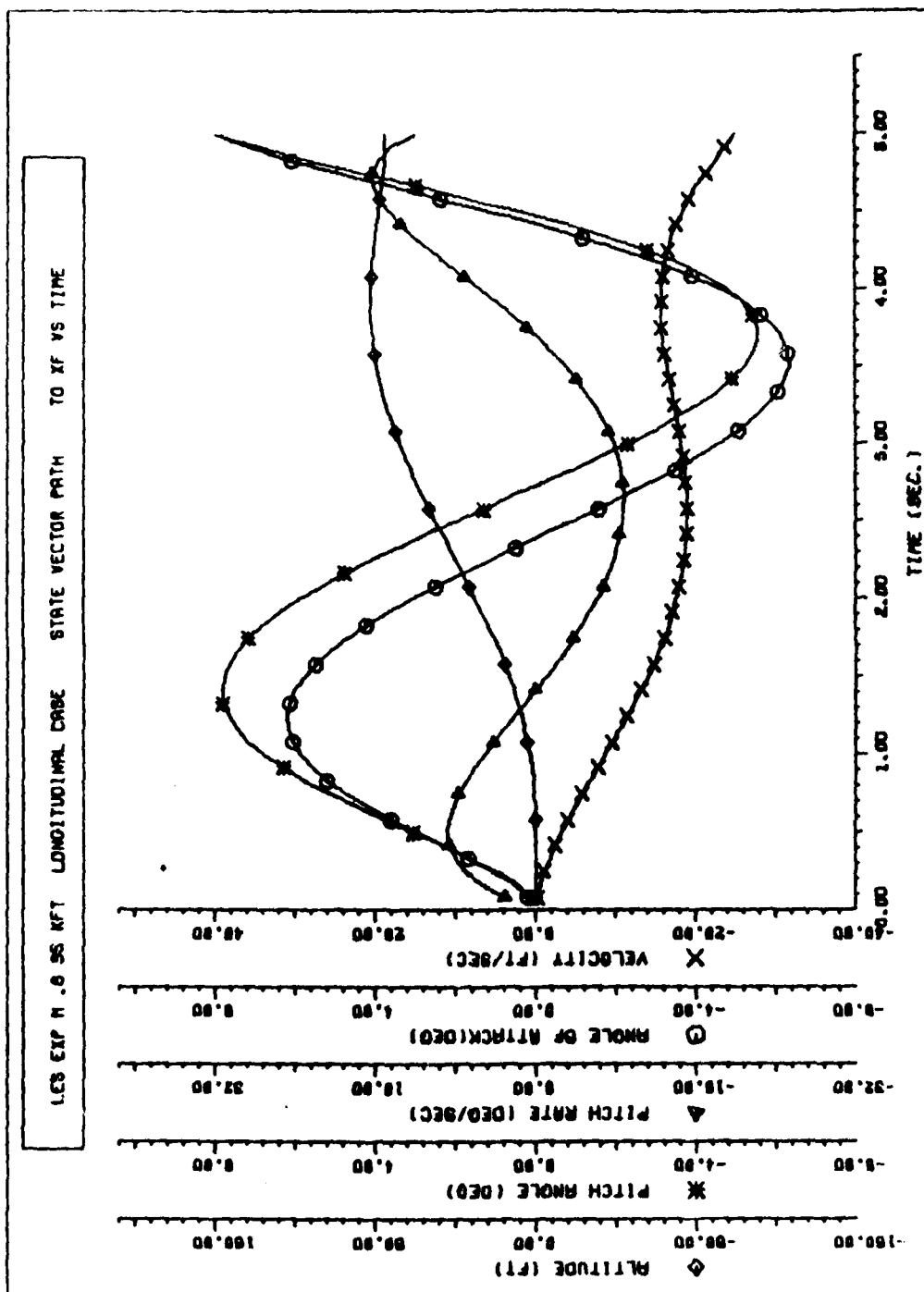


Figure D7 Experimental LES Longitudinal Response to Reach Longitudinal Vector 2

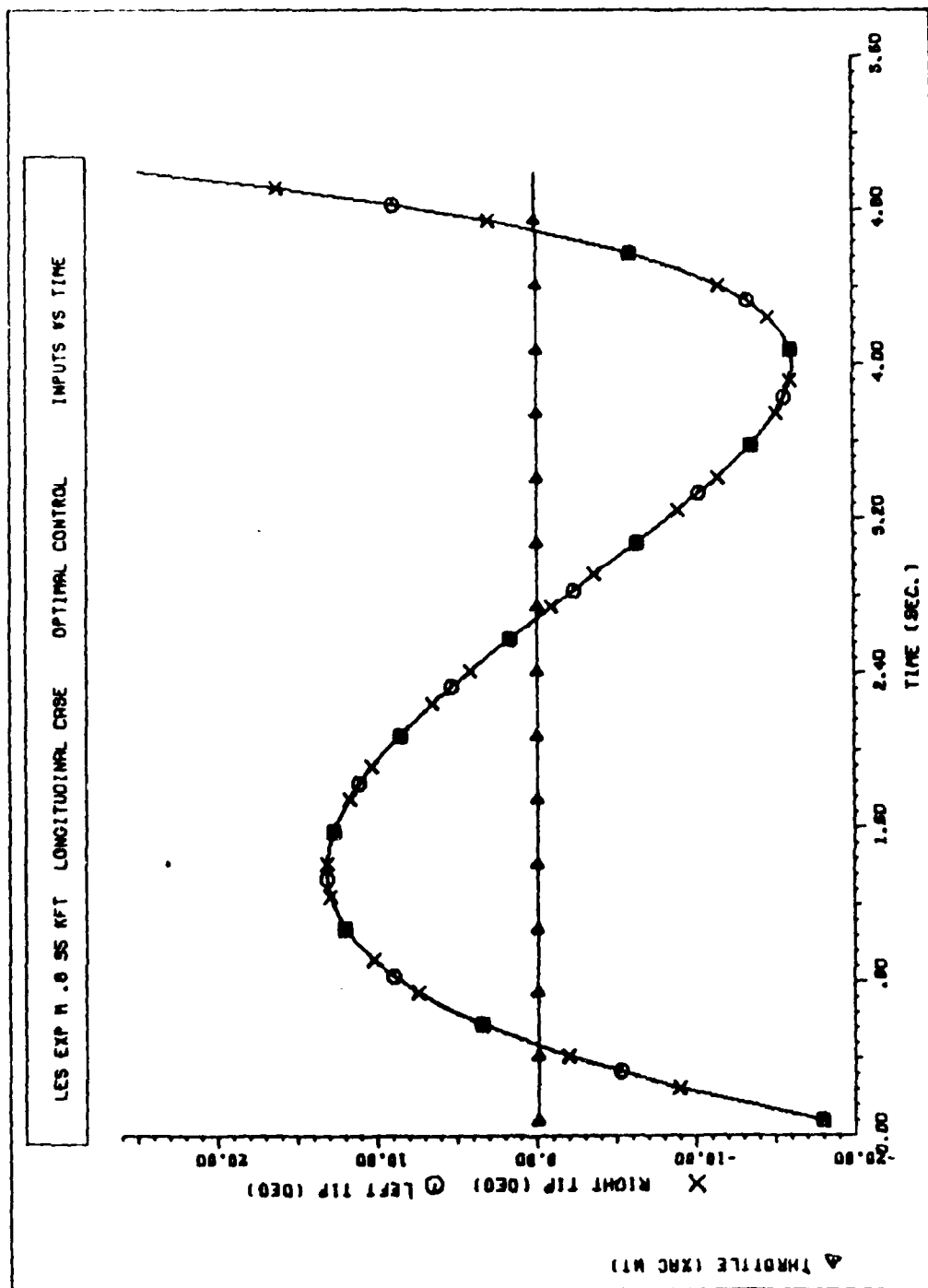


Figure D8 Experimental LES Longitudinal Controls to Reach Longitudinal Vector 2

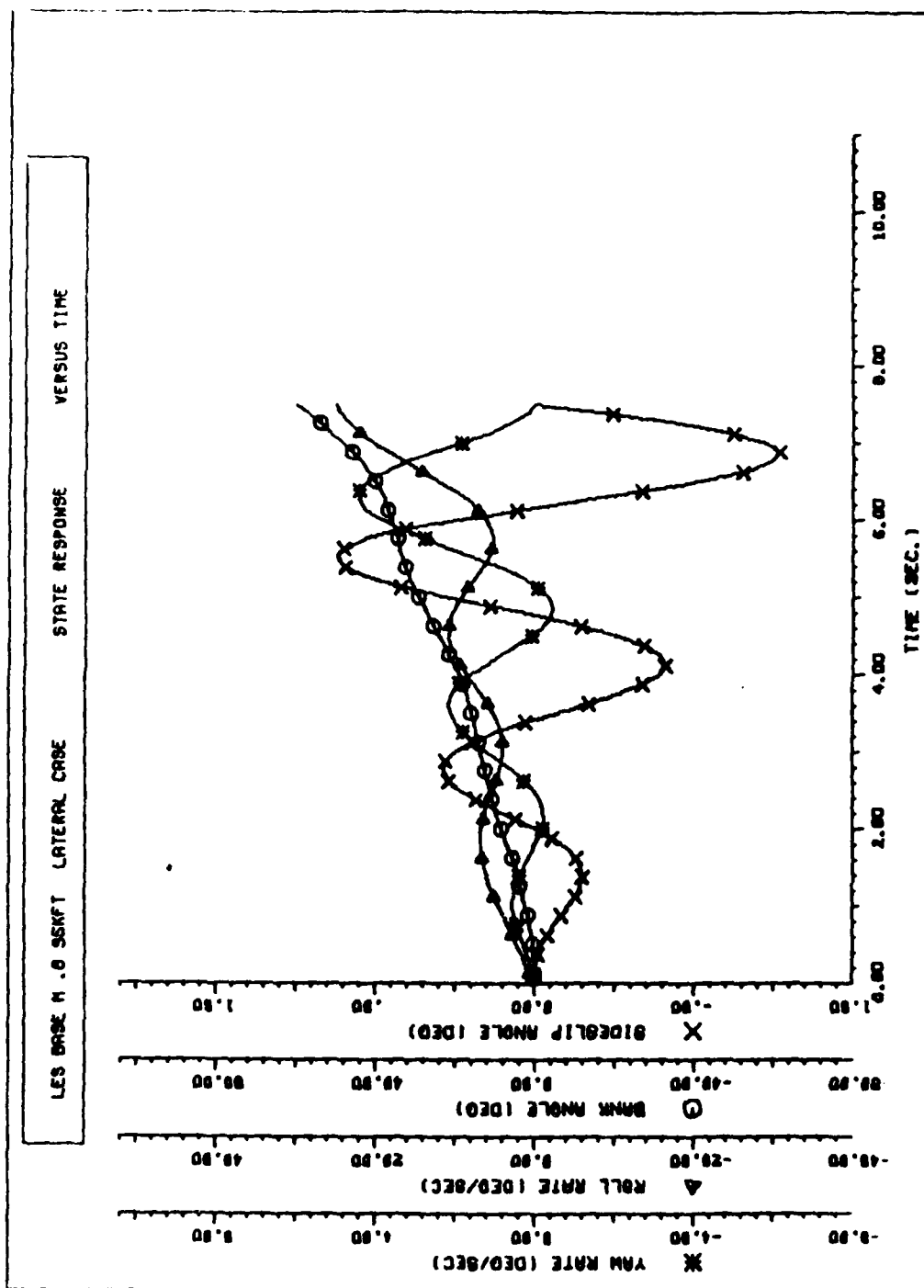


Figure n9 Baseline LES Lateral/Directional Response to Reach Lateral Vector 1

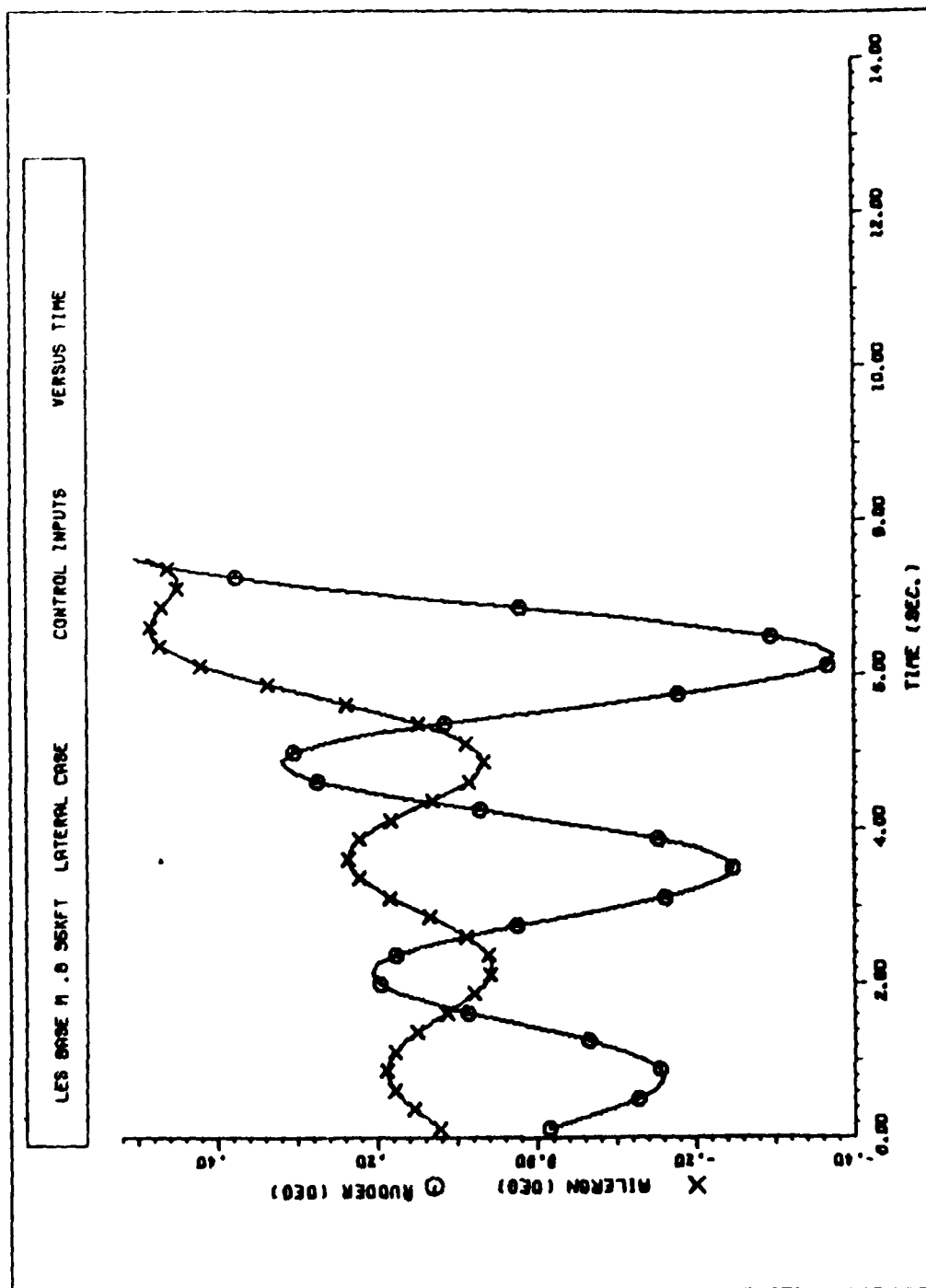


Figure D10 Baseline LES Lateral/Directional Controls to Reach Lateral Vector 1

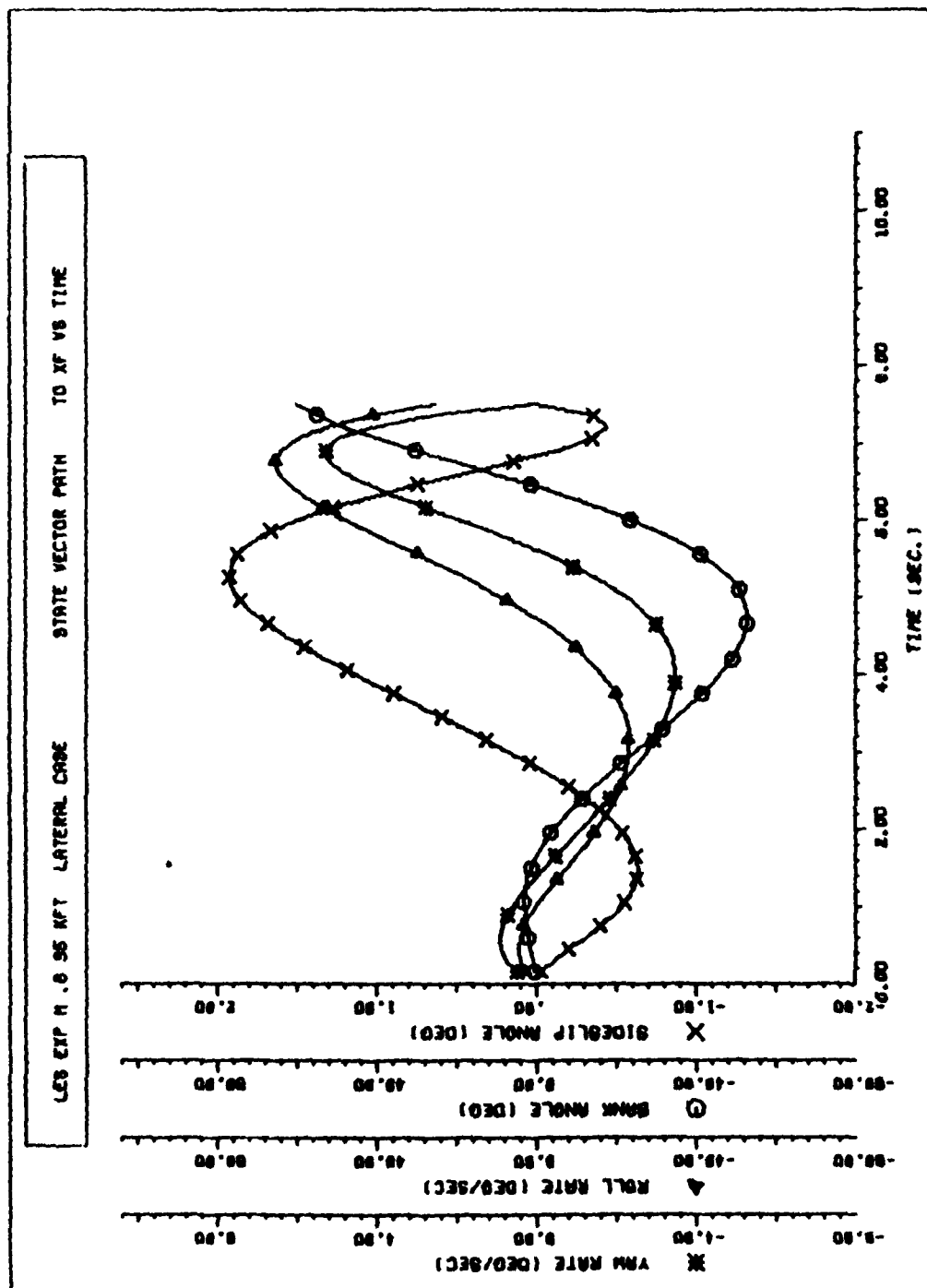


Figure D11 Experimental LES Lateral/Directional Response to Reach Lateral Vector 1

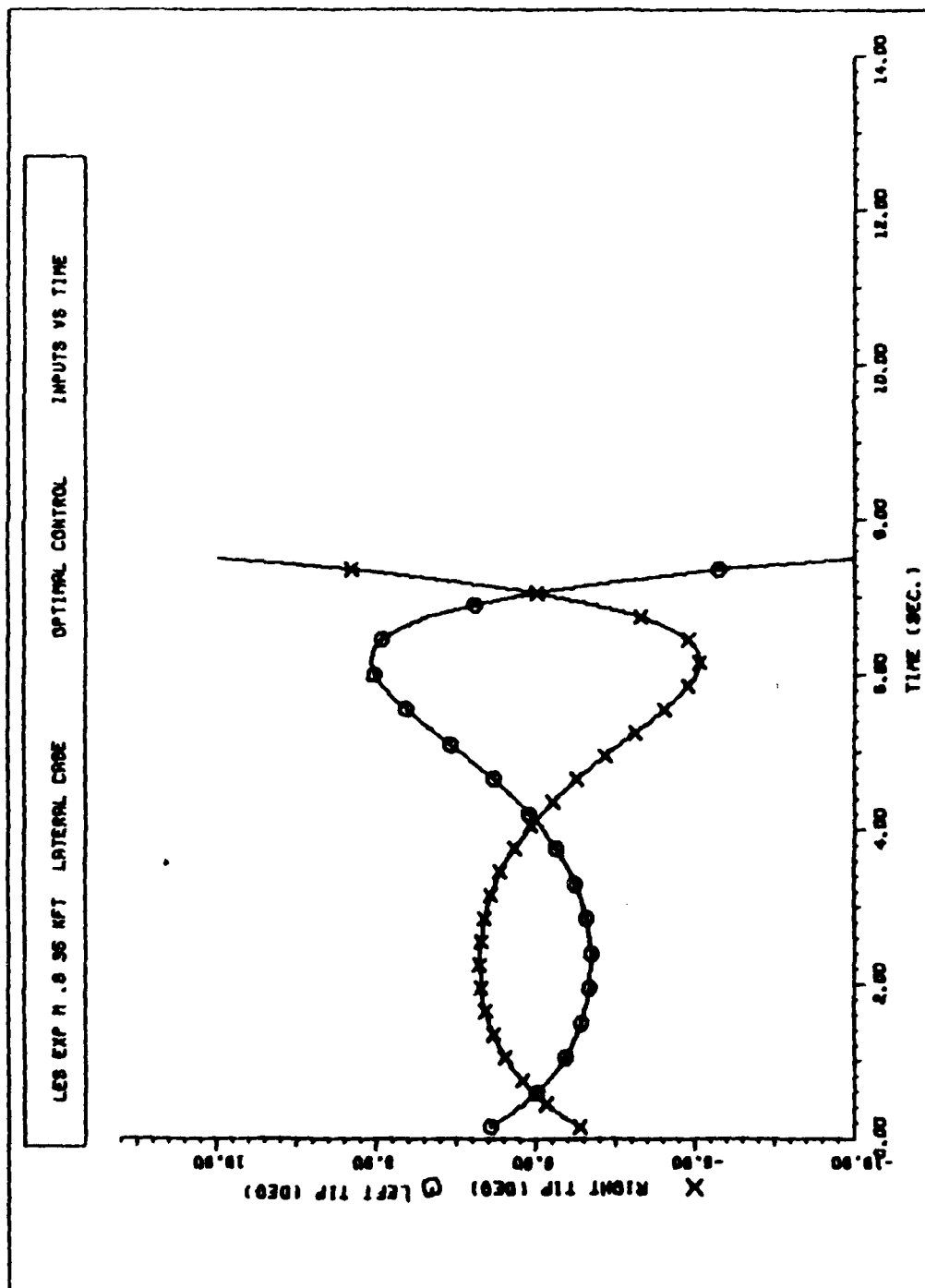


Figure D12 Experimental LES Lateral/Directional Controls to Reach Lateral Vector 1

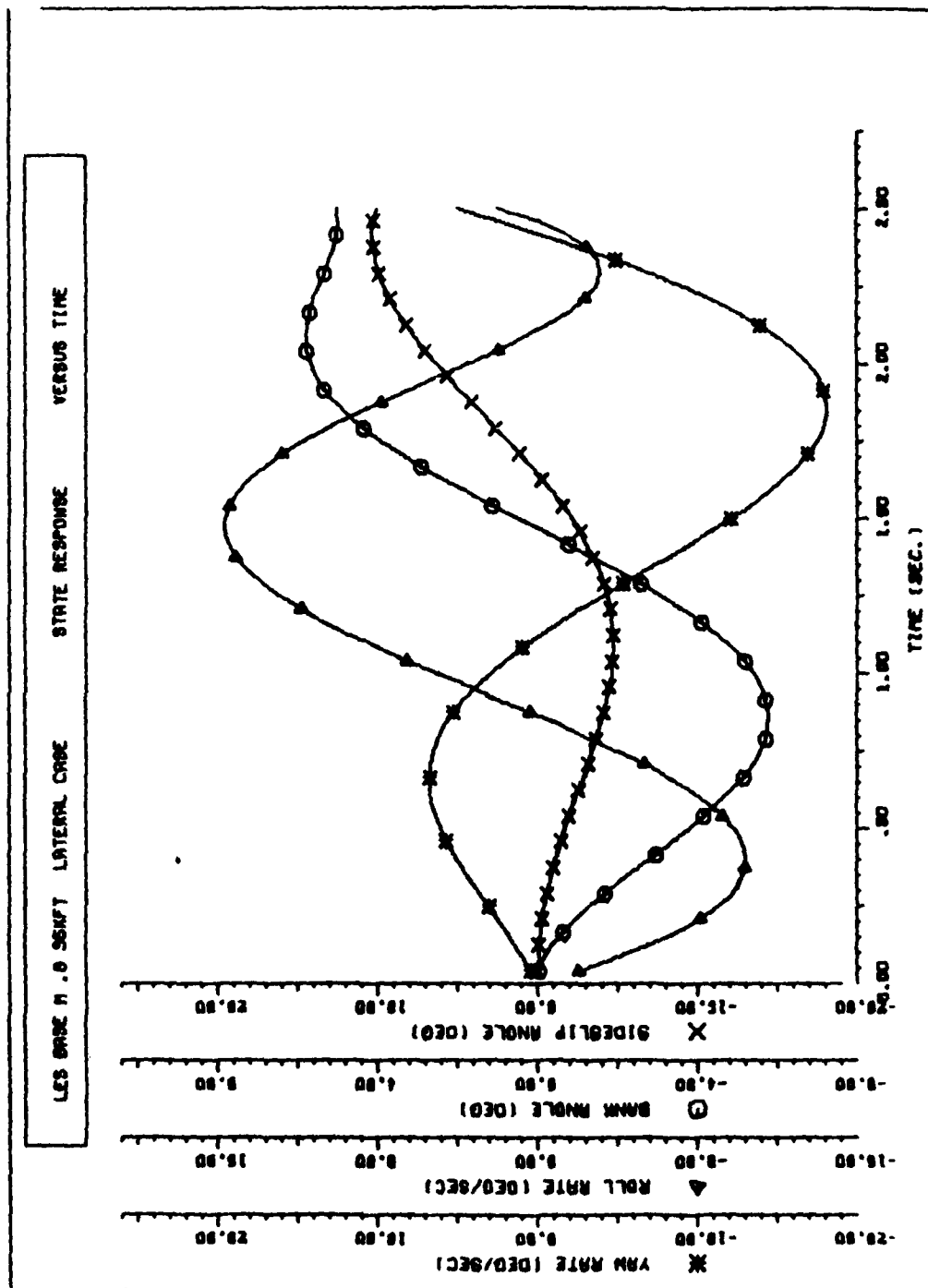


Figure D13 Baseline LES Lateral/Directional Response to Reach Lateral Vector 2

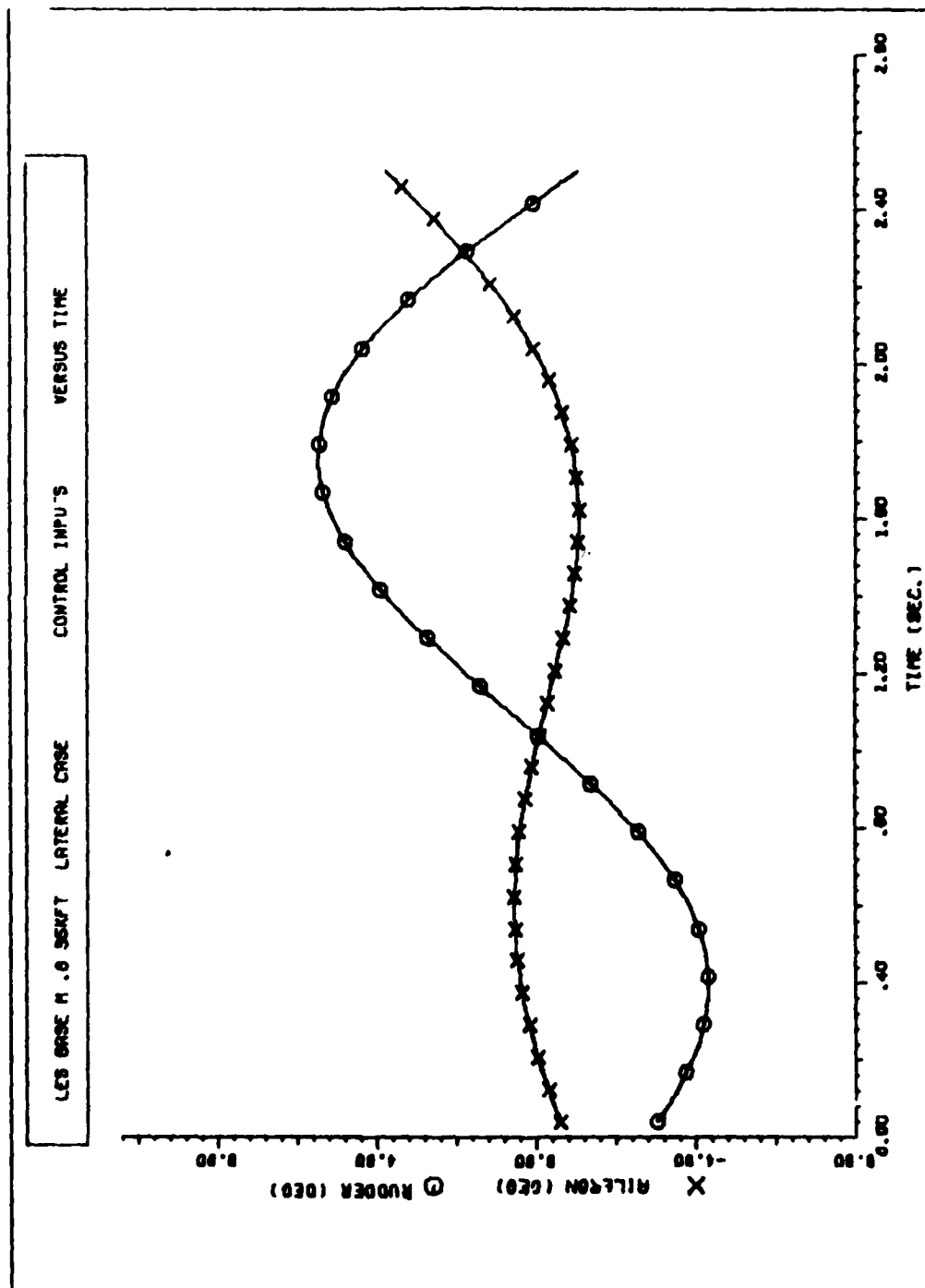


Figure D14 Baseline LES Lateral/Directional Controls to Reach Lateral Vector 2

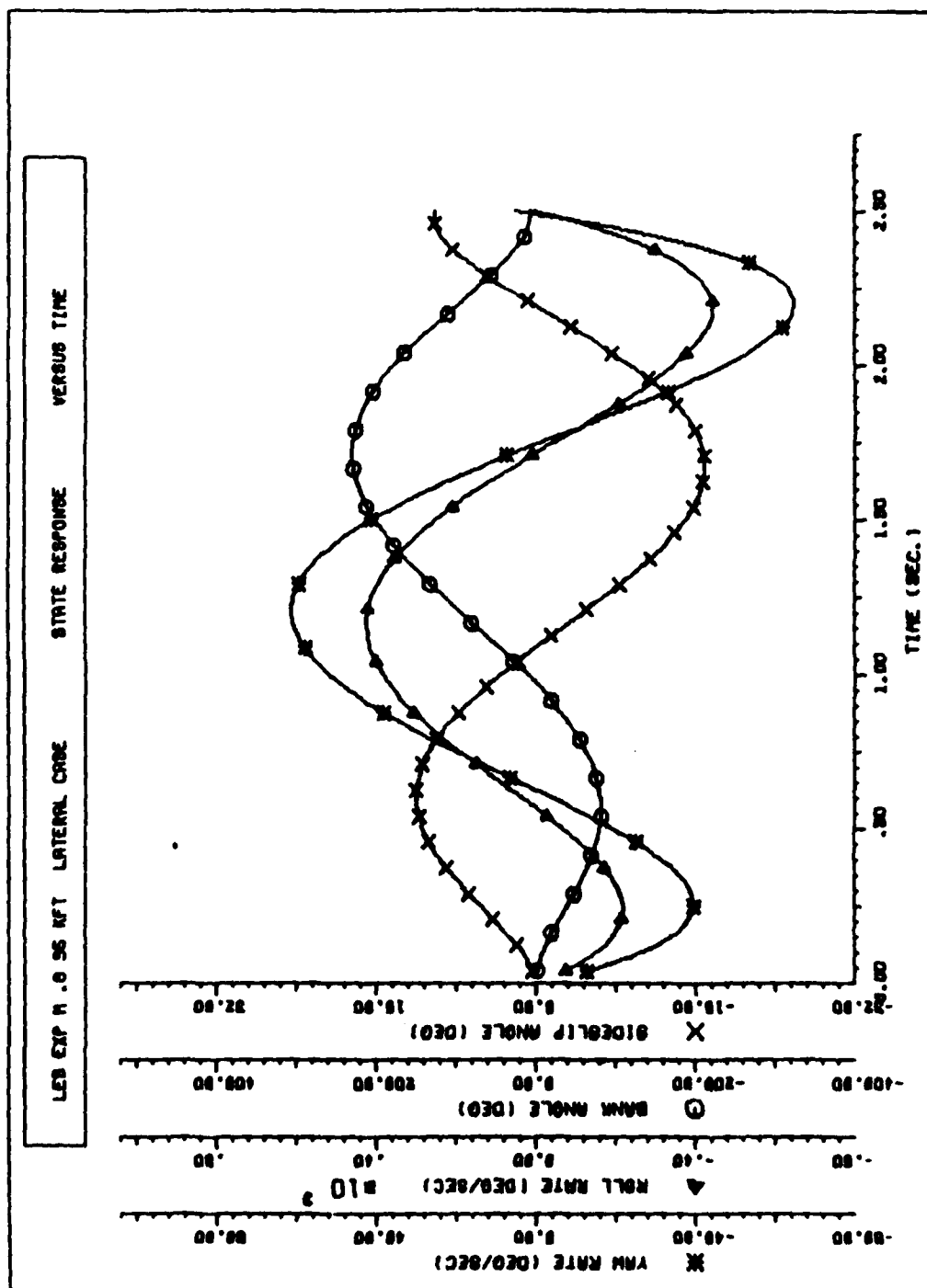


Figure D15 Experimental LES Lateral/Directional Response to Reach Lateral Vector 2

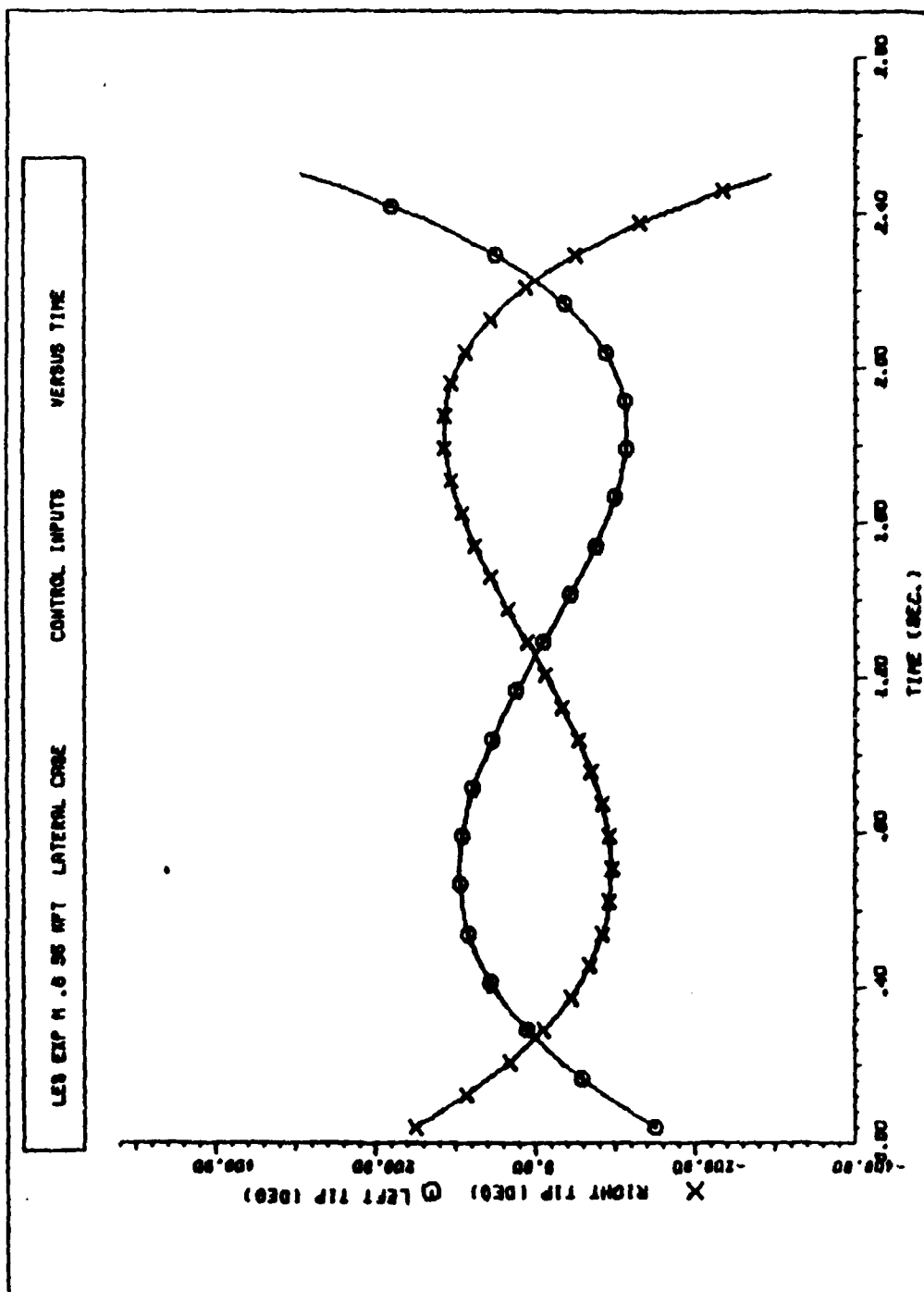


Figure D16 Experimental LES Lateral/Directional Controls to Reach Lateral Vector 2

Appendix E: GRAMOP Program User's Guide

General

This guide describes the detail instructions for using the GRAMOP computer program to analyze the following optimal control problem:

find the optimal control history $\bar{u}^*(t)$ which drives the state variable system from initial state $\bar{x}(0) = \bar{0}$ to the arbitrary user-input final state $\bar{x}(t_f)$, and which also minimizes the cost functional

$$J(\bar{u}(t)) = \frac{1}{2} \int_0^{t_f} \bar{u}^T(\tau) R \bar{u}(\tau) d\tau \quad (E-1)$$

which is subject to the state space constraint

$$\dot{\bar{x}} = A\bar{x} + B\bar{u} \quad (E-2)$$

Matrix R is restricted to a diagonal matrix with non-negative diagonal elements. Details of the theory used in GRAMOP may be found in Chapter IV of the thesis, "Calculating Aircraft Controllability Quality".

GRAMOP contains two basic options:

1) TRAITS option - calculates the controllability characteristics or quality of the linear system throughout the n-dimensional state space. This is done by finding the n time-varying, mutually orthogonal directions in (R^n) made up of:

- 1) $\bar{v}_1(t)$, the easiest direction of all to control in (R^n) ;
- 2) $\bar{v}_2(t)$, the easiest direction of all to control in (R^{n-1}) , that particular subspace of (R^n) which is orthogonal to direction 1;

...

- 1) $\bar{v}_i(t)$, the easiest to control direction in the space (R^{n-i+1}) which is orthogonal to direction (i-1) above;

...
...
...

n) $\bar{V}_n(t)$, the most difficult direction of all to control in (R^n)

2) XUHIST option - calculates both the state history $\bar{x}(t_0, t_f)$, and the optimal control history $\bar{u}^*(t_0, t_f)$ which drives the system from $\bar{x}_0 = \bar{0}$ to $\bar{x}(t_f) = \bar{x}_f$ along the state trajectory $\bar{x}(t_0, t_f)$ for any user-input system, \bar{x}_f , and t_f . This option can be used to investigate some state and time of interest to the user, or to analyze results from the TRAITS option; i.e., obtain sample control and response histories which move the system along a specific "ranked" direction, calculated in the TRAITS option, at a specific final time.

Input data formats are as follows:

CARD NO.	VARIABLE NAME	FORMAT
1	ISTOP	List-directed (LD)

DESCRIPTION - Flag to start (1) or stop (0) GRAMOP execution.

CARD NO.	VARIABLE NAME	FORMAT
2	N,M,I	LD

DESCRIPTION - N = number of state variables, M = number of control variables, and I = computer hardware flag: (1) = INTERCOM, (2) = batch.

CARD NO.	VARIABLE NAME	FORMAT
3,4	ID(1), ID(2)	2A10

DESCRIPTION - First (second) card has 20 characters for first (second) line of plot title box of all plots

CARD NO.	VARIABLE NAME	FORMAT
5	NOUT	LD

DESCRIPTION - Number of variables x_i and/or u_i to be plotted or printed. (must be less than or equal to 5).

<u>CARD NO.</u>	<u>VARIABLE NAME</u>	<u>FORMAT</u>
6,7	YTITLE (1,IM) YTITLE(1,20+IM)	2A10

DESCRIPTION - First (second) card has 20 characters for y-axis print header/plot label for IMth state variable (IMth cost history). There are N (see card 2) pairs of cards 6,7 - a pair for each x_i .

<u>CARD NO.</u>	<u>VARIABLE NAME</u>	<u>FORMAT</u>
8	YTITLE(1,10+IM)	2A10

DESCRIPTION - contains 20 characters of y-axis plot label/print header for IMth control variable. There are M (see card 2) cards 8, one for each u_i .

<u>CARD NO.</u>	<u>VARIABLE NAME</u>	<u>FORMAT</u>
9	IX(J),J=1,NOUT	LD

DESCRIPTION - These are the addresses/subscripts J of all x_j which are to be printed on plotted. (All on one card 9)

<u>CARD NO.</u>	<u>VARIABLE NAME</u>	<u>FORMAT</u>
10	IU(J),J=1,MPL0T	LD

DESCRIPTION - These are the addresses/subscripts J of all u_j which are to be printed or plotted. (All on one card 10)

<u>CARD NO.</u>	<u>VARIABLE NAME</u>	<u>FORMAT</u>
11	L1,L2,YY	LD

DESCRIPTION - Matrix A(B,R) input cards; each $A_{ij}(B_{ij}, R_{ij})$ is input as i,j,A_{ij} . Each card except the last ends with a comma, and the last card for each matrix ends with - "0/". There is one set of cards 11 for each of the three matrices: A,B, and R, in that order.

<u>CARD NO.</u>	<u>VARIABLE NAME</u>	<u>FORMAT</u>
12	KTRAJ	LD

DESCRIPTION - Output option flag; (1) = plot only, (2) = print only, and (3) = both print and plot.

<u>CARD NO.</u>	<u>VARIABLE NAME</u>	<u>FORMAT</u>
13	IXU	LD

DESCRIPTION - This is the XUHIST routine option flag; (1) means run XUHIST, and (0) means do not run XUHIST option.

If IXU = 0, go to card 19; if IXU = 1, the following cards are required:

CARD NO. 14 (TO,TF,NTPTS LD)

DESCRIPTION - TO = user specified initial time; TF = user-specified final time; NTPTS = number of evenly-spaced "sample" points at which output data is calculated in the interval (TO,TF). (Must be less than 100)

CARD NO. 15 $\bar{x}(TF)$ LD

DESCRIPTION - User-specified final state vector at final time TF (see card 14). Same format as card 11.

CARD NO. 16,17 (ID(3),ID(4) LD

DESCRIPTION - First (second) card contains 20 characters of third (fourth) lines of $\bar{x}(t)$ plot title box. Input this card only if KTRAJ (see card 12) is \neq 2.

CARD NO. 18 (NSCALE) LD

DESCRIPTION - The $\bar{x}(t)$ plot y-axes scaling flag; (0) = scale all variables identically; i.e., plot all state variables against a common y-axis; (1) = scale all variables separately; i.e., each variable is plotted against its own scaled y-axis.

A second set of cards 16 - 18 now follows, in identical format, except ID(3),ID(4) are now the titles for the $\bar{u}^*(t)$ plot title box lines 3 and 4, and NSCALE = scaling option for the control variables history plot. For each time interval (TO,TF) and final state ($\bar{x}(TF)$) combination desired, add an additional set of input cards as follows:

- a) one card each 14 and 15, plus
- b) two sets of cards 16-18.

To exit the XUHIST option, input a final card 16 as TO = 0. , TF = 0. , NTPTS = 0

CARD NO. 19 (ITRAIT LD)

DESCRIPTION - This is the TRAITS option flag; (1) = run the TRAITS option, (0) = do not run the TRAITS option.

CARD NO. 20 (TF1,TF2,NTF LD)

DESCRIPTION - These inputs correspond to the same variables as those on card 14.

CARD NO. 21 (IDBUG LD)

DESCRIPTION - print flag; (1) = write debug print onto local
file name TAPE7; (0) = do not write any debug print.

Note: Debug print includes eigenvector time histories, and so is very
desirable to have for later XUHIST use. Remember to include the cards
REWIND, RERUN, COPYSBF, RERUN, OUTPUT in the JCL statements after the
GRAMOP execution card, in order for the print file to be routed to the
printer.

CARD NO. 22, 23 (ID(3),ID(4) LD)

DESCRIPTION - The first N(see card 2) pair of cards contain the 20
characters of the third (fourth) line of each ranked eigenvector plot
title box; the last pair of cards contains the 20 characters for the
ranked cost plot title lines 3 and 4.

A new set of cards 20 - 23 is input for each time interval (TF1,TF2)
desired. To exit TRAITS, input a final card 20 with TF1 = TF2 = "0."
and NTF = "0".

After all option cards for the TRAITS option, the next (or last) card
is another card 1 with ISTOP = 0 to end the GRAMOP run, or with ISTOP =
1 to read another complete set of GRAMOP run input cards.

Sample GRAMOP Input Deck

```

1
1,2,2
CASE TITLE (C 0 0 1
CASE TITLE (C 0 0 2
4
STATE VARIABLE 1
DIRECTION 1 COST
STATE VARIABLE 2
DIRECTION 2 COST
STATE VARIABLE 3
DIRECTION 3 COST
STATE VARIABLE 4
DIRECTION 4 COST
CONTROL 1
CONTROL 2
1,2,3,4
1,2
1 1 2 - .95551E-01
1 1 2 .41248E-01
1 1 3 .31718E-01
1 1 4 -.95844E+00
2 2 1 0.
2 2 2 0.
2 2 3 .10000E+01
2 2 4 -.32335E-01
3 3 1 -.80333E+01
3 3 2 .57828E-03
3 3 3 -.82449E+01
3 3 4 .53411E+00
4 4 1 .51574E+01
4 4 2 .71741E-04
4 4 3 .20823E-02
4 4 4 -.23F43E+00
0 /
1 1 2 .17 64E-02
1 1 2 .42054E-01
2 2 1 0.
2 2 2 0.
2 2 3 .45578E+02
3 3 1 .04278E+01
3 3 2 .28473E+01
4 4 1 -.40450E+01
0 /
1 1 1. 2 2 1. 0 /
3
1 1 1. 25
1 1 1. 97835 2 1 -.8174834 3 1 -.8781281 4 1 .600222 0 /
STATE VECTOR PATH
TO XF VS TIME
1
OPTIMAL CONTROL
INPUTS VS TIME
0.,0.,0
1
0.,10.,50
EASIEST RESPONSE
VECTOR VS TIME
2ND EASIEST RESPONSE
VECTOR VS TIME
3RD EASIEST RESPONSE
VECTOR VS TIME
4TH EASIEST RESPONSE
VECTOR VS TIME
A LOG10 OF EACH BASIS
COST INDEX VS TF
0.,0.,0

```


Vita

John M. Yarger was born Dec. 8, 1950 in Canton, Ohio. He graduated from North Canton Hoover High School in 1968, and received both his Bachelor of Aerospace Engineering degree from the Georgia Institute of Technology and his Air Force commission from ROTC in 1973. He then spent 4 1/2 years as a Minuteman III trajectory engineer and MX trajectory analyst at Headquarters, SAC, Offutt AFB, Nebraska. He entered the AFIT Graduate Aeronautical Engineering program in June, 1978. His home address is:

517 North Central

Fairborn, Ohio 45324

UNCLASSIFIED

SECURITY CLASSIFICATION OF THIS PAGE (When Data Entered)

REPORT DOCUMENTATION PAGE		READ INSTRUCTIONS BEFORE COMPLETING FORM
1. REPORT NUMBER AFIT/GAE/AA/79D-19	2. GOVT ACCESSION NO. AD A115 549	3. RECIPIENT'S CATALOG NUMBER
4. TITLE (and Subtitle) CALCULATING AIRCRAFT CONTROLLABILITY QUALITY		5. TYPE OF REPORT & PERIOD COVERED MS Thesis
7. AUTHOR(s) John M. Yarger Captain, USAF		6. PERFORMING ORG. REPORT NUMBER
9. PERFORMING ORGANIZATION NAME AND ADDRESS Air Force Institute of Technology (AFIT-EN) Wright-Patterson AFB, Ohio 45433		8. CONTRACT OR GRANT NUMBER(s)
11. CONTROLLING OFFICE NAME AND ADDRESS		10. PROGRAM ELEMENT, PROJECT, TASK AREA & WORK UNIT NUMBERS
14. MONITORING AGENCY NAME & ADDRESS (if different from Controlling Office)		12. REPORT DATE December 1981
		13. NUMBER OF PAGES 150
		15. SECURITY CLASS. (of this report) Unclassified
		15a. DECLASSIFICATION DOWNGRADING SCHEDULE
16. DISTRIBUTION STATEMENT (of this Report) Approved for public release; distribution unlimited		
17. DISTRIBUTION STATEMENT (of the abstract entered in Block 20, if different from Report)		
18. SUPPLEMENTARY NOTES Approved for public release; IAW AFR 190-17 FREDRICK C. WYNCH, Major, USAF Director of Public Affairs 15 APR 1982 Dean for Research and Professional Development Air Force Institute of Technology (ATC) Wright-Patterson AFB, OH 45433		
19. KEY WORDS (Continue on reverse side if necessary and identify by block number) Linear System Analysis Controllability Grammian Singular Value Decomposition Optimal Control Aerodynamic Paneling FLEXSTAB Aircraft Dynamics		
20. ABSTRACT (Continue on reverse side if necessary and identify by block number) A quantitative measure of linear system controllability quality was developed, implemented in a software program, and demonstrated through a preliminary evaluation of an experimental aircraft flight control system. A linear state space representation of aircraft perturbation motion was used as the differential constraint equation for a quadratic cost functional which minimizes the control energy required to reach a specified final state. The singular value decomposition of the controllability Grammian, which		

DD FORM 1473

1 JAN 73

EDITION OF 1 NOV 65 IS OBSOLETE

UNCLASSIFIED

SECURITY CLASSIFICATION OF THIS PAGE (When Data Entered)

UNCLASSIFIED

SECURITY CLASSIFICATION OF THIS PAGE (When Data Entered)

appears in the solution to this optimal control problem, yields a unique, time-varying, orthogonal set of basis vectors $(\bar{v}_1, \bar{v}_2, \dots, \bar{v}_n)$ which are ranked by the control energy required to move the linear system along each vector. Each \bar{v}_i is the least costly (in control energy) direction to control in the orthogonal complement to that subspace of (R^n) containing $\bar{v}_j, j=1, 2, \dots, (i-1)$.

The experimental flight control system consists of variable incidence wingtips acting as elevons and rudders, used on a supersonic-cruise light-weight fighter. The evaluation included both comparison of basis vector sets between baseline and modified aircraft and direct comparison of the control magnitudes required to reach sample final states. Results show the experimental controls are unsuitable due to

- (1) poor longitudinal and lateral control power,
- (2) no yaw/rudder control available due to symmetry restrictions in the linear aerodynamics software.

UNCLASSIFIED

SECURITY CLASSIFICATION OF THIS PAGE (When Data Entered)

END

DATE
FILMED

7 82

DTIC